

พฤติกรรมของกำแพงไคอะเฟรมในขณะที่ทำการขุดดินด้วยวิธีการก่อสร้างทอปดาวน์ในดินกรุงเทพ



นาย เนีย ตรง ती

สถาบันวิทยบริการ

วิทยานิพนธ์นี้เป็นส่วนหนึ่งของการศึกษาตามหลักสูตรปริญญาวิศวกรรมศาสตรดุษฎีบัณฑิต

สาขาวิชาวิศวกรรมโยธา ภาควิชาวิศวกรรมโยธา

คณะวิศวกรรมศาสตร์ จุฬาลงกรณ์มหาวิทยาลัย

ปีการศึกษา 2549

ISBN 974- - -

ลิขสิทธิ์ของจุฬาลงกรณ์มหาวิทยาลัย

BEHAVIOR OF DIAPHRAGM WALL DURING EXCAVATION PROCESS USING TOP-DOWN METHOD
IN BANGKOK SUBSOIL



Mr. Nghia Trong Le

สถาบันวิทยบริการ

A Dissertation Submitted in Partial Fulfillment of the Requirements
for the Degree of Doctor of Philosophy Program in Civil Engineering

Department of Civil Engineering

Faculty of Engineering

Chulalongkorn University

Academic year 2006

Copyright of Chulalongkorn University

Thesis Title BEHAVIOR OF DIAPHRAGM WALL DURING EXCAVATION
PROCESS USING TOP-DOWN METHOD IN BANGKOK SUBSOIL

By Mr. Nghia Trong Le

Field of Study Civil Engineering


Thesis Advisor Associate Professor Wanchai Teparaksa, Ph.D.


Thesis Co-Advisor Professor Toshiyuki Mitachi, D.Eng.

Accepted by the Faculty of Engineering, Chulalongkorn University in Partial Fulfillment of
the Requirements for the Doctoral Degree



..... Dean of the Faculty of Engineering
(Professor Direk Lavansiri, Ph.D.)

THESIS COMMITTEE


..... Chairman
(Associate Professor Boonsom Lerthiranwong, Ph.D.)


..... Thesis Advisor
(Associate Professor Wanchai Teparaksa, Ph.D.)


..... Thesis Co-Advisor
(Professor Toshiyuki Mitachi, D.Eng.)


..... Member
(Assistant Professor Tirawat Boonyatee, Ph.D.)


..... Member
(Assistant Professor Korchoke Chantawarangul, Ph.D.)

นาย เนีย ตรง ลี: พฤติกรรมของกำแพงไดอะแฟรมในขณะทำการขุดดินด้วยวิธีการก่อสร้างทอป
 ดาวน์ในดินกรุงเทพ (BEHAVIOR OF DIAPHRAGM WALL DURING EXCAVATION
 PROCESS USING TOP-DOWN METHOD IN BANGKOK SUBSOIL)

อ. ที่ปรึกษา : รศ.ดร. วันชัย เทพรักษ์ , อ.ที่ปรึกษาร่วม : Prof. TOSHIYUKI MITACHI,
 79 หน้า.

การประมาณการเคลื่อนตัวของกำแพงไดอะแฟรมวอลล์เนื่องจากการขุดดินโดยทั่วไปจะทำการประมาณ
 โดยวิธีอีลาสติก แต่ในการขุดดินลึกที่ใหญ่และมีผลของเวลาที่ปล่อยว่างโดยไม่มีกรขุดดินจะต้อง
 ทำการศึกษาพฤติกรรมของดินหลังกำแพงไดอะแฟรมวอลล์ ในการศึกษาพฤติกรรมดังกล่าวได้ทำการ
 วิจัยพฤติกรรมการอัดตัวของดินในสภาพ K_0 (CK_0UC) ทั้งนี้กรณี K_0 Consolidation drained
 และ undrained unloading ผลการศึกษาพบว่ากำลังรับแรงเฉือนของดินจากการทดสอบ CK_0DUC มี
 ค่าเท่ากับค่ากำลังรับแรงเฉือนที่ residual strength ของการทดสอบ CK_0DUC ค่า Young Modulus (E)
 ที่ทุกๆขั้นตอนของการลดแรงดันด้านข้างของดินจากการทดสอบ CK_0DUC จะลดลงเมื่อค่า Deviator
 Stress เพิ่มขึ้น ค่าของต่ำสุดของ Young Modulus (E) มีค่าเท่ากับ 46%, 50% และ 60% ของค่า
 Young's Modulus เริ่มต้น (E_0) ในการทดสอบ CK_0UC , CK_0DUC และ CK_0UUC ตามลำดับ ค่าความ
 ลาดของ Critical State line (CSL) ทั้งการทดสอบ CK_0UC และ CK_0DUC มีค่าเท่ากันเท่ากับ 1.5 ค่า
 อัตราการเคลื่อนตัวในแนวตั้งและแนวรัศมีของทุกๆการลดความดันด้านข้างจากการทดสอบ CK_0DUC
 มีค่าในรูปของเวลา, ความชันของ CSL และ อัตราส่วนของ Deviator and Mean Effective Stress การ
 วิเคราะห์ด้วยไฟไนท์อีลอสเมนต์ 2 มิติ ในการศึกษาโครงการธนาคารแห่งประเทศไทย โดยอิงพฤติกรรม
 การพังทลายของดินในรูปของอีลาสติก พลาสติก สามารถประมาณการเคลื่อนการเคลื่อนตัวได้
 สอดคล้องกับผลของการวัด ในขณะที่การวิเคราะห์ด้วยพฤติกรรมการพังทลายของดินในรูปแบบของ
 Soft Soil Creep (SSC) ควรจะทำการศึกษาเพิ่มเติมเพื่อหาผลจากเวลาที่ปล่อยว่างในการขุดแต่ละ
 ขั้นตอน

สถาบันวิทยบริการ
 จุฬาลงกรณ์มหาวิทยาลัย

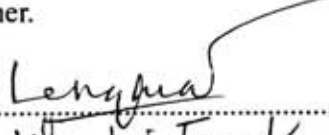
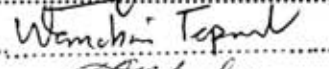

ภาควิชา.....วิศวกรรมโยธา.....ลายมือชื่อนิสิต..... *Lengua*
 สาขาวิชา.....วิศวกรรมโยธา.....ลายมือชื่ออาจารย์ที่ปรึกษา..... *Wanchai Tepul*
 ปีการศึกษา.....2549.....ลายมือชื่ออาจารย์ที่ปรึกษาร่วม..... *Mitachi*

4771847721 : MAJOR CIVIL ENGINEERING

KEY WORD: DIAPHRAGM WALL / LATERAL DISPLACEMENT / ELAPSED TIME / TRIAXIAL TEST / UNLOADING COMPRESSION / PERIODIC DECREMENT / HORIZONTAL PRESSURE

NGHIA TRONG LE : THESIS TITLE. BEHAVIOR OF DIAPHRAGM WALL DURING EXCAVATION PROCESS USING TOP-DOWN METHOD IN BANGKOK SUBSOIL THESIS ADVISOR : WANCHAI TEPARAKSA, THESIS CO-ADVISOR : TOSHIYUKI MITACHI, 79 pp.

The simple linear elastic-perfectly plastic model with soil parameters s_u , E_u and ν of undrained condition is usually applied to predict the displacement of constructed diaphragm wall (DW) on soft soil during excavation. However, that could not explain the continuous increment of lateral displacement of DW for the large and deep excavation area both during the elapsed time without activity of excavation and after finishing excavation. To study the characteristic behaviors of soil behind the DW during those periods, a series of test on Bangkok soft clay samples was simulated in the same manner as stress condition of soil element happening behind diaphragm wall using triaxial tests. Three kinds of triaxial tests were carried out in this research: K_0 consolidated undrained compression (CK_0UC) and K_0 consolidated drained/undrained unloading compression with periodic decrement of horizontal pressure (CK_0DUC and CK_0UUC). The study yields the findings namely the shear strength of series CK_0DUC tests is equal to the residual strength of CK_0UC tests. The Young's modulus determined at each decrement step of the horizontal pressure of soil specimen on CK_0DUC tests decreases with an increase in deviator stress. The decrement of Young's modulus (E) with strain level was observed on CK_0UC , CK_0DUC and CK_0UUC tests. The lower bound E values are equal to 46%, 50% and 60% of initial Young's modulus (E_0) on the CK_0UC , CK_0DUC and CK_0UUC tests, respectively. Besides, the slope of Critical State Line of both CK_0UC and CK_0DUC tests has the same value of 1.5. Moreover, the axial and radial strain rates of each decrement of horizontal pressure step of CK_0DUC tests are established with the function of time, slope of critical state line and ratio of deviator and mean effective stress. The test results are beneficial to the prediction of the diaphragm wall deflection during excavation. The 2D-FE analysis for a case study, Bank of Thailand project, was carried out with elastic-perfectly plastic (EPP) and Soft Soil Creep (SSC) models using PLAXIS program. The EPP soil model was applied to predict effectually the lateral displacement of DW on excavation time and elapsed time by the estimated Young's modulus corresponding to strain level. For the SSC model, the horizontal coefficient of deformation (C_{ar}) which could be applied for FE analysis to predict the lateral displacement of DW versus time should be studied further.

Department Civil Engineering Student's signature..... 
 Field of study Civil Engineering Advisor's signature..... 
 Academic year 2006 Co-advisor signature..... 

ACKNOWLEDGEMENT

I would like to express my profound gratitude and sincere appreciation to Thesis Advisor, Assoc. Prof. Dr. Wanchai Teeparaksa for his valuable suggestions, guidance and encouragement throughout this research. I am also thankful to Thesis Co-advisor Prof. Toshiyuki Mitachi whose invaluable guidance, continuous encouragement and discussion for during 7 months study in Hokkaido University

Thanks to Chair Assoc. Prof. Dr. Boonsom Lerdhiranwong and Assist. Prof. Dr. Tirawat Boonyatee, Assist. Prof. Dr. Korchoke Chantawarangul for their advice while serving as members of my thesis examination committee.

Grateful acknowledgement are also extended to Assoc. Prof. Takayuki Kawaguchi, Dr. Fumihiko Fukuda, Mr. Kudod Yutaka and Mr. Nishida Kohta for enthusiastic guide me doing the Triaxial tests in Hokkaido University

Sincere appreciation is also express to the staffs of management construction of Bank of Thailand project, especially to Mr. Tammarat and Mr. Chakrit for helping me collect the field data. Thanks also to Mr. Chuchart of STS Company for collecting the soil samples.

I would like to thank to Assoc. Prof. Dr. Sangrawee Chopricha for her generous revision and corrections of my thesis draft.

Thanks to AUN-SEED Net JICA for the financial support my studying during 3 years in Chulalongkorn University and Hokkaido University.

Finally, I have profound gratefulness towards all who helped directly and indirectly in the study, especially to my beloved parents, sisters and brothers for their constant love and encouragement.

สถาบันวิทยบริการ
จุฬาลงกรณ์มหาวิทยาลัย

TABLE OF CONTENTS

	Page
Abstract (Thai)	iv
Abstract	v
Acknowledgement	vi
Table of Contents	vii
List of Tables	ix
List of Figures	x
Chapter I Introduction	1
1.1 Background	1
1.2 Objective	2
1.3 Scopes of study	3
1.4 Methodology	3
Chapter II Literature Review	4
2.1 General properties and stratum of subsoil in Bangkok	4
2.2 Resent research of deep excavation	6
2.3 Deep excavation in Bangkok subsoil	8
2.4 Creep behavior of soft soil	10
Chapter III Project Description and Field Experimental Work	15
3.1 Project description	15
3.2 Field Measurements	22
3.3 Summary	24
Chapter IV Laboratory Tests	26
4.1 Material and Testing procedure	26
4.2 Test results and Discussion	29
4.3 Summary	49
Chapter V Finite Element Analysis	52
5.1 Background	52

	Page
5.2 Linear elastic-perfectly plastic model	55
5.3 Soft Soil Creep model	60
Chapter VI Result and Discussion	63
6.1 Parameters of soil models	63
6.2 Finite Element Analysis	65
Chapter VII Conclusion and Recommendation	67
7.1 Summary and Conclusion	67
7.2 Recommendations for Further Research	68
References	69
Appendix	72
Appendix A Data of inclinometers	73
Appendix B Triaxial test Apparatus	76
Vitae	79

สถาบันวิทยบริการ
จุฬาลงกรณ์มหาวิทยาลัย

LIST OF TABLES

Table	Page
3.1. Excavation sequence of BOT case history	16
3.2. The data of lateral displacement of DW on the excavation and elapsed time of nine inclinometers	20
3.3. Summary of properties of subsoil at BOT project	23
4.1. Summary of triaxial test of marine Bangkok clay	29
4.2. Data of secant Young's modulus $E_{u(sec)}$ and un-reloading Young's modulus E_u of CK ₀ UC tests	36
5.1. The properties of diaphragm wall and the basement floors	52
5.2. Parameters for linear elastic-perfectly plastic model	54
5.3. Duration of each construction stage	54
5.4. Parameters for Soft Soil Creep model	55
5.5. Properties of soil for Mohr-Coulomb model (linear elastic-perfectly plastic)	56
5.6. The ratio of undrained Young's modulus and undrained shear strength of soft clay layer	56
5.7. Parameters of soil for Soft Soil Creep model for BOT project.....	60

LIST OF FIGURES

Figure	Page
2.1. Stress path for soil elements near an excavation	7
2.2. Typical Strain Range (Mair, 1993)	9
2.3. Empirical Young's modulus value (Duncan&Buchigani, 1976)	10
2.4. Self-boring pressuremeter test result of Bangkok clay: (a) Soft clay; (b) Stiff clay	10
2.5. Creep curves predicted by the stress-strain-time functions for $m>1$, $m=1$, and $m<1$ for $t_l=1$: (a) Strain versus time and (b) strain versus logarithm of time	12
2.6. (a) Flow surfaces, total stress path, and effective stress in $q-p'$ space, and (b) corresponding ε_v (or ε_m) vs. p' , instant time line, and reference time line for isotropically consolidated undrained test at a constant compression strain rate	14
3.1. Location and divided zones of excavation process of BOT project	15
3.2. Process of excavation and top-down construction in BOT project	16
3.3. Lateral displacement of diaphragm wall on the elapsed time excavated to (a) 8.1 m and (b) 15.2 m	18
3.4. Horizontal displacement of diaphragm wall during basement construction ...	19
3.5. The ratio of the rate of DW lateral displacement on excavation time and on elapsed time	21
3.6. The settlement ground surface behind the DW at line C, D and E position ...	22
3.7. Properties of subsoil in BOT project	24
3.8. BOT project under construction	25
4.1. Undrained shear strength and Young's modulus of CK_0UC tests	27
4.2. Procedure of CK_0DUC and CK_0UUC tests	28
4.3. Ratio of shear strength and overburden effective stress of field-vane-shear test compared with CK_0UC , CK_0UUC and CK_0DUC tests	30
4.4. Relationship between deviator stress (q) and axial strain (ε_a) of CK_0UC , CK_0DUC and CK_0UUC tests	31
4.5. Relationship between deviator stress (q) and axial strain (ε_a) of CK_0UC tests	32
4.6. Definition of un-reloading Young's modulus E_u and secant Young's modulus $E_{u(sec)}$	33

Figure	Page
4.7. Reduction of undrained Young's modulus (E_u) with axial strain level (ϵ_a) of CK ₀ UC tests.....	34
4.8. Comparison secant Young's modulus $E_{u(sec)}$ with un-reloading Young's modulus E_u of CK ₀ UC tests	34
4.9. Ratio of secant Young's modulus $E_{u(sec)}$ and un-reloading Young's modulus E_u of CK ₀ UC tests	35
4.10. Reduction of undrained Young's modulus ratio (E_u/E_{u0}) with axial strain level (ϵ_a) of CK ₀ UC tests	37
4.11. Unloading Young's modulus E_{un}	38
4.12. Relationship between deviator stress (q) and axial strain (ϵ_a) of CK ₀ DUC tests.	38
4.13. Reduction of unloading Young's modulus (E_{un}) with axial strain level (ϵ_a) of CK ₀ DUC tests	39
4.14. Reduction of unloading Young's modulus ratio (E_{un}/E_{un0}) with axial strain level (ϵ_a) of CK ₀ DUC tests	40
4.15. Relationship between deviator stress (q) and axial strain (ϵ_a) of CK ₀ UUC tests	40
4.16. Reduction of unloading Young's modulus (E_{un}) with axial strain level (ϵ_a) of CK ₀ UUC tests	41
4.17. Reduction of unloading Young's modulus ratio (E_{un}/E_{un0}) with axial strain level (ϵ_a) of CK ₀ UUC tests	41
4.18. Relationship between Unloading Young's modulus E_{un} and ratio η/M ...	42
4.19. Slope of the Critical State Line	44
4.20. Strain rate of soil sample at depth 11.0 m under CK ₀ DUC test	45
4.21. Strain rate of soil sample at depth 11.0 m under CK ₀ UUC test	46
4.22. Relationship between strains and time of CK ₀ UUC and CK ₀ DUC tests ...	47
4.23. Strain rate of soil sample under CK ₀ DUC test	48
4.24. Coefficient a_a and b_a of axial strain rate $\dot{\epsilon}_a$	50
4.25. Coefficient a_r and b_r of radial strain rate $\dot{\epsilon}_r$	51

Figure	Page
5.1. Modeling the basement floors of BOT project at section of inclinometer B4	53
5.2. Lateral displacement of DW on stage 2 and stage 4	58
5.3. Lateral displacement of DW on stage 6	59
5.4. Lateral displacement of DW on stage 2, 3, 4 and 5 (SSC model)	61
5.3. Lateral displacement of DW on stage 6 and 7 (SSC model)	62
6.1. Geotechnical properties at BOT site project	64
6.2. Relationship between mean effective stress p' and volume strain ϵ_a of CK_0DUC test	65
6.3. The approximate equation of lateral displacement of DW and time during elapsed time of inclinometer B4 at stage 6	66
A.1. Horizontal displacement of diaphragm wall at inclinometers B1 and B2 during basement construction	73
A.2. Horizontal displacement of diaphragm wall at inclinometers B3 and B6 during basement construction	74
A.3. Horizontal displacement of diaphragm wall at inclinometers B8 and B9 during basement construction	75
B.1. Picture of Triaxial test system for carrying out the CK_0UC , CK_0DUC and CK_0UUC tests	76
B.2. Triaxial test system for carrying out the CK_0UC , CK_0DUC and CK_0UUC tests	77
B.3. Double Negative Pressure (DNP) system for saturation the soil sample	78

CHAPTER I

INTRODUCTION

1.1. Background

The public transportation and high way road systems are being developed in order to reduce gradually the traffic jam in Bangkok capital because it is expanding. The sky train and subway are the parts of transportation systems to solve the traffic problem. The subway project, Metropolitan Rapid Transit (MRT) with about 20 km long twin tunnels, which consists of 18 underground stations, began servicing in July 2004. This subway project makes use of deep excavations. In addition, deep excavations are used increasingly in congested cities around the world to provide underground space. The basements are used for parking lots at a shopping centers of a high building, condominiums and office buildings in urban areas are increasing in more demand. Due to need for more underground space, the deep excavations are conducted widely. Thus, they cause primarily problems needed to be solved namely: their effects to adjacent buildings and controlling the values of ground movement and lateral displacement of retaining wall to be lower than the allowance, etc.

For Bangkok subsoil condition, the cut-and-cover method with braced sheet pile wall, bottom-up with reinforced concrete diaphragm wall propped by steel struts and top-down construction method with reinforced concrete diaphragm wall have been usually selected for retaining structure of the excavation construction. The first method is the most practical system for excavation work in Bangkok subsoil, because it is cheaper than the other two methods. However, the sheet pile bracing system has a low requirement about the horizontal ground movement and also the effects to the existing building. Although, the third method takes a shorter construction time and limits the wall displacement as well as the damage of adjacent buildings by installing the concrete basements floors, it is more expensive and has to achieve higher standard.

Subsoil condition in Bangkok generally consists of a very soft dark gray about 12-14 m thick layer underlain by stiff and very stiff clay to about 23-25 m. The stress-strain behaviors of Bangkok deposit soft soil are nonlinear, irreversible, and time dependent, it causes many problems for deep excavation constructions. In addition, the stratigraphy is continuously followed by the first aquifer dense silty sand

layer, as a result, the dewatering is carried out if the excavation through this sand layer. Thus, the numerical analysis program with appropriate soil model is necessary for predicting and controlling the excavation construction process.

Many studies on deep excavation in Bangkok subsoil have been carried out (Teparaksa W., 1994; P. Tanseng, 1997; P. Tirapong, 1999; Tamrakar S.B., 2001). In almost the research cases, researchers compared the in-situ monitored data from, for instance, inclinometer, settlement point, excess of pore water pressure with these values output from back finite element analysis. The models, e.g., linear-elastic-perfectly plastic, elasto-plastic Mohr-Coulomb, Cam clay (Roscoe and Burland, 1968), modified Cam clay (Cambridge group), and Sekiguchi-Ohta (1977) were used for those analyses by using Plaxis 7.1, Sage-Crisp, and Dacsar (Ver. Dacl4, 1997). These studies concentrated on determining soil parameters for the model and the correlation between the parameters of these models with the others determined from laboratory and in-situ tests.

The undrained creep behavior and degree of pore water pressure dissipation of soft sensitive marine Bangkok clay have never been mentioned in the prediction process of the displacement of retaining wall. The inelastic and time-dependence behavior in soil mechanics play an important role in developing the mathematics model for the reality of the behaviors of soil. The creep deformation and stress relaxation characteristics have a direct impact on the stability on deep excavation. When the excavation goes deeper, this means larger increment of shear stress; the retaining structure increases the primary deformation; as well as the creep deformation follows the time. Therefore, the retaining structure will become deformed over the safety limit or collapsed if the horizontal struts and/or tieback anchors are not installed timely. Moreover, the retaining structure will probably collapsed because of insufficient designing strength and rigidity of diaphragm wall itself since the lateral earth pressure becomes larger and larger during stress relaxation.

Excavation alters the initial stress states in the ground. There are the unloading compression of soil zone behind the wall and unloading extension of excavated soil zone. In a result, the stability and deformation characteristics of an excavation are influenced by stress history and stress state, anticipated field behaviors should be simulated in the laboratory for appropriate determination of shear strength and stiffness parameters.

1.2. Objective

The displacement of diaphragm wall of large excavation zone by top-down method consists of two stages: excavation and elapsed time stages. At the elapsed time stage, the excavation depth remains unchanged. Therefore, there are three objectives of this research:

To determine the parameters of the undrained behavior soil models for the analysis of the displacement of diaphragm wall at the excavation stage.

To analyze the effects of undrained creep or/and pore-water dissipation of soft soil at the elapsed time stage by determining the parameters for creep soft soil model.

To observe the effects of excavation to the settlement, wall movement and tilt of the adjacent buildings from the recorded data yielded from installed instruments.

1.3. Scope of study

The soil behaviors of Bangkok subsoil are characterized by the appropriate models for each kind of soil, e.g., linear elastic-perfectly plastic, elasto-plastic Mohr-Coulomb, modified Cam clay, and Soft Soil Creep model.

The research focuses on reinforced concrete diaphragm wall (DW) of top-down method construction of the BOT (Bank of Thailand) project as the case study.

The back numeral analysis by using PLAXIS program is based on the available field measurement data, laboratory tests, collected data of Bangkok soil from previous studies and correlations of appropriate parameters.

1.4. Methodology

The instrument installed around the site of project monitors the response of case study during basement construction. Especially, the lateral displacement of DW and the ground settlement are observed by inclinometers and settlement points continuously one or two times per week on excavation time and elapsed time. Then, the collected field data is compared with the results of finite element (FE) analysis.

The laboratory test is carried out to determine the soil parameters for soil models so that the results of FE analysis with those soil models can be estimated the response of DW on both excavation time and elapsed time. The unloading compression triaxial tests is realized as the performance of soil element behind the DW during construction time.

CHAPTER II

LITERATURE REVIEW

2.1. General properties and stratum of subsoil in Bangkok

Geotechnical Hazards in Bangkok, the capital of Thailand, are cited with reference to floods, land subsidence and earthquakes, bearing the characteristic subsoil conditions in mind. First, geotechnical engineering works concerning the implementation of flood protection schemes are briefly outlined. Second, the cause of land subsidence, i.e., the drawdown of pore pressures in clay layer induced by water pumping in the aquifer, together with the current situations are described by showing the results of geotechnical site investigation performed recently.

Geology

Subsoil in Bangkok (BKK) area consists of Quaternary deposits, which originated from the sedimentation at the delta of the ancient river in the Chao Phraya. The other soil deposits are marine deposits, which are the result of changes in sea levels during the Quaternary period. Bangkok is situated on the central part of the Chao Phraya plain about 20km north of Gulf of Thailand. It is bordered on the west by Tanowsri Mountain range and on the East by Horat Plateau. The major drainage system of the plain is the Chao Phraya River and its tributaries from the surrounding highlands. The terrestrial elevation is about 0 to 5m above the mean sea level. The Chao Phraya basin is filled with sedimentary soil deposits, which form alternative layers of sand, gravel and clay. The marine clay is the uppermost clay layer, and it is generally found in the lower deltaic area of Bangkok plain, which extends from 200 to 250km in the East-West direction and 250 to 300km in the North-South direction. Formation of the uppermost layer, known as Bangkok clay, is believed to approximately start 4000 years ago.

The top 80m thick soil layer in Bangkok subsoil investigated for every project is basically divided into four layers.

(1) Crust: The crust, dark gray and hard layer from 1 to 3 m in thickness, showing the shear strength of about 40kPa on average. It is resulted due to weathering and desiccation processes. The weathering process includes such features as fluctuation of ground water level, leaching, ion exchange and precipitation of cementitious materials due to drying and wetting during dry and wet season.

(2) Soft clay: The thickness of soft clay layer is about 14m in central of Bangkok and varies from 12 to 17 m from the north to the south of Bangkok. This layer is highly compressible with the over-consolidation ratio OCR of 1 to 1.5. Its general properties are: natural water content $w_n=60$ to 100%, liquid limit $w_L=50$ to 100%, plasticity index $I_p=30$ to 80 and undrained shear strength $s_u=10$ to 25 kPa

(3) Stiff clay: A distinct unconformity exists between the base of the soft clay and underlying first stiff clay layer. It is also hard in nature and the stiffness of this layer is seemingly due to desiccation and some extent due to erosion (AIT, 1981). In many places, it is mottled, fissured, with red and yellow colors indicating that it is exposed to sub-aerial processes of desiccation and chemical weathering before burial by the soft clay (Moh et al., 1969). Sub-aerial processes take place in the zone below ground level and above the groundwater table. There is also evidence that the first stiff clay have been eroded in places prior to deposition of soft clay. Thickness of the first stiff clay varies between 7 to 14m in the central of Bangkok. Low compressibility, high OCR and low natural water content w_n as compared to soft clay are some of it properties. The shear strength tends to increase with depth, having the strength of about 100kPa on average. This layer is light gray and yellow-brown in color.

(4) Sand (aquifer): The sand layer of the Bangkok Aquifer System start below the first stiff clay layer and extend up to 70 m below the ground level (Rau and Nutalaya, 1981). This part of the information is broadly divided into three parts namely: (i) upper sand, (ii) stiff clay and (iii) lower sand. The upper sand, classified as silty sand (SM), have medium to high density with 10 to 15 m thick. The SPT blow count in upper sand layer is about 30 blows/ft whereas the SPT value in the lower sand layer is more than 50 blows/ft.

The city of Bangkok is located on a low land plain. In predicting the deformation behavior of soft clay ground prior to such excavations, the profile of elastic stiffness should be manifested by performing in-situ seismic survey, and the result maybe properly plugged into the elastic FE analysis as demonstrated by Tamrakar et al. (2001).

General soil properties and ground water condition

- Properties of subsoil in Bangkok
 - Unit weight, partial grain size, specific gravity
 - Natural water content, Atterberg limits and Plasticity and Liquidity index

- Undrained strength, Shear modulus, and SPT value
 - Ground water conditions

The piezometer profile identified for Bangkok is hydrostatic from 1-2 m below the ground surface to the depth of about 7-10 m. But, beyond this depth, owing to water pumping from the aquifer underneath the clay, non-hydrostatic distribution can be seen, which in turn exhibits underdrainage effectively within the stiff clays and the sand. It should be mentioned that the water pressure is virtually zero at the bottom of the stiff clay layer.

2.2. Recent studies on deep excavation

The behaviors of ground around the excavated zone are different. Such as the sample A and sample B on Figure 2.1 have different stress path, sample A and B are compression unloading and extension unloading, respectively.

In soil, time effects on its stress-strain behavior are common features, especially in clayey soil (Zhu, J.-G, et al 1999). Two types of time-dependent phenomena can be distinguished. One is due to the dissipation of excess pore-water pressure. The other is caused by the inherent viscous characteristics of soil skeleton, such as creep, stress relaxation, and strain rate dependency. It depends on the soil behavior under drained or undrained situation.

Ou, C.Y., and Lai C.H. (1994) used a combination of the hyperbolic and the modified Cam-clay models, respectively, for drained behavior of cohesionless soil and undrained behavior of cohesive soil to finite-element analysis of deep excavation in layered sand and clayey soil deposits. It was considered the pore-water pressure dissipation during the actual elapsed time for each excavation phase on the analysis process. The results indicated that the calculated displacement of a retaining wall during excavation was smaller than that given by undrained analysis. **The authors also concluded that some degree of pore-water pressure dissipation actually occurs during the intermediate excavation stages, in the result, in a decrease the final deformation of the wall and ground-surface settlement than would be predicted by undrained analysis.**

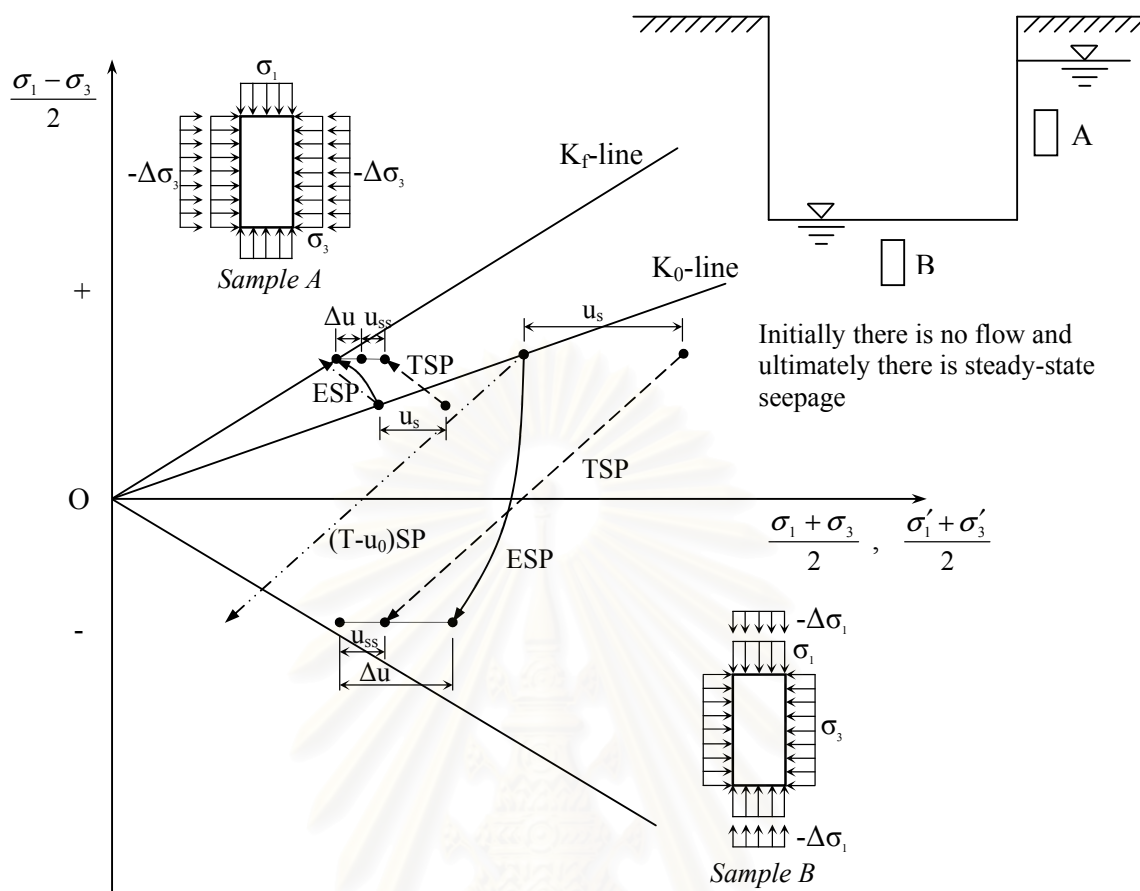


Figure 2.1. Stress path for soil elements near an excavation

Ou, C.Y., et al. (1998) observed the performance of the excavation (TNEC project, Taiwan) using top-down the construction method by measuring strut loads, wall displacement, wall bending moment, ground surface settlement, pore water pressure and bottom heave. The authors suggested that it should consider the effects of the dissipation of excess pore-water pressure and/or creep behavior on soil, significantly, on the deformation behavior of wall and soil because the top-down method used concrete floor slabs to support the wall sometimes required a long periods of time between two successive excavation stages to construct the floor slab. They found that the wall deflection and settlement gradually increased with time while excavation depth remained unchanged (with elapsed time). In more detail, the maximum lateral deflection rate of wall was in the range of 0.1 to 0.6 mm/day. In addition, when the excavation proceeded to 15.2 m depth, the accumulated wall deflection at 10 and 12 m depth were 30% and 36%, respectively, and the accumulated ground settlement at distance 13 m from the wall was 44%. The

monitored piezometers data showed that the pore-water pressure in the soil outside the excavation dropped significantly during excavation time and increase gradually on the elapsed time, except for the soil near the wall and above the excavation surface.

Lin D.G. and Woo S.M. (2005) analysed the lateral wall movement of top-down method construction zone of Taipei International Financial Center (Taipei 101) and concluded that a creep rate of 0.34 mm/day for 24 days creep time duration (elapsed time) was observed at 13 m depth of wall after completing 3rd stage excavation with 13.15 m of depth. The two-dimensional undrained creep analysis with Creep Soft Soil (*C-S-S*) model was used to simulate the creep deformation of deep excavation and the author experienced that the creep parameter μ^* in *C-S-S* model was dependent on creep stress level and needed to be adjusted with the creep rate ($d\varepsilon/dt$).

2.3. Deep excavation in Bangkok subsoil

On short-term behavior of soft soil in Bangkok, undrained condition of soil with the parameters for elasto-perfectly plastic s_u , E_u and ν was used to analyze and to predict the responses of construction on soil such as deep excavation, embankment, and foundation. Folk (1980) concluded that the response of soft foundation clay during and immediately after construction was usually undrained after he analyzed fills on soft clay involving normal rates of loading, fill/subsoil geometry and boundary drainage condition.

Many researchers have conducted studies on the correlation between undrained Young's modulus E_u and undrained shear strength s_u of Bangkok soft soil. After back analysis the behavior of diaphragm wall for deep excavation in Bangkok subsoil, W. Teeparaksa et al. (1999) suggested that the ratio of soil stiffness in terms of Young's modulus and undrained shear strength E_u/s_u is equal to 500 and 2000 for soft Bangkok clay and stiff clay, respectively. The different stiffness of diaphragm wall and sheet pile wall affected the deformation of soil behind the wall as well as the strain level. Pornpot Tanseng (1997) also concluded that the E_u/s_u ratios were 500 and 2000 for soft clay and stiff clay, respectively, for back analysis on diaphragm wall and those ratios were 150 and 1000 for sheet pile wall.

Moreover, according to another research, that ratio varied. It could be 200~500 (Bowels, 1988) and 280~350 (Hock, 1997) for soft clay, and 1200~1600 for

stiff clay (Hock, 1997). Actually, the ratio E_u/s_u was a function of many variables, e.g., the strain level (Figure 2.2 and 2.4), plasticity index and OCR (Figure 2.3). Based on that correlation, the small variation of magnitude of s_u affected significantly to the soil stiffness - undrained Young's modulus E_u as well as the displacement of retaining wall.

P. Thirapong (1999) predicted the deformation behavior of braced excavation in Bangkok clay by using the DACSAR program (Iizuka, 1988) with Sekiguchi-Ohta model and it yielded encouraging results. The author concluded that, in elastoplastic model, initial recompression index κ_r should be employed rather than common swelling κ in order to take rebound history and apparent sensitivity into account.

Tamrakar S.B. (2001) determined the design parameters for elasto-plastic finite element analysis using SAGE-CRISP and suggested that the FE analysis by using the linear-elastic soil model with $E' = E'_{max} / 2$ probably be the simplest and adequate to the standard for predicting relatively small ground deformation associated with excavation work with rigid wall, e. g., diaphragm wall. Moreover, poisson's ratio is suggested 0.2-0.3 in excavation analysis. It seems to be the same as elastic material problem.

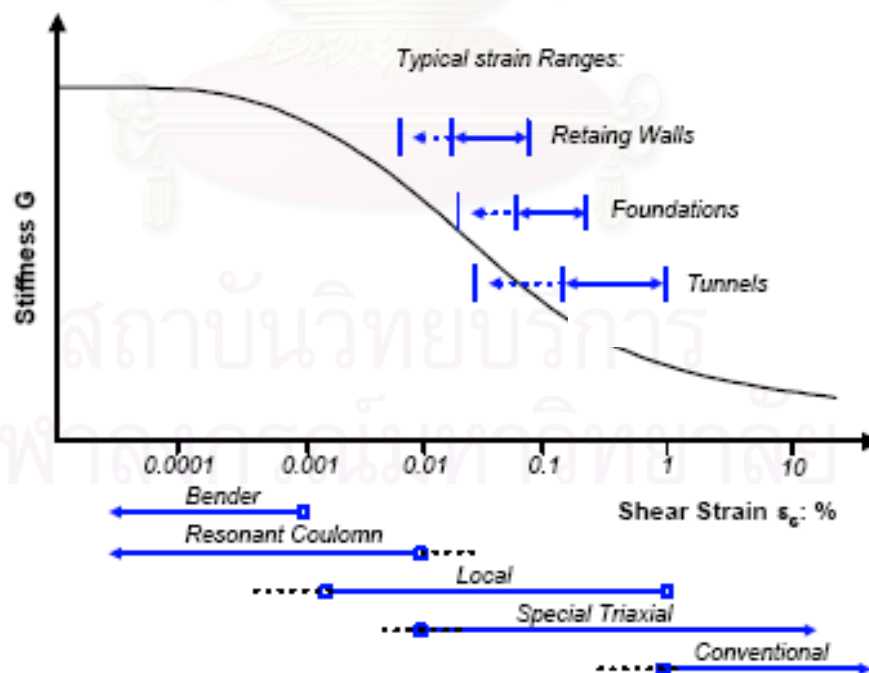


Figure 2.2. Typical Strain Range (Mair, 1993)

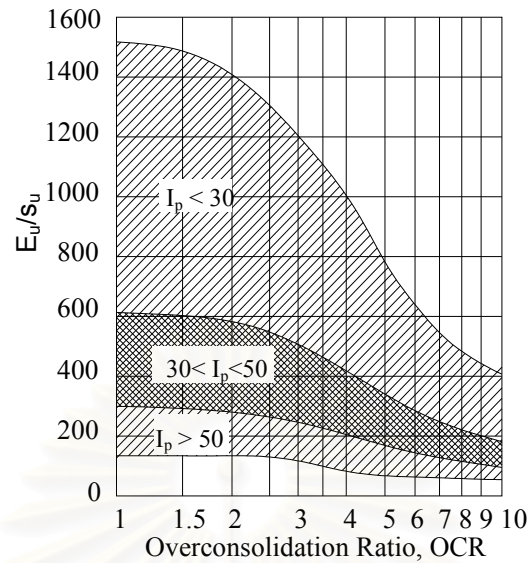


Figure 2.3. Empirical Young's modulus value (Duncan&Buchigani, 1976)

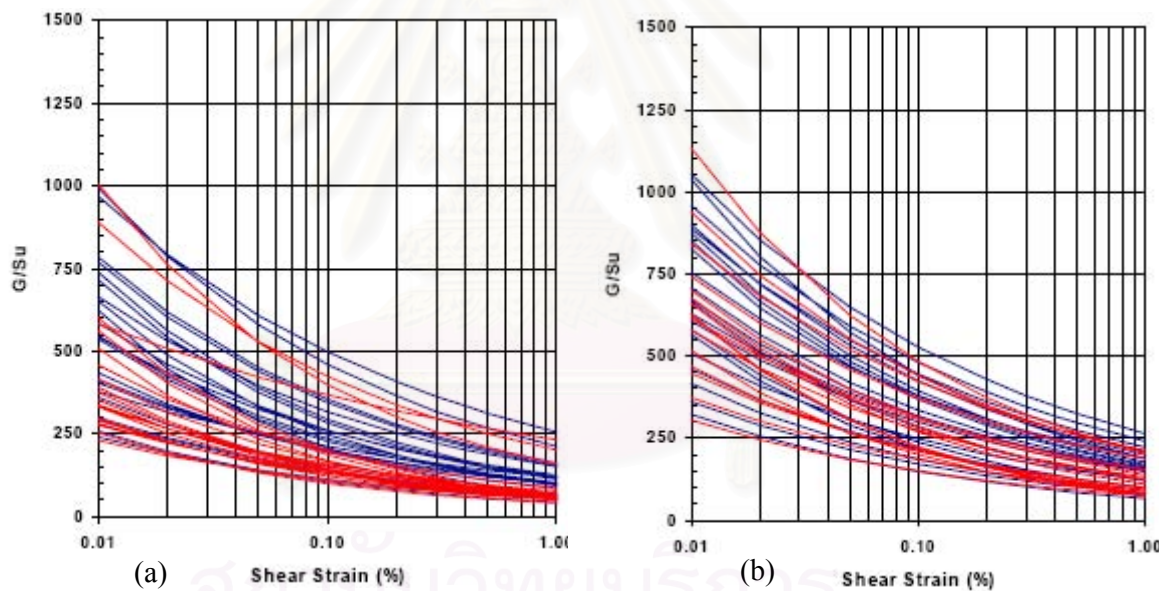


Figure 2.4. Self-boring pressuremeter test result of Bangkok clay: (a) Soft clay; (b) Stiff clay

2.4. Creep modeling of soil

1. Singh and Mitchell's creep model

Based on the analysis of drained and undrained triaxial creep tests on several clays, Singh and Mitchell (1968) suggested that a simple three-parameter phenomenological equation might be used to describe the strain-rate-time relation of clayey soil when subjected to constant stress. The model describes the creep behavior of clayey soils over the range of engineering interest, that is stresses from about 30%

to as high as 90% or more of the initial strength. Observing a general relationship between the logarithm of the axial strain rate and the logarithm of time, irrespective of whether the strain versus logarithm of time is linear or nonlinear can be described as

$$\dot{\varepsilon} = Ae^{\alpha \bar{D}} \left(\frac{t_1}{t} \right) \quad (2.1)$$

where

$$\bar{\alpha} = \alpha D_{\max}; \quad \bar{D} = \frac{D}{D_{\max}}$$

A - soil property that reflects composition, structure, and stress history.

α - is the slope of the linear part of the log strain rate versus stress plot; this parameter indicates the stress intensity effect on the creep rate.

m - the absolute value of the slope of the straight line on the log strain rate versus log time plot, this parameter controls the rate at which the axial strain rate decreases with time; $m = 0.7 \div 1.3$ for triaxial creep test.

D - deviator creep stress.

\bar{D} - the deviator stress level expressed as the ratio of the creep stress D with respect to the strength D_{\max} at the beginning of the creep process.

Integration of the creep rate function in Eq. (2.1) produces a general relationship between time and axial strain may be obtained. There are two solutions obtained depending on the value of m . If $\varepsilon = \varepsilon_1$ at $t = 1$ and $t_1 = 1$, then

$$\varepsilon = \varepsilon_1 + \frac{A}{1-m} e^{\alpha D} (t^{1-m} - 1) \quad (m \neq 1) \quad (2.2)$$

and

$$\varepsilon = \varepsilon_1 + Ae^{\alpha D} \ln t \quad (m = 1) \quad (2.3)$$

Creep curve shapes corresponding to these relationships are shown in Figure 2.5. A similar equation to equation (2.2) was developed by Mesri et al. (1981) from equation (2.1). The initial time-independent strain was neglected, and the resulting equation was

$$\varepsilon = \frac{At_1}{(1-m)} e^{\alpha D} \left(\frac{t}{t_1} \right)^{(1-m)} \quad (2.4)$$

Three parameters A , α , and m can be determined by a few ordinary creep tests for any given soil. For a particular soil, m is assumed to be constant, however, other

creep curves at different stress levels probably involved different value of m for the same soil.

The model only describes the creep behavior at a constant level of stress in one-dimensional condition and is only valid for the first time loading.

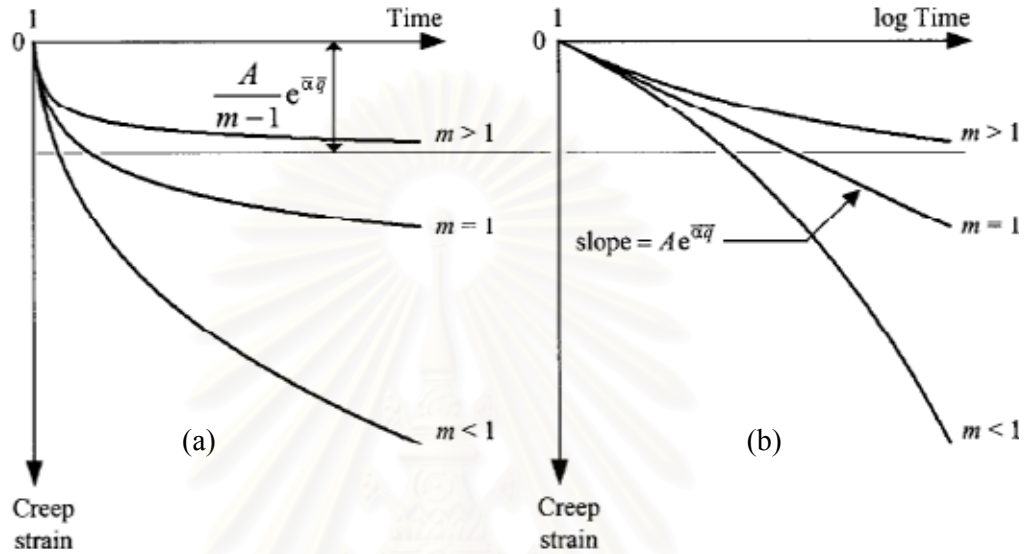


Figure 2.5. Creep curves predicted by the stress–strain–time functions for $m > 1$, $m = 1$, and $m < 1$ for $t_l = 1$: (a) Strain versus time and (b) strain versus logarithm of time.

2. 3D elastic viscoplastic (EVP) model (Yin, J.-H., and Graham, J., 1999).

This model is based on the total strain rates $\dot{\epsilon}_{ij}$ which are the sum of elastic strain rates $\dot{\epsilon}_{ij}^e$ and viscoplastic strain rates $\dot{\epsilon}_{ij}^{vp}$:

$$\dot{\epsilon}_{ij} = \dot{\epsilon}_{ij}^e + \dot{\epsilon}_{ij}^{vp} \quad (2.5)$$

A separate elastic relationship is suggested to relate the elastic strain rates $\dot{\epsilon}_{ij}^e$ in eq. (2.5) to effective stress rates $\dot{\sigma}'_{kl}$:

$$\dot{\epsilon}_{ij}^e = C_{ijkl} \dot{\sigma}'_{kl} \quad (2.6)$$

where C_{ijkl} is a fourth-order compliance tensor with subindices $k = 1, 2, 3$ and $l = 1, 2, 3$.

Viscoplastic strain rates $\dot{\epsilon}_{ij}^{vp}$ in eq. (2.5) are calculated from the flow rule

$$\dot{\epsilon}_{ij}^{vp} = \gamma \langle \phi(F) \rangle \frac{\partial Q}{\partial \sigma'_{ij}} = S \frac{\partial Q}{\partial \sigma'_{ij}} \quad (2.7)$$

where the scaling function $S = \gamma \langle \phi(F) \rangle$ and Q is a viscoplastic potential function, called a plasticity potential function in Perzyna's framework.

The approach is based on the framework of Modified Cam-Clay (Roscoe and Burland 1968) and is assumed that the viscoplastic potential Q in eq. (2.7) is equal to the flow-surface function F , which depends on stress level and hardening history k :

$$Q = F(\sigma'_{ij}, k) = 0 \quad (2.8)$$

and

$$F = p'^2 - p'p'_m + \frac{q^2}{M^2} = 0 \quad (2.9)$$

where

$$p' = (\sigma'_{11} + \sigma'_{22} + \sigma'_{33})/3 \text{ is the mean effective stress;}$$

$$q = \left(\frac{3}{2} S_{ij} S_{ij} \right)^{1/2} \text{ is the generalized deviator stress, where } S_{ij} = \sigma'_{ij} - \delta_{ij} p', \text{ and}$$

$$\delta_{ij} = 1 \text{ for } i=j \text{ or } \delta_{ij} = 0 \text{ for } i \neq j$$

M is the slope of the strength envelope

$$M = M_c = 6 \sin \phi' / (3 - \sin \phi') \text{ in compression,}$$

$$\text{and } M = M_e = 6 \sin \phi' / (3 + \sin \phi') \text{ in extension.}$$

The volume strain rate and shear strain rate are proved as below

$$\begin{cases} \dot{\epsilon}_v = \frac{1}{K^e} \dot{p}' + \frac{1}{J^e} \dot{q} + S(2p' - p'_m) \\ \dot{\epsilon}_s = \frac{1}{J^e} \dot{p}' + \frac{1}{3G^e} \dot{q} + S \frac{2q}{M^2} \end{cases} \quad (2.10)$$

where

K_e - elastic bulk modulus,

G_e - elastic shear modulus,

J_e - a coupling modulus, which is used to describe shear-induced compression-dilation or mean stress induced shear strain.

S - scaling function.

$$S = \frac{\psi/V}{t_0} \exp \left[-(\epsilon_{vm} - \epsilon_{vm0}) \frac{V}{\psi} \right] \left[\left(\frac{p'_m}{p'_{m0}} \right)^{\frac{\lambda}{\psi}} \frac{1}{2p' - p'_m} \right] \quad (2.11)$$

$$\begin{cases} \kappa \approx \frac{C_r}{\ln(10)}, & \lambda \approx \frac{C_c}{\ln(10)} \\ \varepsilon_{vm0}^{ep} = \varepsilon_{vc,24} \quad (\text{or } \varepsilon_{vc,EOP}), & p'_{m0} = p'_{c,24} \quad (\text{or } p'_{c,EOP}) \\ \psi \approx \frac{C_{ae}}{\ln(10)}, & t_0 = t_{24} \quad (\text{or } t_{EOP}) \end{cases}$$

p'_m is the effective mean stress where an elliptical locus meets the p' axis.

$$C_{ae} = \frac{e_1 - e_2}{\log\left(\frac{t_2}{t_1}\right)} \quad \text{or} \quad C_{ae} = \frac{\varepsilon_{vm2} - \varepsilon_{vm1}}{\log\left(\frac{t_2}{t_1}\right)}$$

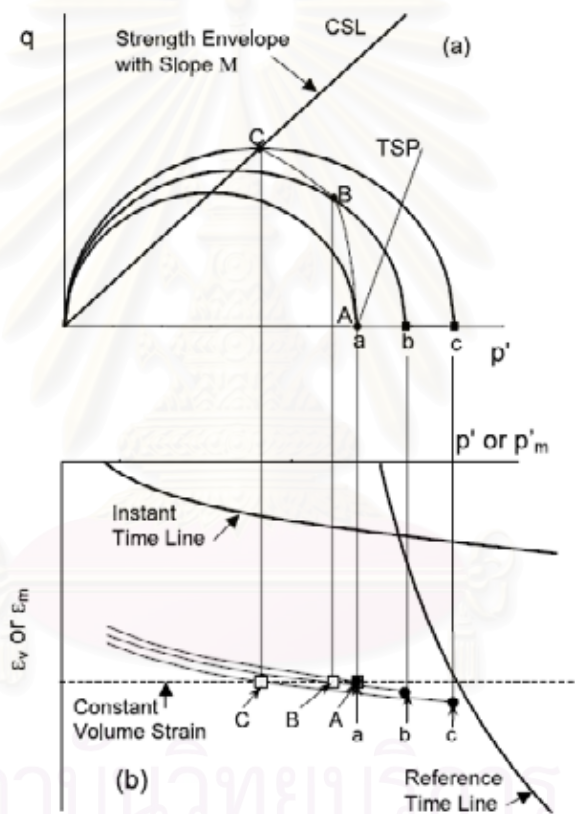


Figure 2.6. (a) Flow surfaces, total stress path, and effective stress in q - p' space, and (b) corresponding ε_v (or ε_m) vs. p' , instant time line, and reference time line for isotropically consolidated undrained test at a constant compression strain rate.

2.5. Summary

CHAPTER III

PROJECT DESCRIPTION AND FIELD MEASUREMENTS

3.1. Project description

The new Head Office of the Bank of Thailand (BOT), located on the Chao Praya River bank, Bangkok, is used as a case study of this research. As shown in Figure 3.1, the project is near the existing office building and the old historic palaces. The BOT consists of five underground basement floors with the total depth of excavation about 15.2 m and the fifth floor basement is a mat foundation. The project took more than one year to finish all the excavation and top-down construction for the basement floors.

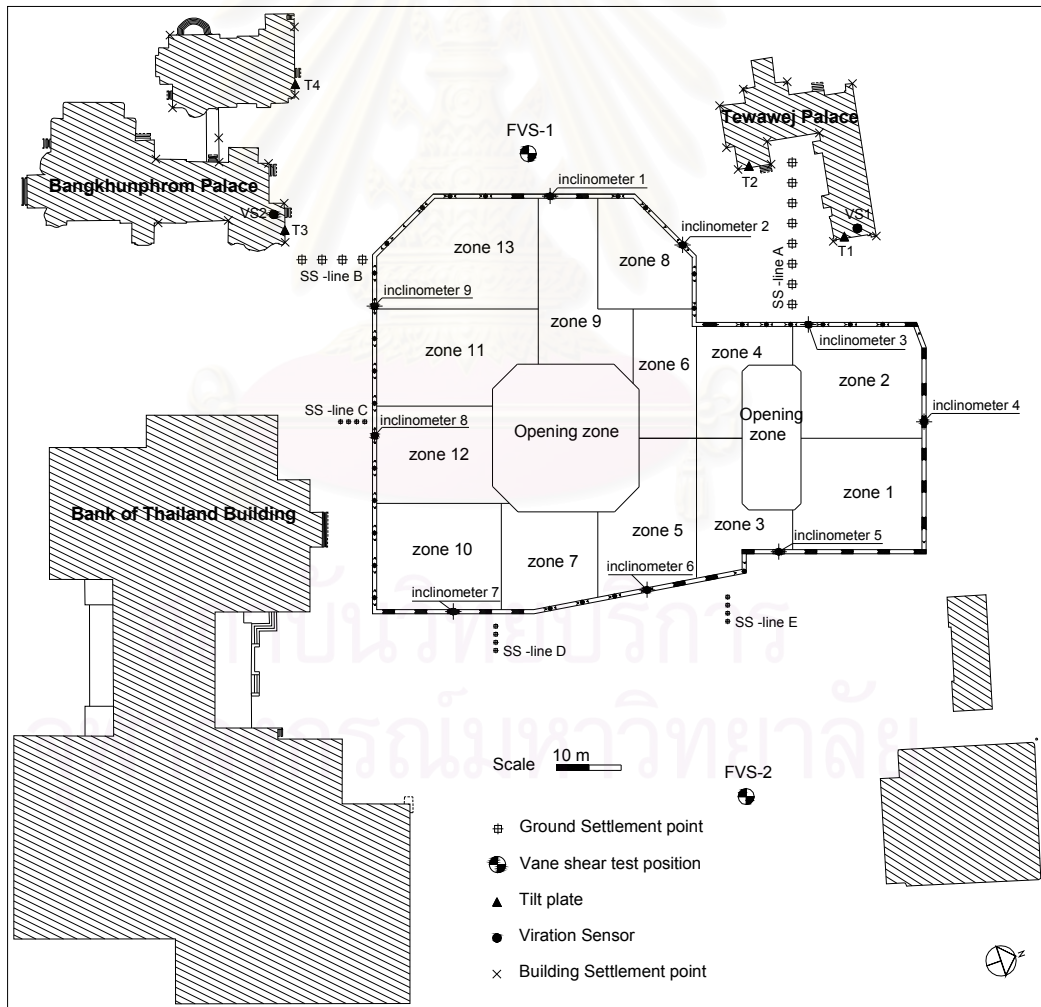


Figure 3.1. Location and divided zones of excavation process of BOT project

The area of excavation is larger than 10,790 m², and was divided into thirteen constructed zones. The sequence of basement construction at each zone is shown in Figure 3.2 and Table 3.1. The excavation was paused at three main excavated stages 2, 4 and 6 at the depth of 1.25 m, 8.1 m and 15.2 m, respectively. At those stages, there were the elapsed times of excavation to concrete the basement floors before continuing the excavation deeper, while the displacement of DW was continuously increasing. The lateral displacement of DW was monitored by nine inclinometers installed around the project (Figure 3.1).

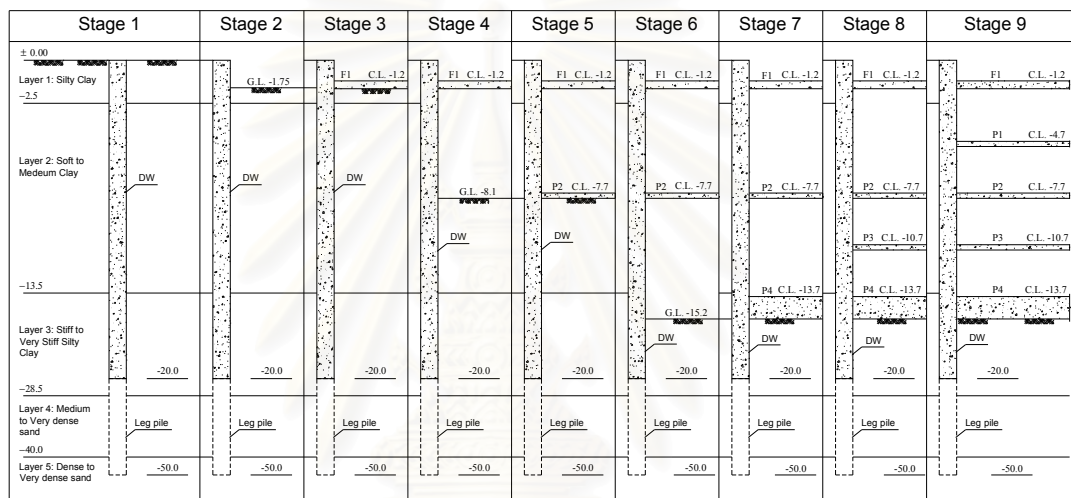


Figure 3.2. Process of excavation and top-down construction in BOT project

Table 3.1. Excavation sequence of BOT case history

Stage (1)	Interval (day) (2)	Construction activities (3)
1	1 – 234	Construct diaphragm wall, stanchion and bored pile
2	251 – 313	Excavate to elevation of -1.75 m.
3	330 – 387	Cast floor slab (F1) at elevation of -1.2m
4	381 – 487	Excavate to elevation of -8.1m
5	412 – 502	Cast floor slab (P2) at elevation of -7.7m
6	495 – 642	Excavate to elevation of -15.2m
7	538 – 662	Cast floor slab (P4) at elevation of -13.7m
8	517 – 706	Cast floor slab (P3) at elevation of -10.7m
9	591 – 737	Cast floor slab (P1) at elevation of -4.7m

The diaphragm wall, which was 1 m thick and 20 m deep, was retained around the periphery of excavation zone as a temporary wall during construction, and then it was incorporated into the permanent structure upon completion of the building. The DW had the leg piles at certain positions to support the columns from the upper structure and to balance as well as to reduce the settlement of the whole building. The entire building was supported by bored piles which was 1.5m in diameter. They were constructed by using a wet process with polymer slurry.

Installation of the inclinometers and settlement points was carried out to monitor the displacement of diaphragm wall and ground settlement during the excavation and construction process. Nine inclinometers were installed through the depth of the wall and the leg pile in order to observe the lateral movement of the bottom of the wall. In addition, the building settlement points, vibration sensors and tilt plates were installed on the old palaces and buildings around the excavation zone to observe the effects of excavation by recording the settlement, vibration, and the tilt to those buildings (Figure 3.1).

Figure 3.3 shows the data of the lateral displacement of some inclinometers (B1 to B9) around the periphery of DW at 8.1m and 15.2m of excavated depth. As the excavation paused at 8.1m deep to cast the floor slab F1, the largest value of lateral displacement appeared at around 2.0m deeper than the excavated level. It took nearly 3 months to cast the F1 floor, and during this period, the inclinometer data monitored biweekly showed a non-stop increase. Especially, in Figure 3.3(b), the excavation went through the stiff clayey layer to 15.2m deep. The maximum of lateral displacement, which occurred at the depth around 12.5m of soft clay layer, still increased after 6 months even though the excavation was over at inclinometers B1 and B9.

There are two different rates of DW lateral displacement on the excavation time and on the elapsed time as shown in Figure 3.4. Table 3.2 displays nine collected inclinometers data during nearly one year of excavation and construction of the basement floors. It was apparent that the data collected from nine inclinometers which were installed at different section of DW were different. Some positions were at the existing opening zone for the staircase functions of basement floors. The rate of DW lateral displacement on excavation time is the ratio of lateral displacement increment (Δh) and the duration of excavation (Δt). Similarly, the rate of DW lateral

displacement on elapsed time is the ratio of lateral displacement increment (Δh) and the elapsed time without excavation activity (Δt). As shown in Figure 3.5, the ratios of the rate of horizontal displacement $\left(\frac{\Delta h}{\Delta t}\right)_{\text{excavation time}} / \left(\frac{\Delta h}{\Delta t}\right)_{\text{elapsed time}}$ of diaphragm wall during excavation and elapsed time is from 2.6 to 13.0 as the excavated depth is 8.1 m. That ratio is from 1.2 to 9.6 as the excavated depth is 15.2 m depth. In other words, when the excavation is deeper the increment of lateral displacement on elapsed time is larger.

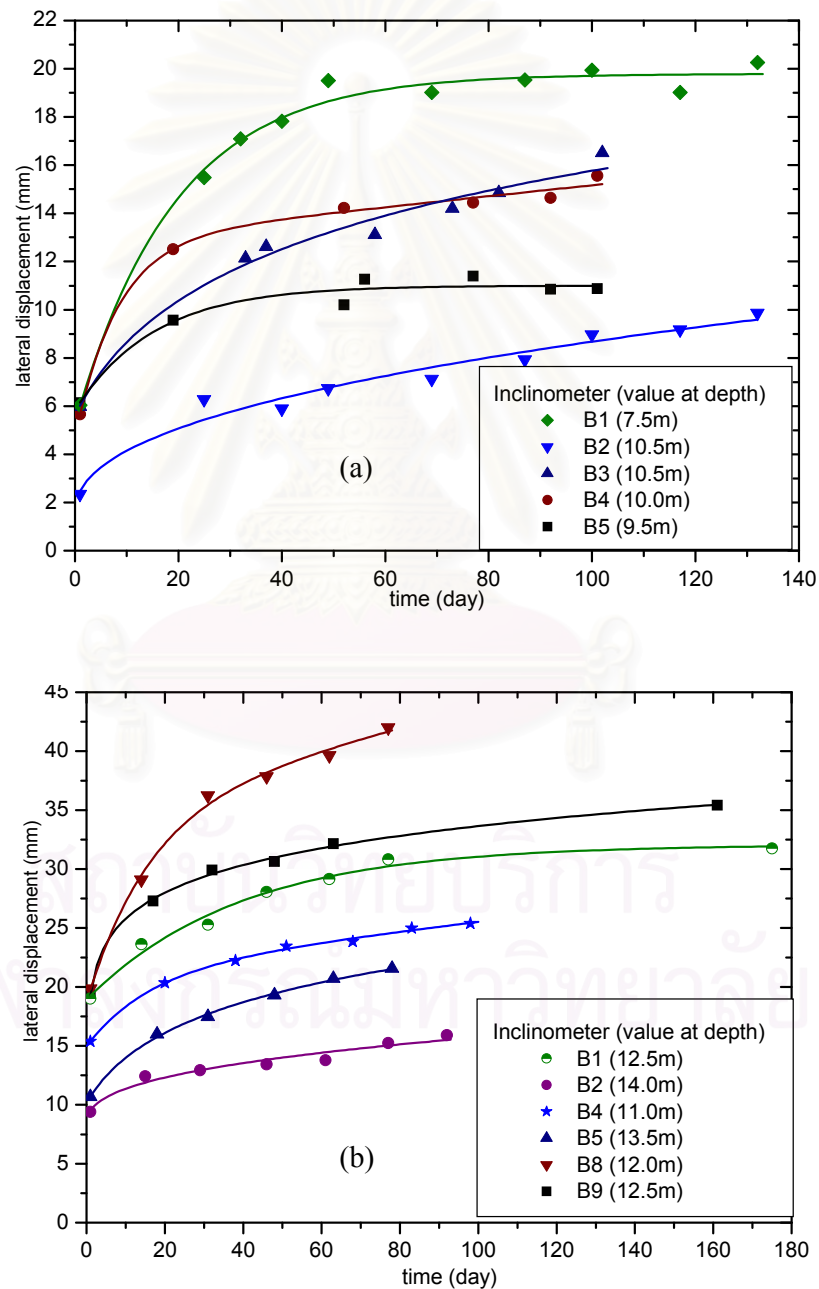
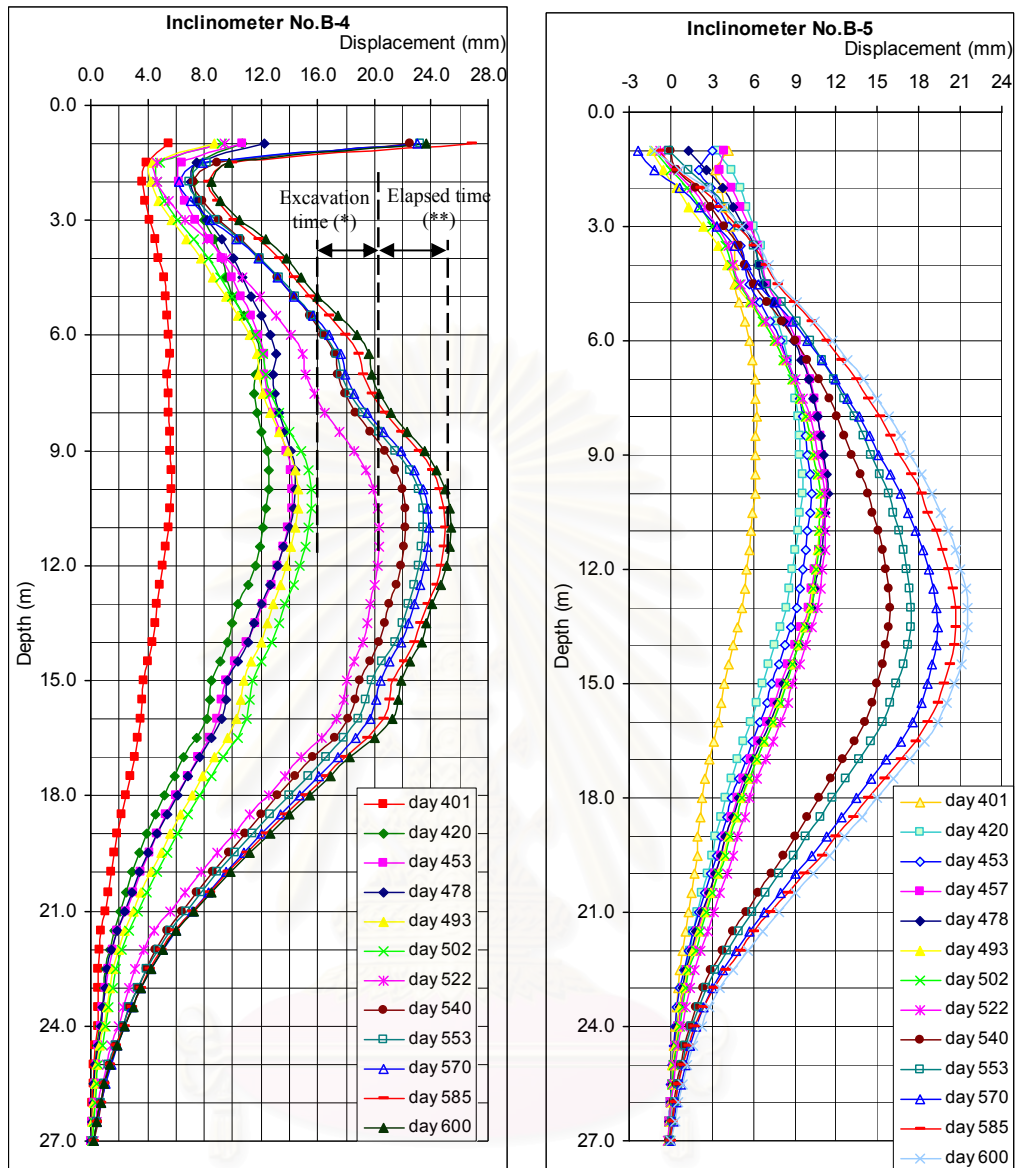


Figure 3.3. Lateral displacement of diaphragm wall on the elapsed time excavated to (a) 8.1 m and (b) 15.2 m.



(*) Excavation time: Duration happening excavation activities at the zone of installed inclinometer.

(**) Elapsed time: Duration without excavation activities at the zone of installed inclinometer.

Figure 3.4. Horizontal displacement of diaphragm wall during basement construction

Figure 3.4 showed the typical data of two inclinometers at position B4 and B5. The data collected from the other inclinometers shown in the Appendix II also displayed two groups of lines of DW lateral displacement measured during elapsed time. For example, the data collected in inclinometer B4 (Figure 3.4(a)) showed two groups of lines. The first group of lines was recorded from day 420 to day 502 during elapsed time of excavation at position of inclinometer B4 when the ground was excavated to 8.1m deep. The second group of lines showed lines of day 522 to day

600 of the DW lateral displacement data during elapsed time when the depth of excavation is 15.2m.

Table 3.2. The data of lateral displacement of DW on the excavation and elapsed time of nine inclinometers

Inclinometer	Stage	Excavated level (m)	Interval (day)	Δt (day)	Depth ^(*) (m)	Max. of $\Delta h^{(**)}$ (mm)	$\Delta h/\Delta t$ (mm/day)	Ratio ^(***)
B1	3_4	1.75 - 8.1	452 - 475	24	5.0	9.49	0.395	8.43
	4_5	8.1	476 - 584	109	11.5	5.11	0.047	
	5_6	8.1 - 15.2	585 - 600	16	15.0	5.71	0.357	
	6_7	15.2	601 - 677	77	15.5	10.48	0.136	
B2	3_4	1.75 - 8.1	452 - 467	16	10.0	3.54	0.221	6.18
	4_5	8.1	468 - 584	117	12.0	4.19	0.036	
	5_6	8.1 - 15.2	585 - 600	16	16.0	3.51	0.219	
	6_7	15.2	601 - 677	77	15.5	4.15	0.054	
B3	3_4	1.75 - 8.1	401 - 423	23	10.5	4.46	0.194	2.24
	4_5	8.1	424 - 521	97	13.0	8.40	0.087	
	5_6	8.1 - 15.2	522 - 535	14	14.5	2.50	0.179	
	6_7	15.2	536 - 571	46	15.0	5.67	0.123	
B4	3_4	1.75 - 8.1	401 - 420	20	9.5	6.86	0.343	8.27
	4_5	8.1	421 - 501	81	13.0	3.36	0.041	
	5_6	8.1 - 15.2	502 - 522	21	15.0	6.6	0.314	
	6_7	15.2	523 - 570	48	10.5	3.52	0.073	
B5	3_4	1.75 - 8.1	391 - 420	30	10.5	5.45	0.182	7.97
	4_5	8.1	421 - 522	100	13.0	2.28	0.023	
	5_6	8.1 - 15.2	523 - 536	14	15.5	5.88	0.420	
	6_7	15.2	537 - 583	47	14.5	5.14	0.109	
B6	3_4	1.75 - 8.1	432 - 452	21	11.5	6.68	0.318	5.88
	4_5	8.1	453 - 553	101	11.0	5.46	0.054	
	5_6	8.1 - 15.2	454 - 570	17	15.0	6.45	0.379	
	6_7	15.2	571 - 611	41	14.0	5.7	0.139	
B7	3_4	1.75 - 8.1	452 - 478	27	10.5	10.47	0.388	5.72
	4_5	8.1	479 - 599	121	13.0	8.21	0.068	
	5_6	8.1 - 15.2	600 - 614	15	13.0	2.54	0.169	
	6_7	15.2	615 - 646	32	13.0	4.59	0.143	
B8	3_4	1.75 - 8.1	478 - 493	16	8.5	8.85	0.553	7.23
	4_5	8.1	494 - 599	106	6.0	8.11	0.077	
	5_6	8.1 - 15.2	600 - 631	32	13.5	16.88	0.528	
	6_7	15.2	632 - 677	144	12.0	23.54	0.163	
B9	3_4	1.75 - 8.1	473 - 487	15	11.0	8.54	0.569	12.43
	4_5	8.1	488 - 613	126	10.5	5.77	0.046	
	5_6	8.1 - 15.2	614 - 631	18	15.5	9.79	0.544	
	6_7	15.2	632 - 677	46	14.5	5.33	0.116	

(*) The depth at which the lateral displacement (Δh) reaches the largest value.

(**) The maximum of lateral displacement of diaphragm wall.

(***) The ratio of the rate of DW lateral displacement ($\Delta h/\Delta t$) on the excavation time and on the elapsed time.

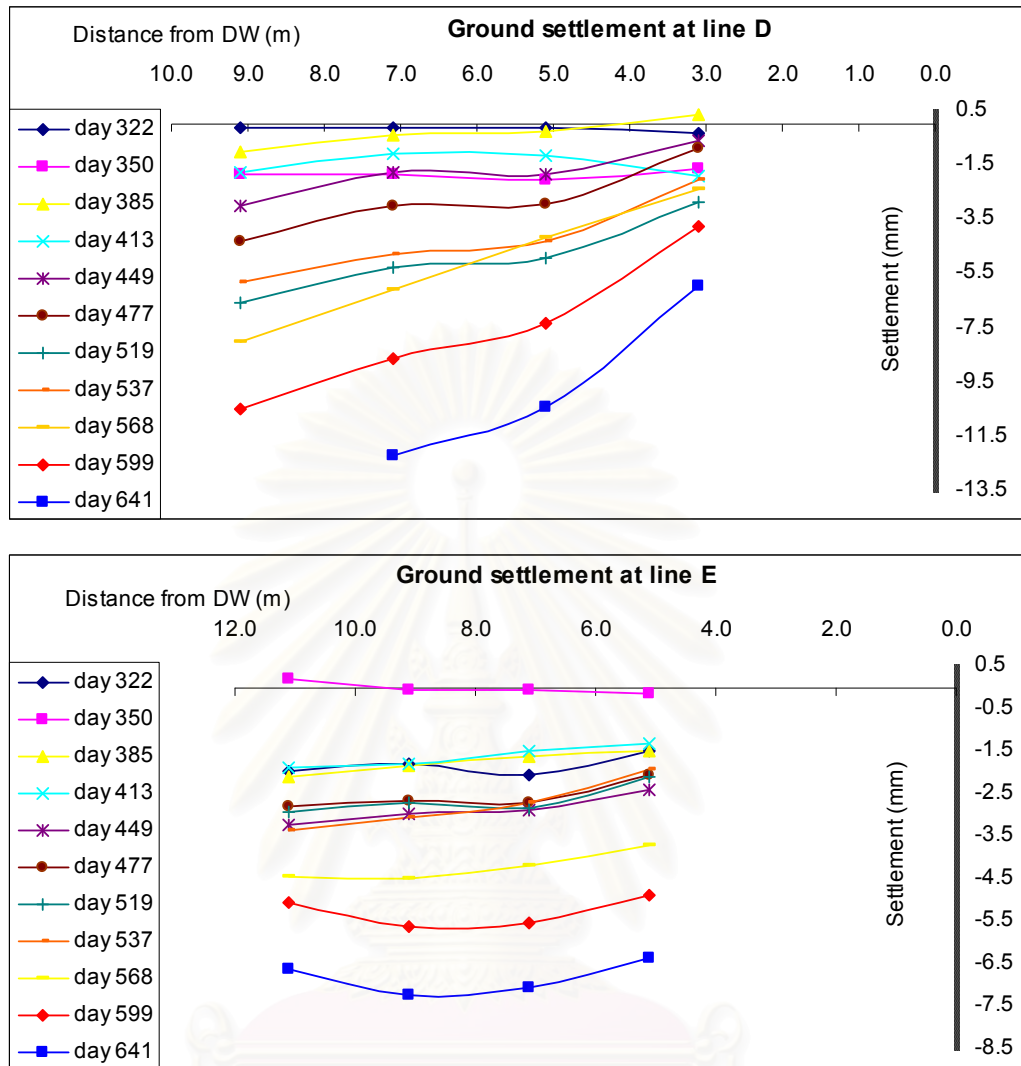


Figure 3.6. The settlement ground surface behind the DW at line C, D and E position

3.2. Field Measurements

Soft Bangkok clay is young marine sediment that covers a total area of about 10,000 km² of the Lower Central Plain of Thailand. It varies in thickness from about 15m at the coast of the Gulf of Thailand to 7 m at the border of Ayutthaya province, which is 100 km north of Bangkok. The water content decreases from about 150% to 90% in the same region and the vane shear strength at shallow depths increase from less than 10 kPa near the coast to about 30 kPa in Ayuthaya. The Atterberg limits decrease with distance from the sea and the plasticity index also decreases northwards from about 90% to less than 55% (E. W. Brand, 1983).

The stratum of the subsoil at BOT project consists of seven layers from the ground surface to borehole bottom and the main properties of each soil layer is shown in the Table 3.3. The undrained shear strength s_u of clay layers is determined by unconfined compression test. The ground water table exists around -2.0m deep after 24 hours boring.

Table 3.3. Summary of properties of subsoil at BOT project

Soil Type	Depth (m)	W (%)	Unit weight, γ_t (kN/m ³)	c_u (UC) (kN/m ²)	SPT-N (blows)
Crust (silt clay+sand fill)	0-2.5	32-35	17.1	-	7
Soft to Medium Clay	2.5-13.5	40-80	16.7	16.7	-
Stiff to Very Stiff Silty Clay	13.5-28.5	18-35	17.5	65.6	29
Medium to Very Dense Sand	28.5-38.5	10-22	19.0	-	45
Hard Silty to Sandy Clay	38.5-40.5	18-21	20.9	-	58
Dense to Very Dense Sand	40.5-70.3	10-26	20.0	-	75
Hard Silty Clay	70.3-80.4	11-20	20.9	-	79

Vane shear test

During the excavation process, the soil behind the DW had the unloading compression stress path. The mean effective stress decreased and the vertical strain appeared because of the decompression of horizontal stress. To examine the effect of the change of stress state of soil behind the DW to its shear strength, the field-vane-shear (FV) test was carried out to determine the undrained shear strength (s_u) at the beginning and at the end of excavation process.

The change of undrained shear strength s_u versus time due to the change of effective stress state was observed and determined at two positions. The first one, at which the soil was considered without effect of excavation activities, was as close as possible to the excavation site and not farther than the excavation depth. However, the second position, at which the soil affected by excavation activities, was farther away from the excavation site than the first one but not closer than four times excavation depth (based on the effect of excavation zone by Peck). The two positions of field-vane-shear test were pointed out in Figure 3.1. The vane blade of FV test was 55×110mm. and the test results was shown in Figure 3.7.

Undrained shear strength was determined by both field-vane-shear tests (FV) on site and unconfined compression (UC) laboratory test; the values were shown in Figure 3.7. There was a slight difference between the results of s_u by UC tests at three boreholes because of the inhomogeneity of the soil at the site. However, the values of shear strength from UC tests were clearly smaller than those values from FV tests. The main reason was that the horizontal pressure on UC tests was zero.

The properties of soil at site was investigated and showed more details in Figure 3.7, the natural water content mostly lay inside the range of plasticity index and lightly increasing with depth on the soft soil layer.

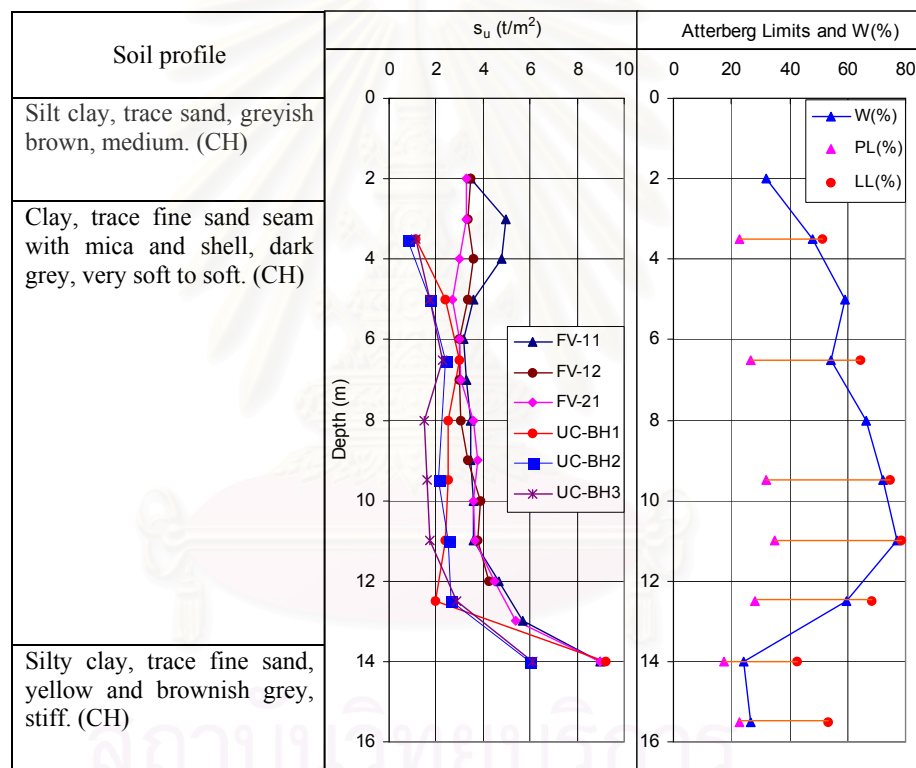


Figure 3.7. Properties of subsoil in BOT project

3.3. Summary

The BOT project applied the top-down construction method for building basement floors and upper structure. The large and deep excavation area of this project took long time and many steps to complete. During the period of basement construction, the lateral displacement of DW was measured biweekly by nine inclinometers installed around the periphery of excavation zone. Based on the data

collected continuously, it was found that the lateral displacement of DW was an even non-stop increase during the elapsed time without the excavation activities. Beside that, the ground settlement and the settlement, tilt and vibration of the adjacent buildings were observed carefully by using the settlement points, tilt plates and vibration sensors.

The summary of the borehole log (summarized in Table 3.3 and Figure 3.7), which consisted of the general test results, was not enough to study the behavior of soft soil on the DW during basement construction. The parameters for FE back analysis the project could not obtained fully from that test results. Therefore, more field experiment and laboratory tests were needed for further analysis.

The field-vane-shear test was carried out at the BOT project site for initial step to evaluate the effects of the change of stress state to the shear strength of the soil behind the DW. Moreover, the behavior of soil element behind the DW is studied in more details with the simulation of soil sample by the laboratorial triaxial tests in Chapter IV. These triaxial tests yield the parameters for back FE analysis.



Figure 3.8. BOT project under construction

CHAPTER IV

LABORATORY TESTS

The lateral displacement of diaphragm wall on elapsed time was non-stop increasing as discussed in chapter 3. Hence, to understand the behavior of soft soil behind the diaphragm wall and find out the parameters of soft soil for back finite element analysis, the laboratory triaxial tests were conducted. Three kinds of triaxial tests were carried out in this research: K_0 consolidated undrained compression (CK_0UC) and K_0 consolidated drained/undrained unloading compression with periodic decrement of horizontal pressure (CK_0DUC and CK_0UUC). In these tests, the soil specimens were simulated under the same stress condition as the soil element behind diaphragm wall on the excavation process. The shear strength and the slope of Critical State Line were determined with applied load continuously in CK_0UC test and periodically in CK_0DUC and CK_0UUC tests. Besides, the reduction of Young's modulus with strain level was observed in those tests. Moreover, the characteristic of creep deformation of soil sample was also determined in the latter two tests.

4.1 Material and Testing procedure

The undisturbed soil samples, with the height of 150 mm and diameter of 75 mm, were taken from two 25.0 m deep boreholes of BOT project near the bank of Chao Praya River in Bangkok. The properties of those samples were presented in Table 3.3 and Figure 3.6. Soil specimens of 100 mm height and 50 mm in diameter, were trimmed from those undisturbed samples and then saturated under 15 kPa of cell pressure and 5 kPa of back pressure at the beginning and gradually increase to final stage at 200 kPa of back pressure and 210 kPa of cell pressure. Those values of pressures dissolve sufficient air on the specimens. The excess of pore water pressure was measured by means of B-value to check the saturation degree of the specimen. Then, all the samples were consolidated automatically to obtain K_0 condition with the vertical effective stress equal to estimated overburden effective stress at the depth of each sample. The vertical effective stress was increased in 0.5 kPa/min while the cell pressure was automatically controlled to keep the radial strain of specimen equal to zero. Time duration to stop the K_0 process was after the completion of primary consolidation based on the 3t method of Standards of Japanese Geotechnical Society

for Laboratory Shear Test (English version). Eight filter paper strips were put around the side of the soil specimen to enhance the radial drainage during consolidation. Subsequently, the samples were continued carrying out the following tests:

(1) CK₀UC (K₀ Consolidated Undrained Compression test): the specimens were sheared under undrained condition as conventional triaxial compression test at 0.1 %/min of axial strain rate. In addition, the relationship between deviator stress and axial strain was automatically recorded nearly 100 steps until the axial strain reached 0.01%. The undrained shear strength (s_u) and undrained Young's modulus at 0.01% of axial strain ($E_{u(0.01\%)}$) of the samples were determined and shown in Figure. 4.1. Moreover, the undrained Young's modulus was also measured at 0.01, 0.02, 0.04, 0.07, 0.1, 0.2, 0.4, 0.7, 1, 2, 4, 7 and 10% of axial strain level.

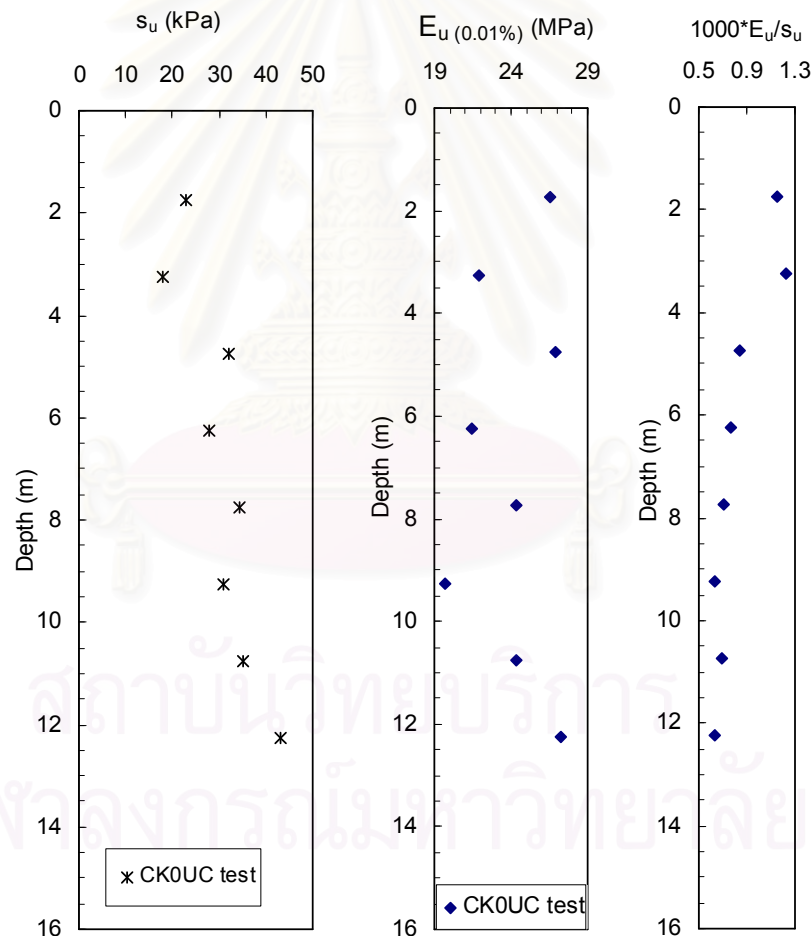


Figure 4.1. Undrained shear strength and Young's modulus of CK₀UC tests

(2) CK₀DUC (Anisotropically Consolidated Drained Unloading Compression test): after anisotropic consolidation to be K₀ condition, the specimens were swelled

(unloading compression) by periodically decreasing horizontal stress step-by-step while the axial effective stress was maintained constantly. The amplitude of the decrement step of horizontal stress was controlled by the decrement step of stress ratio (ΔK) from initial stress ratio ($K_0 = \sigma'_{h0}/\sigma'_{v0}$) to that value at failure ($K_f = \sigma'_{hf}/\sigma'_{vf}$) values as shown in Figure 4.2.

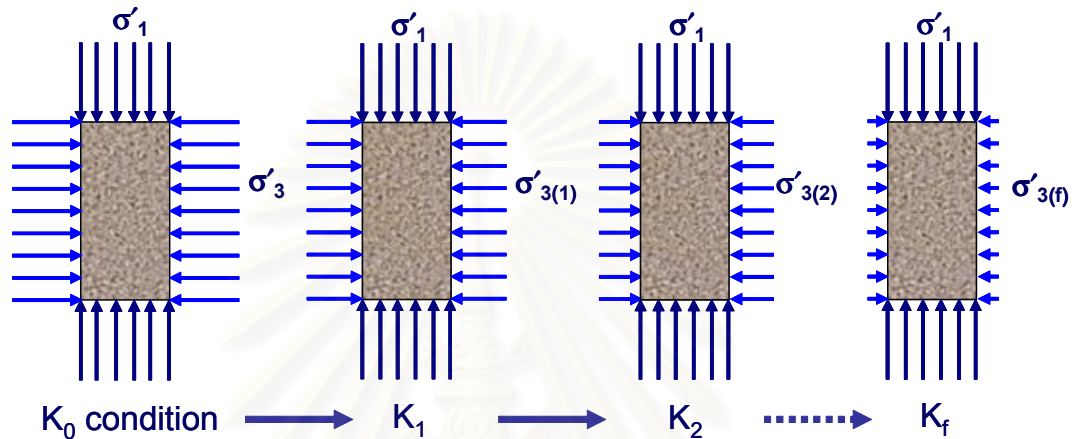


Figure 4.2. Procedure of CK₀DUC and CK₀UUC tests

Each reduced value of horizontal stress was kept for 24 hours or 48 hours in some steps. During that time, the cell pressure and axial load were controlled automatically to maintain the vertical and horizontal effective stresses to be unchanged. The valve of back pressure was opened for drained condition, and the back pressure was supplied continuously the value 200 kPa as the final value of K_0 consolidation step. The volume strain of the sample was determined from the volume of water in the burette by a differential pressure transducer.

(3) CK₀UUC (Anisotropically Consolidated Undrained Unloading Compression test): this test is the same as the test number (2); however, the drainage valve was closed for undrained condition.

It was only considered the behaviors of soil effect to displacement of DW during excavation; therefore, for tests (2) and (3), the maintenance time for each loading step (each K_i value in Figure 4.2) was only 24 hours or 48 hours for some steps. To eliminate the influence of temperature as a variable, the temperature during the experiments was kept as constant to be 24 ± 1 °C. Seventeen soil samples were carried out with three kinds of tests and these test results were summarized in Table 4.1.

Table 4.1. Summary of triaxial test of marine Bangkok clay

Test No.	Depth (m)	Test Condition	ω (%)	e_0	$q_{max}/2\sigma'_{v0}$	ϕ'_r ($^\circ$)	ϕ'_p ($^\circ$)	M	B-value (%)
1	2.0	CK ₀ UC	43.6	1.30	0.818	46.3	52.8	2.17	97.8
2	3.5		40.6	1.14	0.612	39.5	42.4	1.74	100.1
3	5.0		62.2	1.68	0.642	43.3	52.3	2.15	99.2
4	8.0		81.6	2.26	0.413	35.3	36.7	1.49	99.7
5	9.5		72.9	2.01	0.412	36.9	37.9	1.54	97.1
6	11.0		64.4	1.76	0.440	34.9	38.1	1.55	91.4
7	12.5		59.9	1.67	0.456	34.0	38.1	1.53	98.1
8	5.0	CK ₀ DUC ($\Delta K=-0.05$)	55.4	1.56	0.453	-	62.8	2.53	99.1
9	6.5		55.7	1.54	0.419	-	33.4	1.35	99.8
10	8.0		64.2	1.79	0.374	-	39.7	1.61	97.1
11	9.5		64.8	1.78	0.368	-	38.7	1.55	92.1
12	11.0		71.8	2.00	0.360	-	36.9	1.50	100.1
13	10.5	CK ₀ DUC ($\Delta K=-0.10$)	74.3	2.06	0.344	-	33.4	1.35	100.3
14	12.0		64.4	1.82	0.381	-	38.7	1.58	98.3
15	6.0	CK ₀ UUC ($\Delta K=-0.05$)	71.3	2.04	0.443	-	38.7	1.58	96.7
16	9.5		77.7	2.12	0.351	-	40.6	1.66	97.3
17	11.0		76.1	2.12	0.505	-	33.4	1.35	97.0

4.2 Test results and Discussion

4.2.1 Shear Strength and Young's Modulus

The ratio of shear strength and overburden effective stress (s_u/σ'_{v0}) versus depth was shown in Figure 4.3. The overburden effective stress was estimated from the total unit weight of the tested soil samples and 2m depth of ground water table. It was found that the ratio s_u/σ'_{v0} of CK₀UC tests was approximately equal to the value of field-vane-shear (FVS) test. Upper 6.0m depth, this ratio was larger than 0.5 because of the effect of weathered consolidation to this clay layer. The ratio s_u/σ'_{v0} was around 0.45 for the depth from 6.0m to 12.0m. This finding was similar to the result of the test at 11.0m depth in Sutthisan area by Tanaka, H. et. al. (2001).

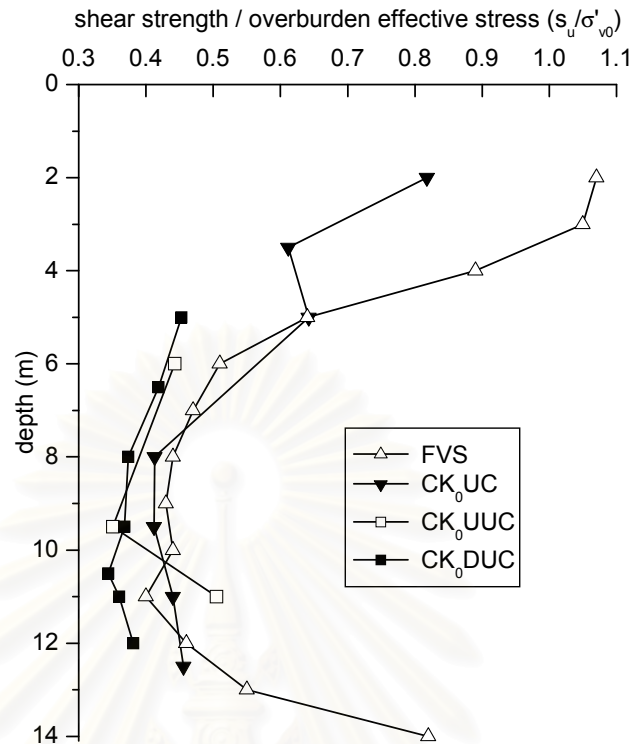


Figure 4.3. Ratio of shear strength and overburden effective stress of field-vane-shear test compared with CK₀UC, CK₀UUC and CK₀DUC tests

Many researchers have studied the values of the ratio E_u/s_u on Bangkok soft clay. Their main purpose is to reduce the input parameters of elasto-perfectly plastic soil model for applying finite element analysis on the retaining wall structure. Some values of this ratio were predicted by back analysis of the lateral displacement of the wall. They have found that the ratio varies of 200~500 (Bowels, 1988) and 280~350 for soft clay, and 1200~1600 for stiff clay (Hock, 1997), 500 and 2000 for Bangkok soft clay and stiff clay (W. Teparaksa et al., 1999). Actually, the ratio E_u/s_u was a function of many variables, e.g., the strain level (Mair, 1993), plasticity index and OCR (Duncan and Buchigani, 1976). As shown in Figure 4.4, the undrained shear strength absolutely depended on the strain value at which the ratio of shear strength and overburden effective stress $[(\sigma_1 - \sigma_3)/2]/\sigma'_{v0}$ reached its peak.

The system of triaxial test is automated to record the data, therefore, the relationship between deviator stress ($q = \sigma_1 - \sigma_3$) and axial strain (ϵ_a) of the CK₀UC tests was recorded nearly 100 times when the axial was lesser than 0.01%. From that obtained data, the initial undrained Young's modulus or undrained Young's modulus

of lesser than 0.01% axial strain $E_{u(0.01\%)}$ was exactly calculated. The ratio $E_{u(0.01\%)/s_u}$ gets high from 1100 to 1300 for weathered clay layer upper 4 m depth and 600 to 800 for normal soft soil layer as shown in Figure 4.1. In addition, the undrained shear strength of the CK_0UC tests was approximately close to the values of field-vane-shear tests $s_{u(FVS)}$ in Figure 4.3; therefore, the E_u values at a small strain ($\epsilon_a \leq 0.01\%$) could be estimated from $s_{u(FVS)}$ instead of undrained shear strength of unconfined compression test (UC).

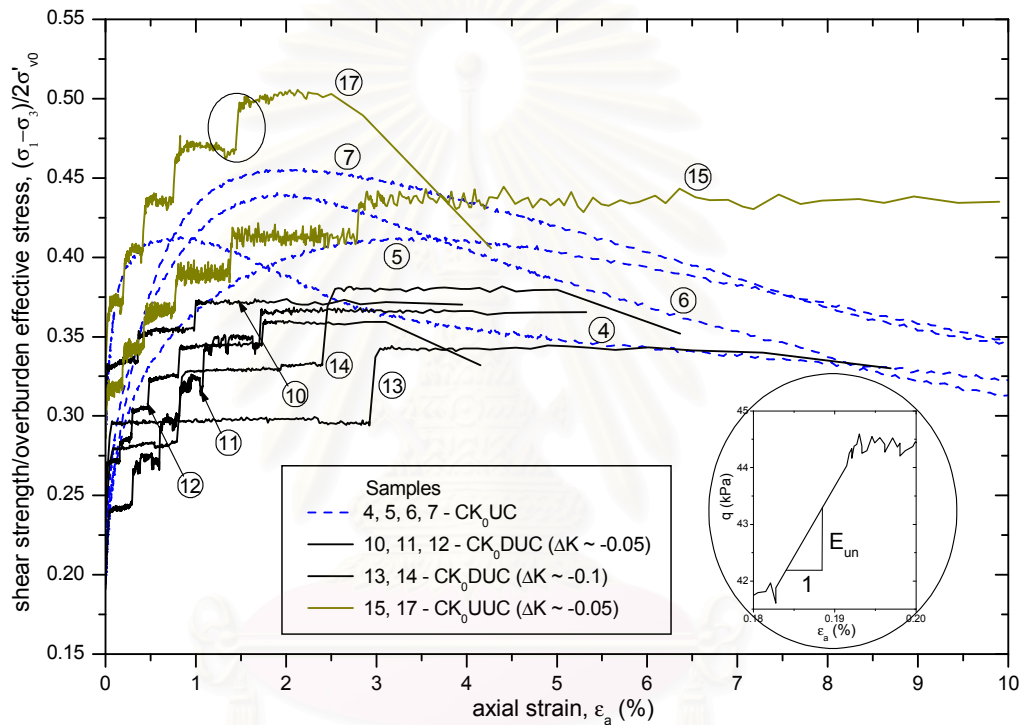


Figure 4.4. Relationship between deviator stress (q) and axial strain (ϵ_a) of CK_0UC , CK_0DUC and CK_0UUC tests.

In Figure 4.4, the ratio $[(\sigma_1 - \sigma_3)/2]/\sigma'_{v0}$ of the CK_0DUC tests of the samples below 6 m deep were lesser than 0.40 (except the samples of CK_0UUC test) and smaller than that value of CK_0UC tests. It could be explained based on early concept of Hvorslev that the shear strength was composed of an effective friction increasing linearly with the effective stress and an effective cohesion. The cohesion component was mobilized with a small strain and would cause a gradual transfer of shear stresses to the more stable frictional contact points (Schmertmann and Osterberg, 1961). In case of CK_0DUC test, the load was applied discontinuously by keeping the same state

of effective stresses for 24 hours. Therefore, the cohesion component was not mobilized completely while the frictional strength was quickly mobilized by drained condition. As a result, the shear strength of clay of CK₀DUC tests was only equal to the residual strength of CK₀UC tests.

Many studies have shown that Young's modulus depends on the strain level. In this study, two K₀ consolidated undrained compression tests on Bangkok soft soil was carried out with samples at -6.5m and -9.5m depth. The test result was shown in Figure 4.5. On these tests, the undrained Young's modulus was determined with the axial strain levels at 0.01, 0.02, 0.04, 0.07, 0.1, 0.2, 0.4, 0.7, 1, 2, 4, 7, 10 and 15%. The undrained Young's modulus was measured with 0.01% of unloading-reloading of axial strain. For example, measuring the undrained Young's modulus at 1% of axial strain level, when the axial strain of tested sample reached 1% the sample was unloaded until the axial strain obtained 0.99%; then, it was reloaded. When the axial strain level was still small in values such as 0.01, 0.02, 0.04%, the unloading and reloading lines were almost coincided. However, when the axial strain was larger than 0.04%, the unloading and reloading curves were separated. In this case, the undrained Young's modulus was calculated based on the slope of reloading line.

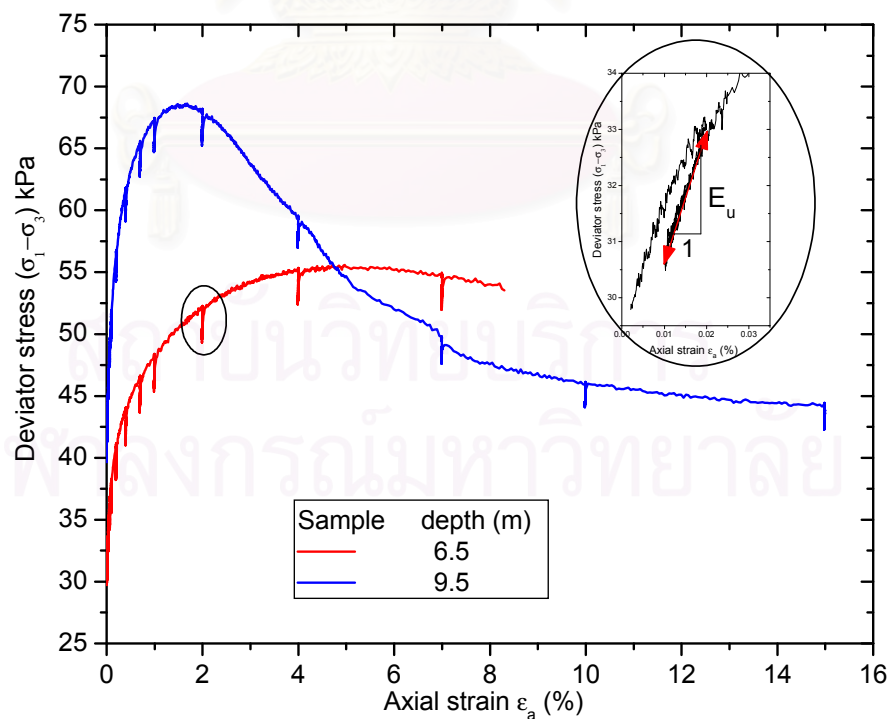


Figure 4.5. Relationship of deviator stress (q) and axial strain (ϵ_a) of CK₀UC tests.

There are two moduli concerned on this research: un-reloading and secant moduli, which were determined from the relationship line between deviator stress and axial strain. As shown in Figure 4.6, the un-reloading modulus E_u was determined by unloading and reloading the deviator stress with 0.01% of axial strain. The secant modulus $E_{u(sec)}$ was the slope of the line from the point at beginning the application of the deviator stress to the point of each strain level. These Young's moduli would be applied for FE analysis to predict the lateral displacement of DW by using the linear elastic-perfectly plastic soil model.

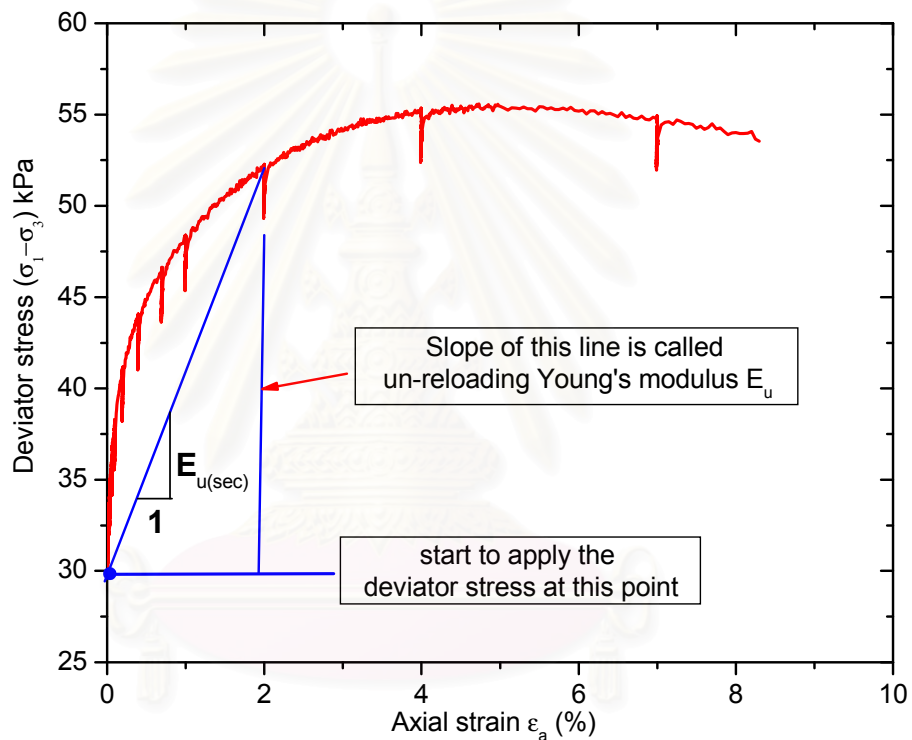


Figure 4.6. Definition of un-reloading Young's modulus E_u and secant Young's modulus $E_{u(sec)}$

Figure 4.7 shows the values of Young's modulus versus axial strain level of two above tests. The initial undrained Young's modulus or the Young's modulus at 0.01% of axial strain was largest value. The Young's modulus reduces rapidly from the initial value at 0.01% until around 1% of axial strain. However, this value was almost constant when the axial strain was larger than 1%. Conclusively, the Young's modulus was considered to reduce versus small axial strain and to be constant with large axial strain.

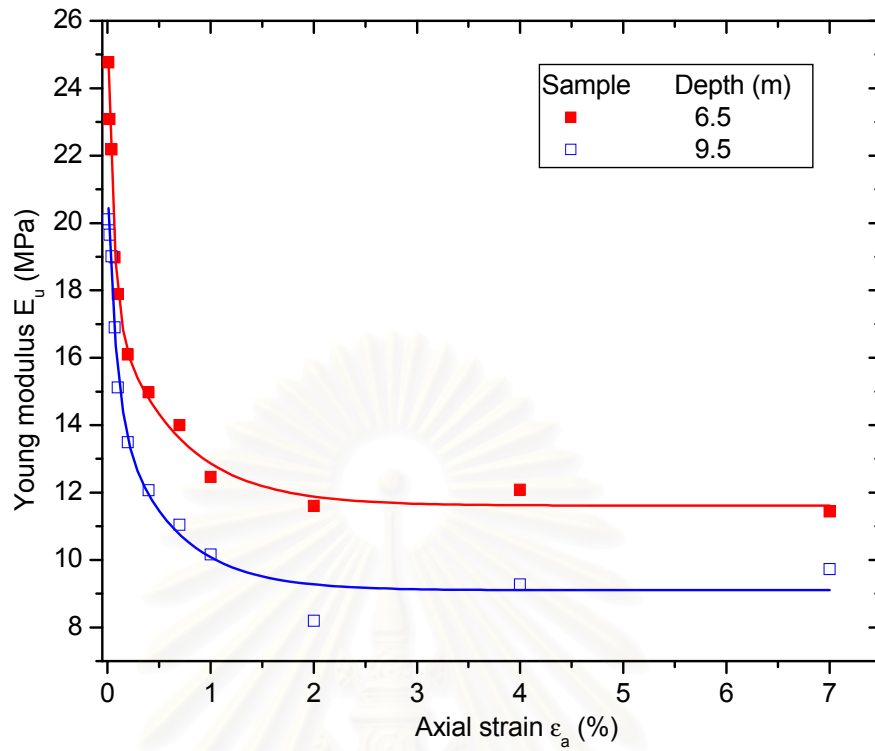


Figure 4.7. Reduction of undrained Young's modulus (E_u) with axial strain level (ϵ_a) of CK_0UC tests

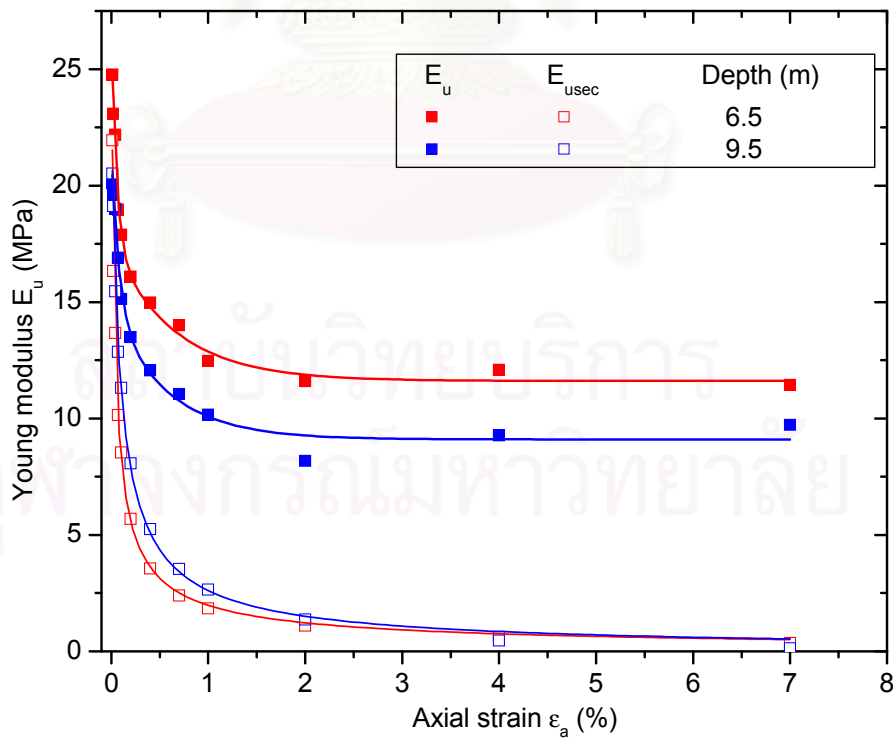


Figure 4.8. Comparison secant Young's modulus $E_{u(sec)}$ with un-reloading Young's modulus E_u of CK_0UC tests

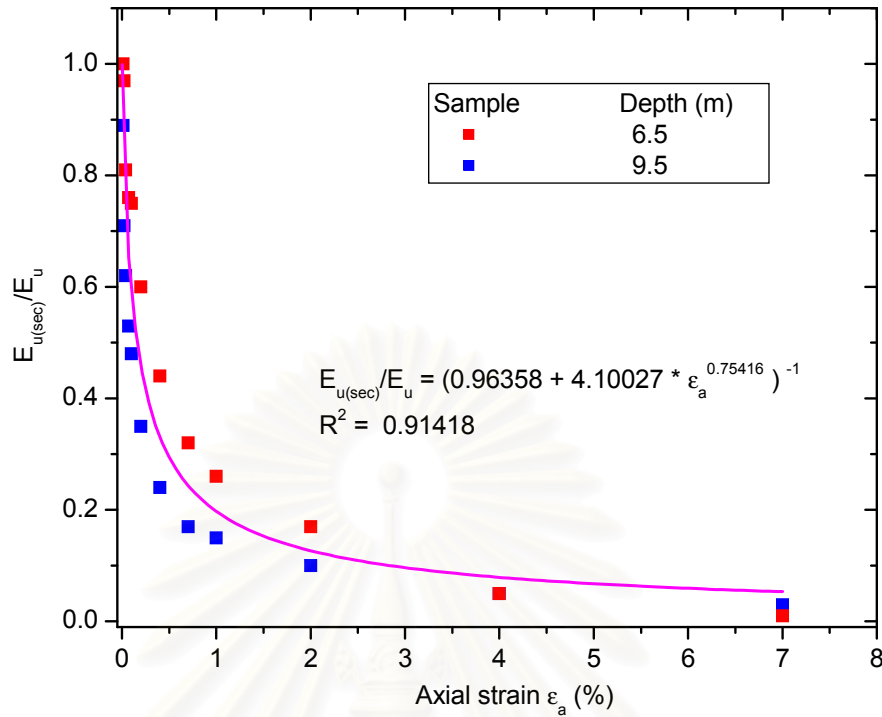


Figure 4.9. Ratio of secant Young's modulus $E_{u(sec)}$ and un-reloading Young's modulus E_u of CK₀UC tests

Figure 4.8 showed the data of secant Young's modulus of two soil samples at the depth of 6.5 m and 9.5 m. The $E_{u(sec)}$ reduced rapidly to the lower bound value when axial strain was smaller than 0.5%. The lower bound value was equal to round 10% of initial value. The initial value of secant and un-reloading Young's moduli were almost equal. When the soil sample got the critical state, the secant Young's modulus had very small value about 10% of its initial value while the un-reloading modulus still had a large value about 46% of its initial value.

Figure 4.9 showed the relationship between ratio of $E_{u(sec)}/E_u$ and axial strain level. The more detail of this ratio value was on Table 4.2. The initial value of secant Young's modulus and un-reloading Young's modulus was equal. When the axial strain increased, the secant Young's modulus reduced faster than the un-reloading Young's modulus. The ratio of $E_{u(sec)}/E_u$ was equal to round 0.1 when the sample reached the critical state. The different between the value of $E_{u(sec)}$ and E_u because of the difference of axial strain. The secant Young's modulus was calculated by axial strain, which included the components of elastic and plastic axial strains. Meanwhile, the un-reloading Young's modulus was determined by only the elastic axial strain.

Table 4.2. Data of secant Young's modulus $E_{u(sec)}$ and un-reloading Young's modulus E_u of CK_0UC tests

Depth of soil sample (m)	Axial strain ϵ_a (%)	$E_{u(sec)}$ (MPa)	E_u (MPa)	$E_{u(sec)}/E_u$
6.5	0.01	24.77	21.94	0.89
	0.02	23.08	16.34	0.71
	0.04	22.19	13.67	0.62
	0.07	18.98	10.14	0.53
	0.1	17.89	8.55	0.48
	0.2	16.10	5.69	0.35
	0.4	14.98	3.56	0.24
	0.7	14.00	2.40	0.17
	1.0	12.47	1.85	0.15
	2.0	11.61	1.12	0.10
	4.0	12.08	0.63	0.05
	7.0	11.44	0.36	0.03
9.5	0.01	20.11	20.52	1.02
	0.02	19.65	19.13	0.97
	0.04	19.01	15.47	0.81
	0.07	16.90	12.86	0.76
	0.1	15.12	11.32	0.75
	0.2	13.49	8.08	0.60
	0.4	12.08	5.26	0.44
	0.7	11.05	3.54	0.32
	1.0	10.16	2.66	0.26
	2.0	8.19	1.37	0.17
	4.0	9.27	0.47	0.05
	7.0	9.73	0.13	0.01

On the condition that the effect of the depth soil sample was neglected on CK_0UC test, the undrained Young's modulus at each axial strain level was compared with the initial undrained Young's modulus at 0.01% of axial strain. The ratio of Young modulus at each axial strain level and initial Young's modulus (E_u/E_{u0}) versus axial strain (ϵ_a) was plotted in Figure 4.10. The ratio (E_u/E_{u0}) was rapidly reduced from 1.0 to around 0.5 and, after that; it was kept constant. As a result, the minimum of undrained Young's modulus to which could be reduced was equal to around 50% value of initial undrained Young's modulus determined in CK_0UC tests.

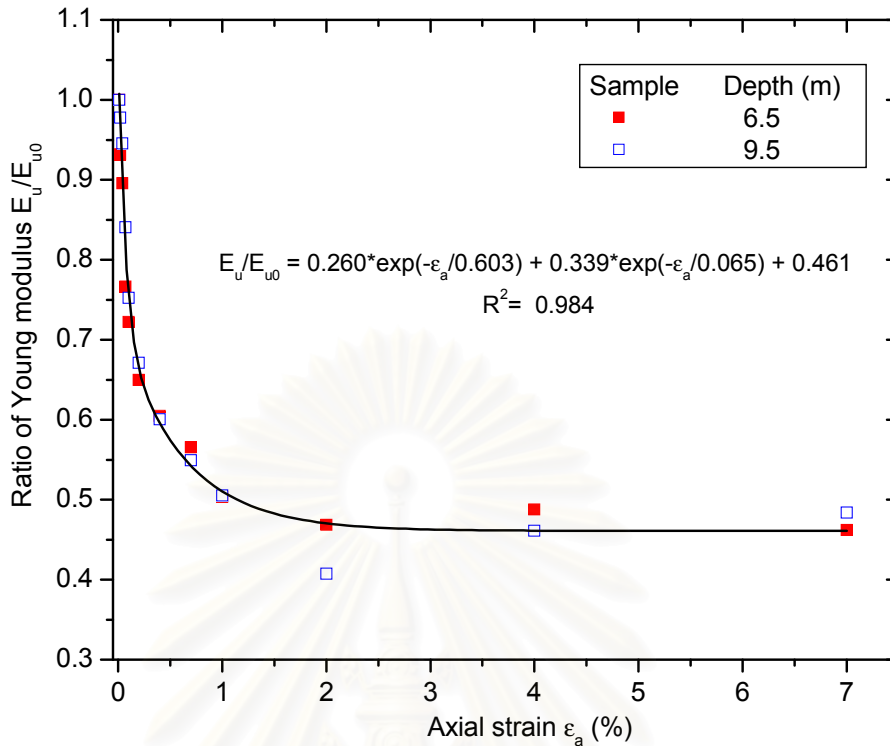


Figure 4.10. Reduction of undrained Young's modulus ratio (E_u/E_{u0}) with axial strain level (ϵ_a) of CK₀UC tests.

On CK₀DUC tests, the strain of each step of K-value could be divided into two parts, initial and creep strains. The initial strain happened immediately after applying the reduction of cell pressure value. At this moment, the pore water excess was negative and the axial strain increased rapidly with an increase of deviator stress. As shown in the circle of Figure 4.4 and in Figure 4.11, the slope of the straight line which was the relationship between increment of deviator stress Δq and initial axial strain $\Delta \epsilon_a$ was called unloading Young's modulus E_{un} .

The results of three CK₀DUC tests shown in Figure 4.12 were the relationship between deviator stress $q = (\sigma_1 - \sigma_3)$ and axial strain ϵ_a of three soil samples at 5.0, 6.5 and 11.0m deep. In this figure, the axial strain was accumulated at the beginning of horizontal unloading process. The unloading Young's modulus E_{un} was defined as the slope of the relationship line between Δq and $\Delta \epsilon_a$ immediately after unloading the horizontal stress. These tests were a failure before the axial strain reached 2%. This axial strain value was approximately equal to the axial strain at peak of q - ϵ_a curve of CK₀UC tests.

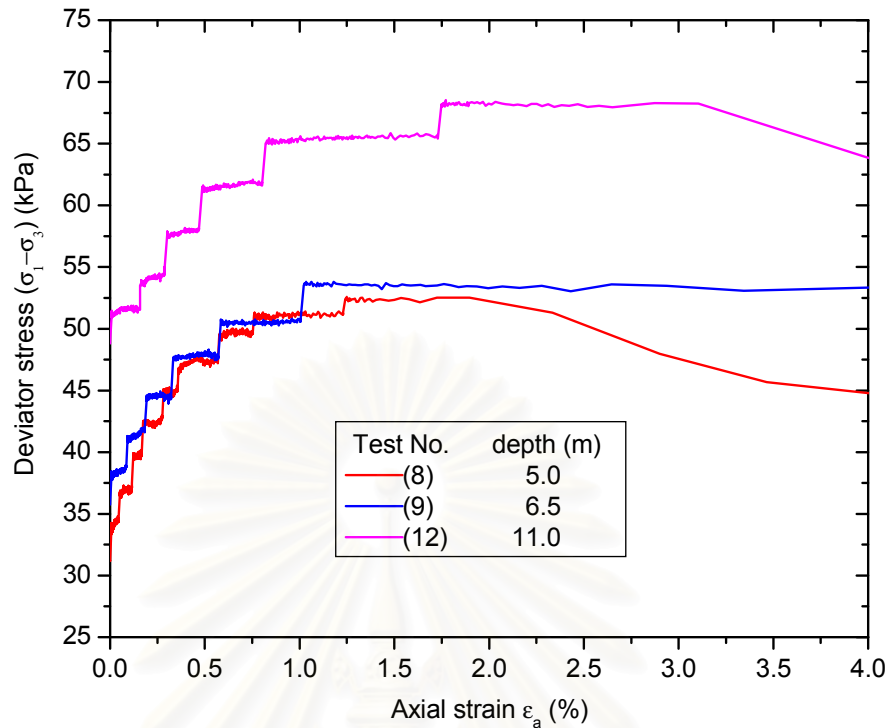


Figure 4.12. Relationship between deviator stress (q) and axial strain (ϵ_a) of CK_0DUC tests.

The unloading Young's modulus (E_{un}) of each step of horizontal stress decrement was calculated and shown in Figure 4.13. All the E_{un} values were calculated with increment of axial strain ($\Delta\epsilon_a$) from 0.007% to less than 0.02%. Because of the specificity of the CK_0DUC tests, the E_{un} values were only measured until the samples was a failure or the axial strain was less than 2%. Similar to the undrained Young's modulus of CK_0UC tests, this E_{un} Young's modulus was also decreased rapidly when axial strains were still small in values.

To examine the rate of decrement of unloading Young's modulus with axial strain, the ratio of unloading Young's modulus at each level of axial strain and that initial value was calculated and shown in Figure 4.14. The E_{un} value was decreased about 25% of the initial E_{un} value when

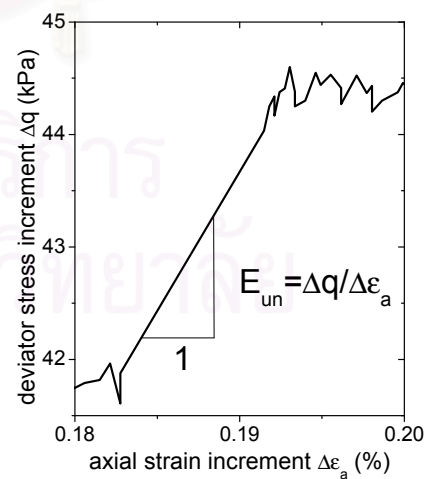


Figure 4.11. Unloading Young's modulus E_{un}

axial strain was around 0.2%. In addition, the minimum of E_{un} value was equal to 50% of initial of that value when the axial strain was lesser than around 2%.

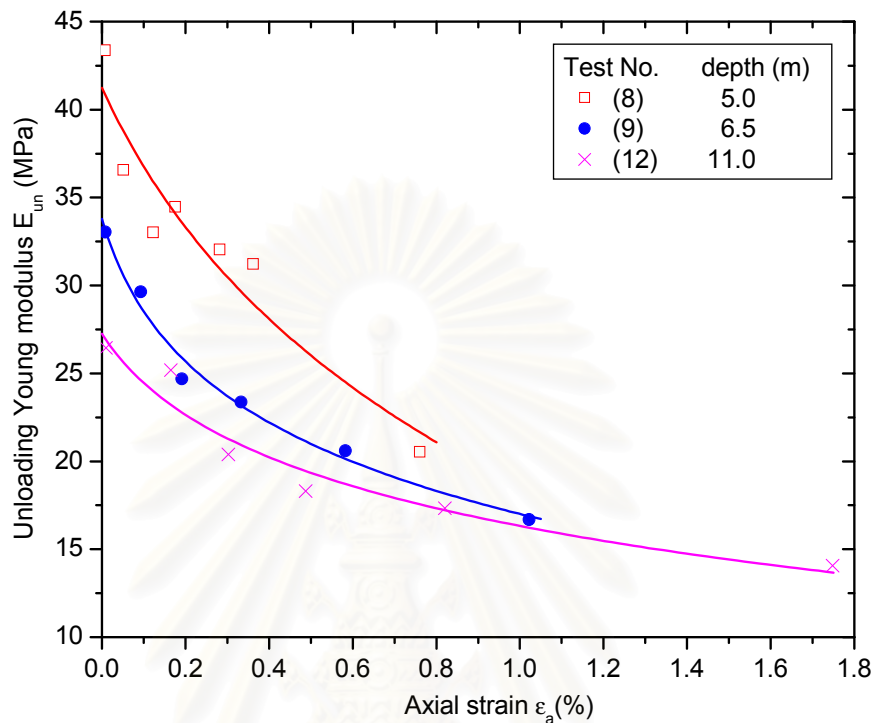


Figure 4.13. Reduction of unloading Young's modulus (E_{un}) with axial strain level (ϵ_a) of CK₀DUC tests.

Figure 4.15 showed the relationship between deviator stress and axial strain of two CK₀UUC tests at the depth of 9.5m and 11.0 m. Similar to two kinds of previous CK₀UC and CK₀DUC tests, the unloading Young's modulus was also determined from this data. On these undrained tests, the Young's modulus had unsmooth reduction with the axial strain as shown in Figure 4.16. The Young's modulus decreased slightly with initial strain. The E_{un} value at each strain level was compared with the initial value and plotted in Figure 4.16. The minimum of E_{un} was calculated before the sample obtained a failure. As a result, this minimum value of E_{un} was equal to about 60% of the initial of E_{un} as shown in Figure 4.17.

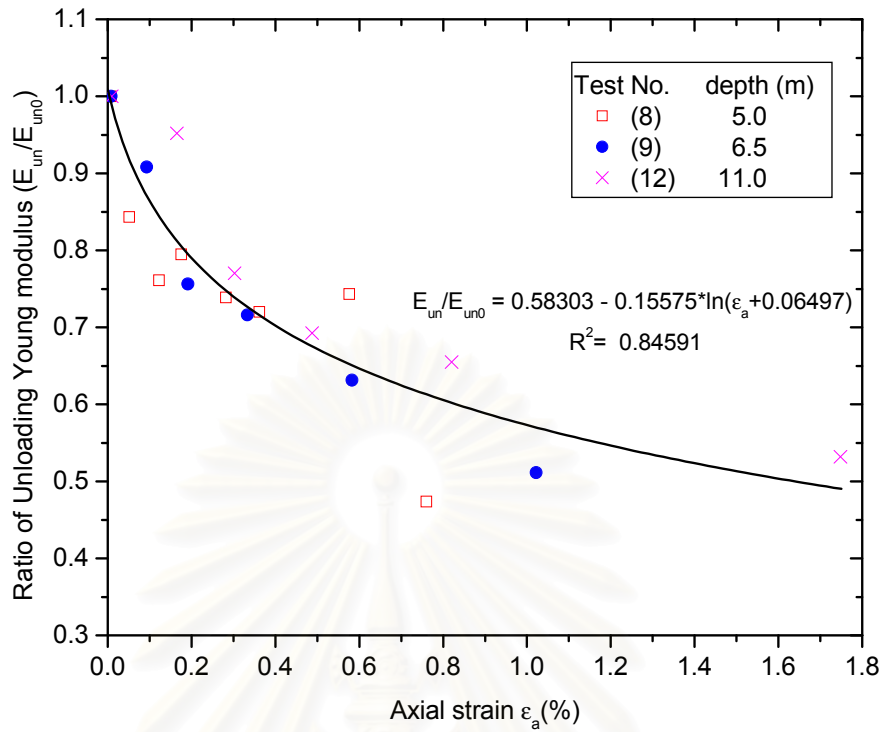


Figure 4.14. Reduction of unloading Young's modulus ratio (E_{un}/E_{un0}) with axial strain level (ϵ_a) of CK₀DUC tests.

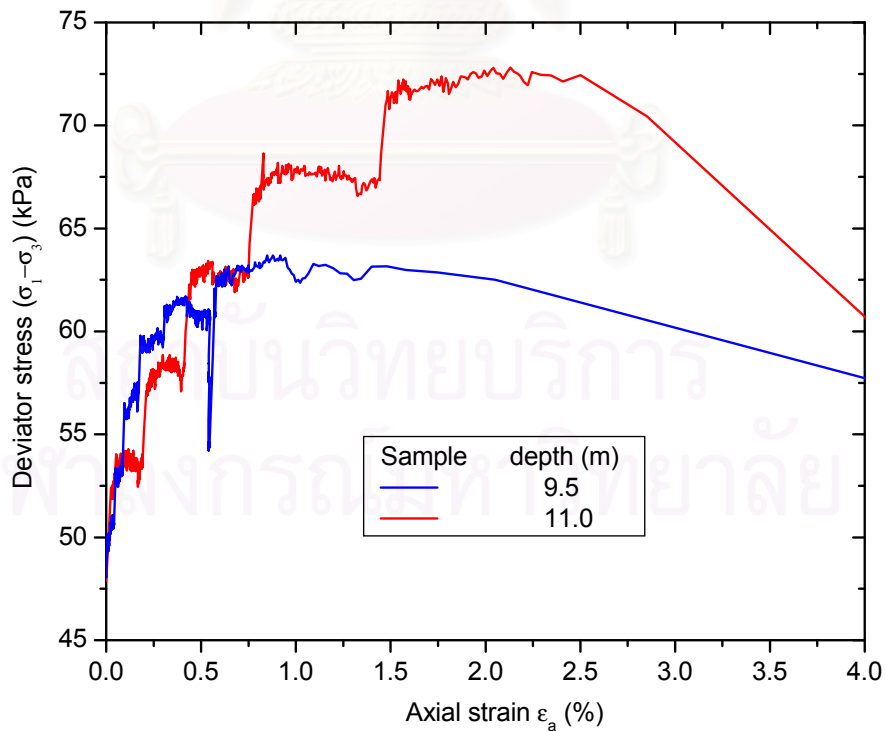


Figure 4.15. Relationship between deviator stress (q) and axial strain (ϵ_a) of CK₀UUC tests.

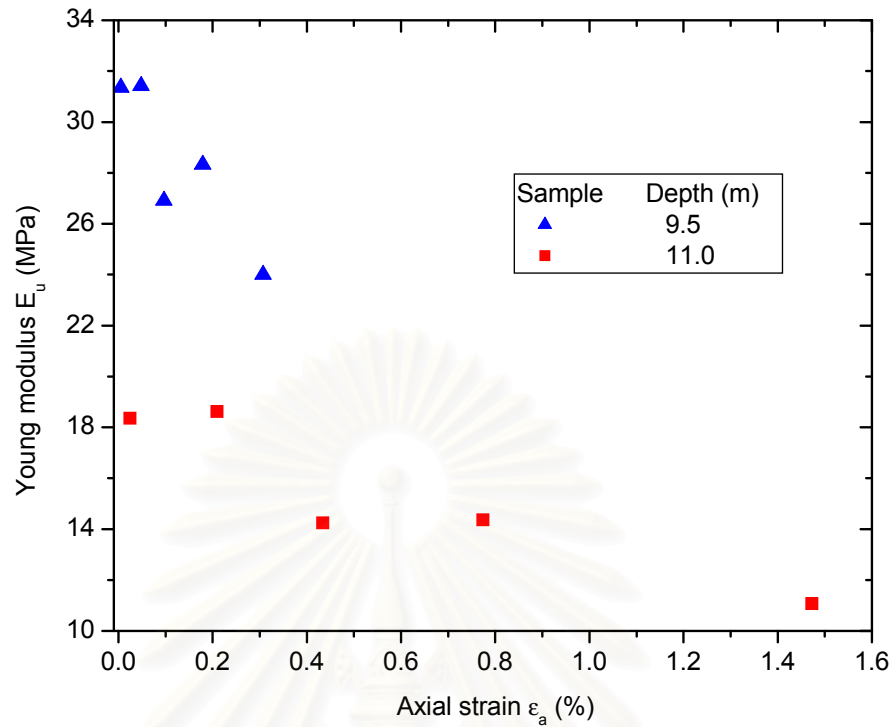


Figure 4.16. Reduction of unloading Young's modulus (E_{un}) with axial strain level (ϵ_a) of CK₀UUC tests.

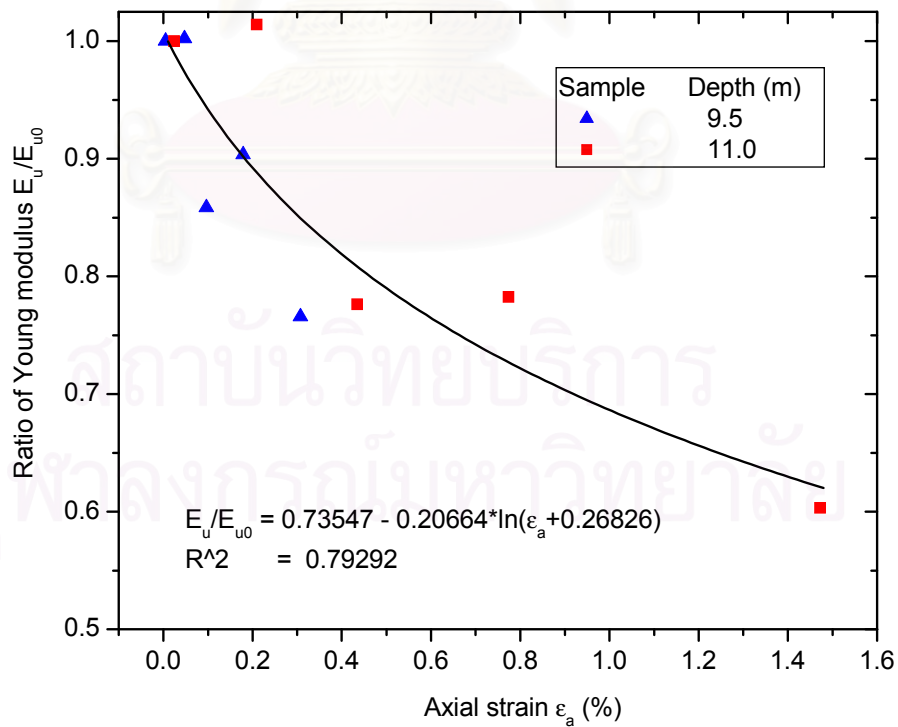


Figure 4.17. Reduction of unloading Young's modulus ratio (E_{un}/E_{un0}) with axial strain level (ϵ_a) of CK₀UUC tests.

The relationship between unloading Young's modulus E_{un} on CK_0DUC test and the stress state was established based on the slope of stress path in $(p':q)$ space ($\eta = q/p'$). In the lower right corner as shown in Figure 4.19, the slope of the relationship between deviator stress and mean effective stress was called η ($\eta = q/p'$) at each decrement step of horizontal stress or K value; and M ($M = q_f/p'_f$) at the critical state. As shown in Figure 4.18, the E_{un} values, which were calculated with the increment of axial strain $\Delta\epsilon_a$ less than 0.02% (Figure 4.11), decreased with the ratio η/M . In other words, the Young's modulus of soil behind the diaphragm wall during excavation process decreased.

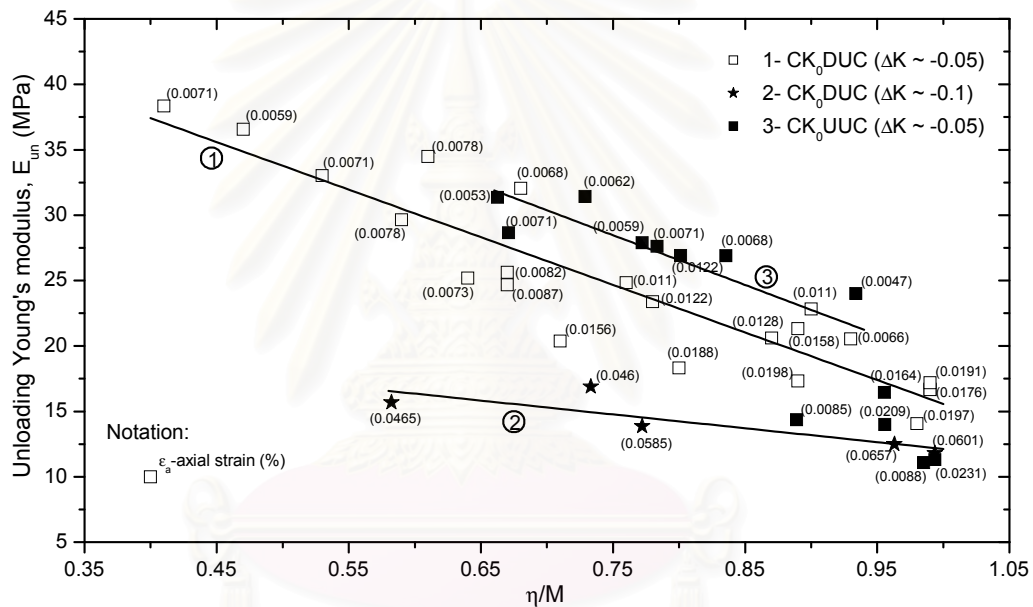


Figure 4.18. Relationship between Unloading Young's modulus E_{un} and ratio η/M

In the unloading compression triaxial tests, the rate of lateral stress reduction was -1.0 kPa/min and the axial effective stress was controlled automatically to maintain as constant. The E_{un} values of the first unloading step of CK_0DUC tests were larger than the E_u of CK_0UC tests because of the difference of axial strains.

In Figure 4.18, the unloading Young's moduli of CK_0DUC tests were performed and shown signified by square ($\Delta K = -0.05$) and solid stars ($\Delta K = -0.1$) symbols. On comparing line 1 and line 2, when the decrement step of horizontal pressure was large, the Young's moduli E_{un} values were found to be small. The initial axial strain after sudden decrease of the horizontal pressure was large as noted on the

observed points shown in the figure. Moreover, when the samples were still strong enough ($\eta/M < 0.85$) the E_{un} of CK_0UUC tests was larger than its values of CK_0DUC tests (line 2 and 3).

4.2.2 Slope of Critical State Line

The decrement step of horizontal stress of all the unloading compression triaxial tests was controlled by the stress ratio ($K = \sigma'_h/\sigma'_v$) or the slope of stress path in ($p':q$) space ($\eta = q/p'$). Based on the data shown in Table 4.1, the slope of Critical State Line (M) had two different values. The soil samples at upper 6.0 m deep were overconsolidated clay because of weathering effects and the M values were around 2.0. Meanwhile, the soil at lower 6.0 m deep was slightly overconsolidated clay and the M values were equal to 1.50 ($\phi' = 37^\circ$) as shown in Figure 4.19. Compared with the M value 1.05 ($\phi' = 26^\circ$) obtained from series of isotropically consolidated undrained triaxial test (Balasubramaniam, A. S. and Chaudry A. R., 1978) the M value around 2.0 of CK_0UC tests of this study was larger due to the difference of test procedures. However, when comparing with CK_0UC tests carried out by Tanaka H., et. al. (2001) on Bangkok clay, the slope of the critical line was the same ($M=1.5$ or $\phi' = 37^\circ$).

In the series of CK_0DUC and CK_0UUC tests, when the decrement steps of horizontal pressure were small ($\Delta K = -0.05$, test No. 8 to 12) the M values were approximately equal to the M values of CK_0UC tests (Figure 4.19). However, on 13 and 14 tests, the decrement step of horizontal pressure ($\Delta K = -0.1$) was twice as larger as that on 8 to 12 tests, the M values were smaller than those values of 8 to 12 tests.

สถาบันวิทยบริการ
จุฬาลงกรณ์มหาวิทยาลัย

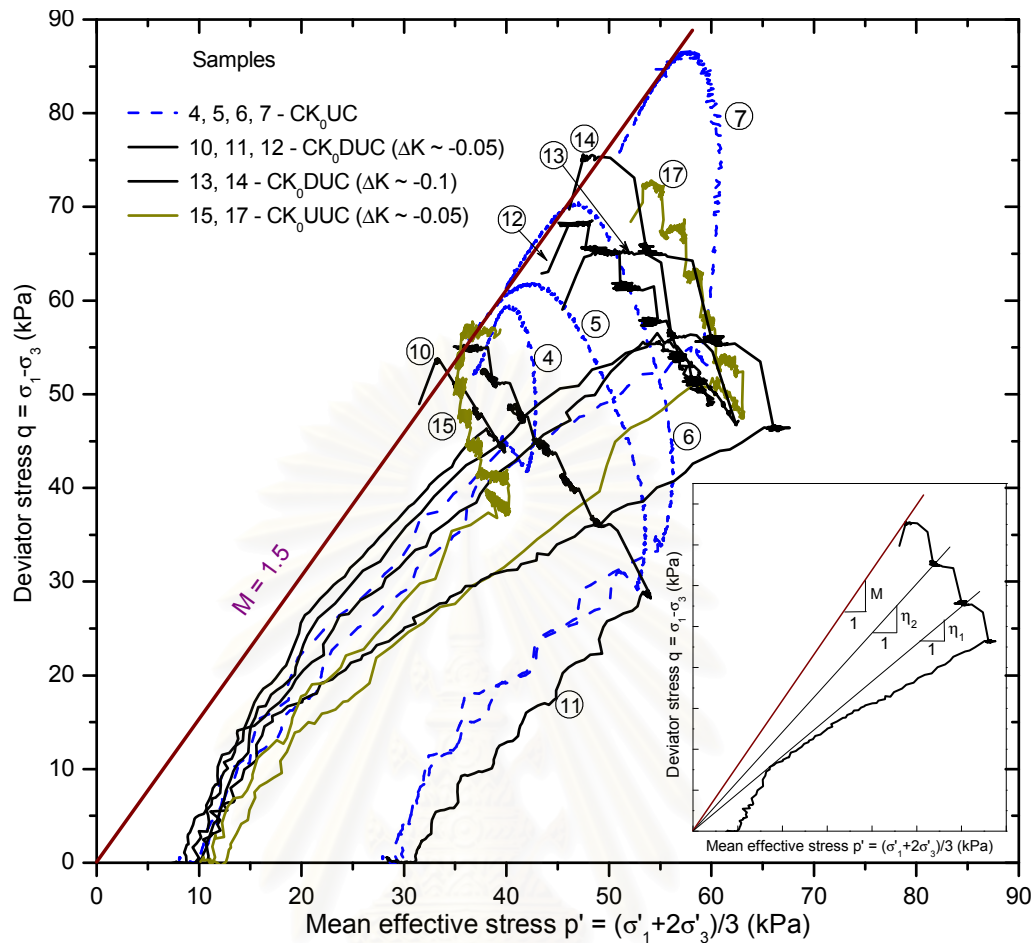


Figure 4.19. Slope of the Critical State Line

4.2.3 Creep deformation

Figures 4.20 and 4.21 show the axial and radial strain versus time and strain rate versus time relationships obtained from CK₀DUC and CK₀UUC tests. The strain rate curves were the derivative of strain rate functions, which were approximately determined from the exponential function of time. These curves immediately reached the large value after unloading horizontal pressure then they reduced virtually linear versus time as shown in Figures 4.20b and 4.21b. The axial and lateral strain rates of both CK₀DUC and CK₀UUC tests increased with deviator stress and decreased with time. These strain rate values were not constant during 24 hours of maintaining applied loading as shown in Figures 4.20 and 4.21.

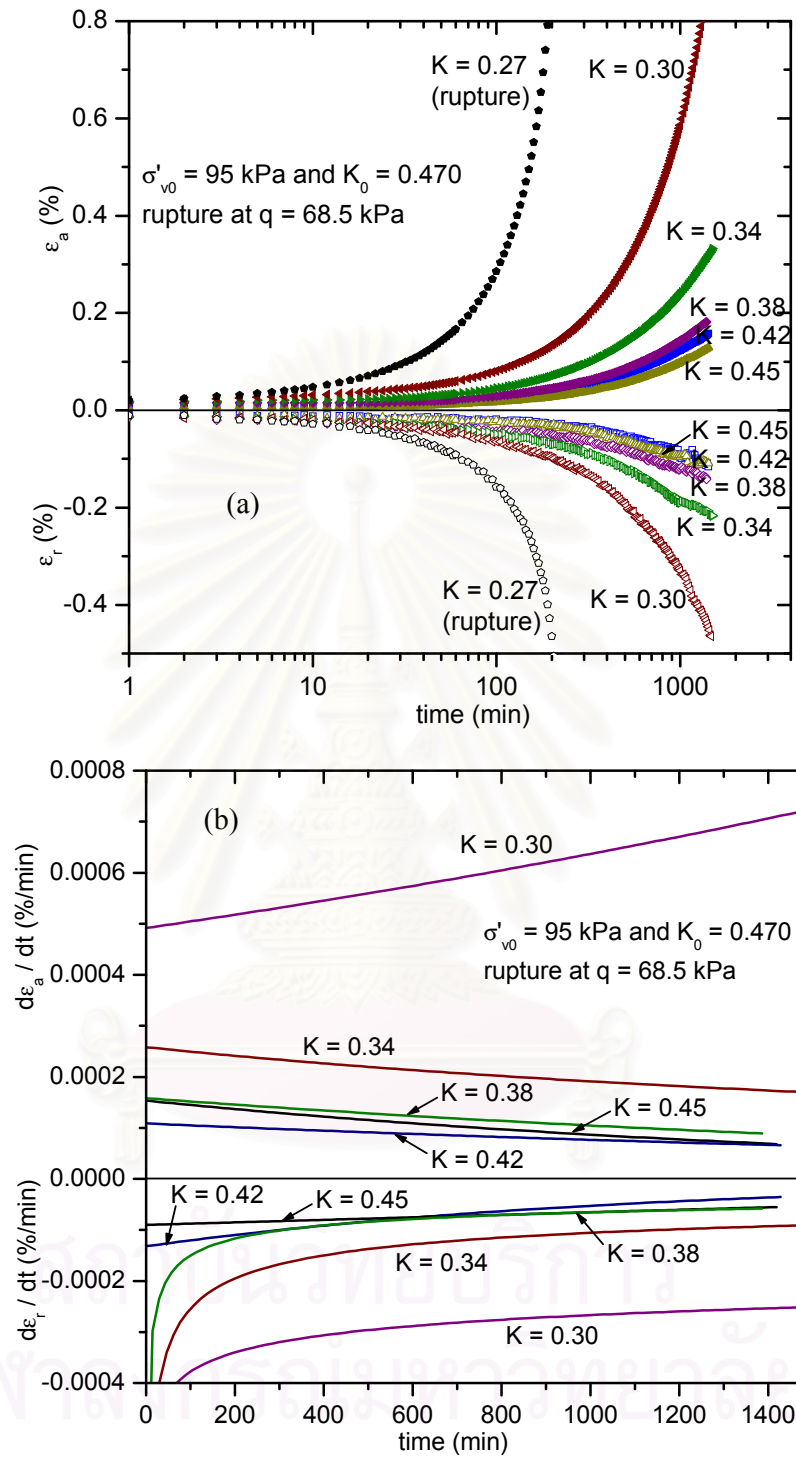


Figure 4.20. Strain rate of soil sample at 11.0 m depth under CK_0 DUC test.

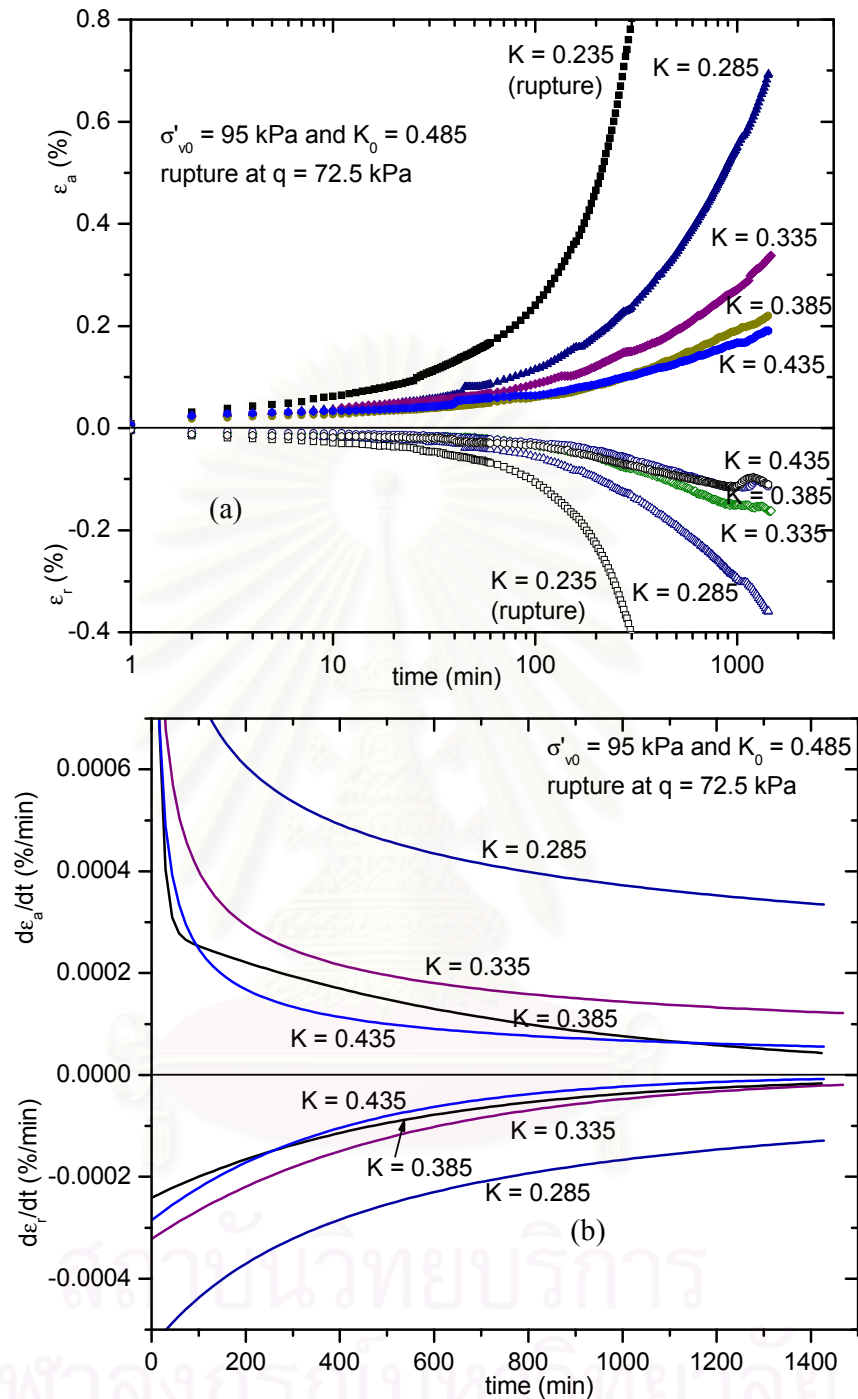


Figure 4.21. Strain rate of soil sample at 11.0 m depth under CK₀UUC test.

Figure 4.22 shows the relationship of axial, volume and radial strains and time of soil samples of both CK₀UUC and CK₀DUC tests. With the soil samples at the same depth and decrement horizontal pressure step ($\Delta K = -0.05$), the strain of CK₀UUC tests (No. 15 and 17) was larger than that of CK₀DUC tests (No. 9 and 12).

However, when the decrement horizontal pressure step increased twice ($\Delta K=-0.1$), in No. 13 and 14 tests, the volume strain suddenly dropped down to negative peak, but it then increased and achieved a positive value. Therefore, the volume strain of the soil sample depended not only on the drainage condition but also on the amplitude of the lateral decrement load.

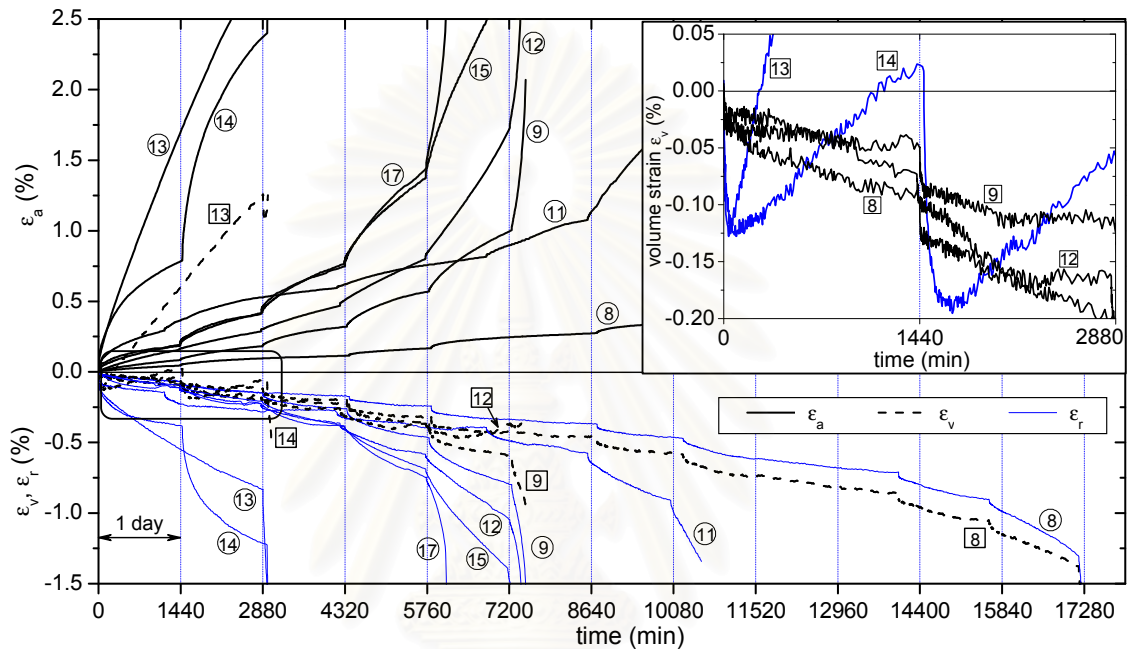


Figure 4.22. Relationship between strains and time of CK_0UUC and CK_0DUC tests.

The strain rates of axial and lateral strain of five CK_0DUC tests (No. 8 to 12 tests), shown in Figure 23, could be approximated by the linear logarithmic equations

$$\dot{\epsilon}_a = a_a + b_a \log t - \text{axial strain rate} \quad [4.1]$$

$$\text{and } \dot{\epsilon}_r = a_r + b_r \log t - \text{lateral strain rate.} \quad [4.2]$$

The coefficients a_a , b_a and a_r , b_r shown in Figures 4.24 and 4.25 related a linear line to the ratio $\eta/(M-\eta)$. In Figure 4.23, the strain rate of each η value of stress state was shown by one curve line. At the same value of time, the closer M value of η value got, the larger absolute value of strain rate became. Hence, the strain rates increased when the stress state approached the value of stresses at failure.

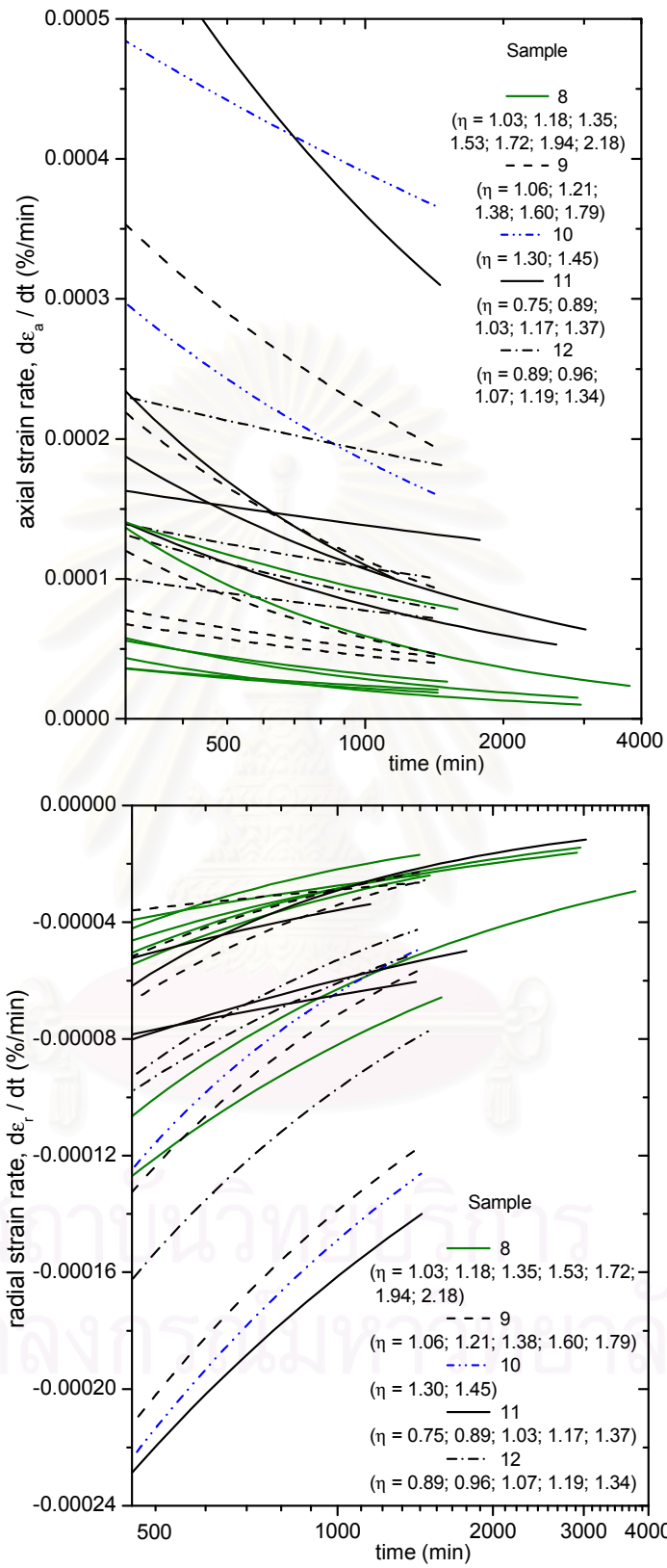


Figure 4.23. Strain rate of soil samples under CK_0 DUC test.

The coefficient of deformation with time (C_α) of clay soil was usually determined from vertical strain of oedometer test or the volumetric strain of the triaxial consolidation test. According to Tavenas F. et. al. (1978), the expression of the relationship of C_α and strain rate was shown in Equation [4.3].

$$\dot{\varepsilon} = C_\alpha / t(1 + e_0) \text{ or } C_\alpha = \dot{\varepsilon} \times t \times (1 + e_0) \quad [4.3]$$

while $\dot{\varepsilon}$ was axial strain of oedometer test or volume strain of triaxial test.

In the unloading compression triaxial test, both axial and radial strain rates were considered. From Equation [4.3], the coefficient of deformation of both axial ($C_{\alpha a}$) and radial ($C_{\alpha r}$) directions could be calculated by substituting $\dot{\varepsilon}$ by $\dot{\varepsilon}_a$ and $\dot{\varepsilon}_r$.

$$C_{\alpha a} = \dot{\varepsilon}_a \times t \times (1 + e_0) \text{ - coefficient of axial deformation} \quad [4.4]$$

$$\text{and } C_{\alpha r} = \dot{\varepsilon}_r \times t \times (1 + e_0) \text{ - coefficient of radial deformation} \quad [4.5]$$

Therefore, the coefficient of deformation as well as strain rate depended on the deviator stress level, time and the direction of deformation.

4.3 Summary

The undrained shear strength s_u , which was determined by CK_0UC test, was larger than that value of unconfined compression test and was approximately equal to the value of field-vane-shear test. Moreover, the shear strength determined by CK_0DUC test was only equal to the residual strength of CK_0UC test. The ratio of shear strength and overburden effective stress with depth was calculated. This ratio got large value on the weathered consolidation soil layer from the ground surface to around 4m deep. Decreasingly, it was equal to around 0.4 on the soft soil layer deeper than 4 m.

The ratio of initial undrained Young's modulus $E_{u(0.01\%)}$ and undrained shear strength s_u of CK_0UC test got high values from 1100 to 1300 for weathered consolidation clay layer upper 4 m depth and 600 to 800 for normal soft soil layer.

The decrement of Young's modulus with strain level was observed on CK_0UC , CK_0DUC and CK_0UUC tests. On the first two tests, the Young's modulus decreased rapidly on the small range of initial strain. Moreover, the minimum of Young's modulus was equal to around 50% of initial Young's modulus. Nevertheless, on the third test, the Young's modulus decreased roughly with strain and the minimum of E_{un} value was equal to about 60% of that initial value. That value was larger than the value of the first two tests.

Besides, the relationship between Young's modulus and stress state of CK₀DUC and CK₀UUC tests was also discovered. The stress state was defined as the ratio η/M . As a result, the Young's modulus reduced as the ratio η/M increased or the stress state approached to failure.

The slope of Critical State Line M was determined from three kinds of test CK₀UC, CK₀DUC and CK₀UUC. The M value was almost the same on those tests and equal to around 1.5.

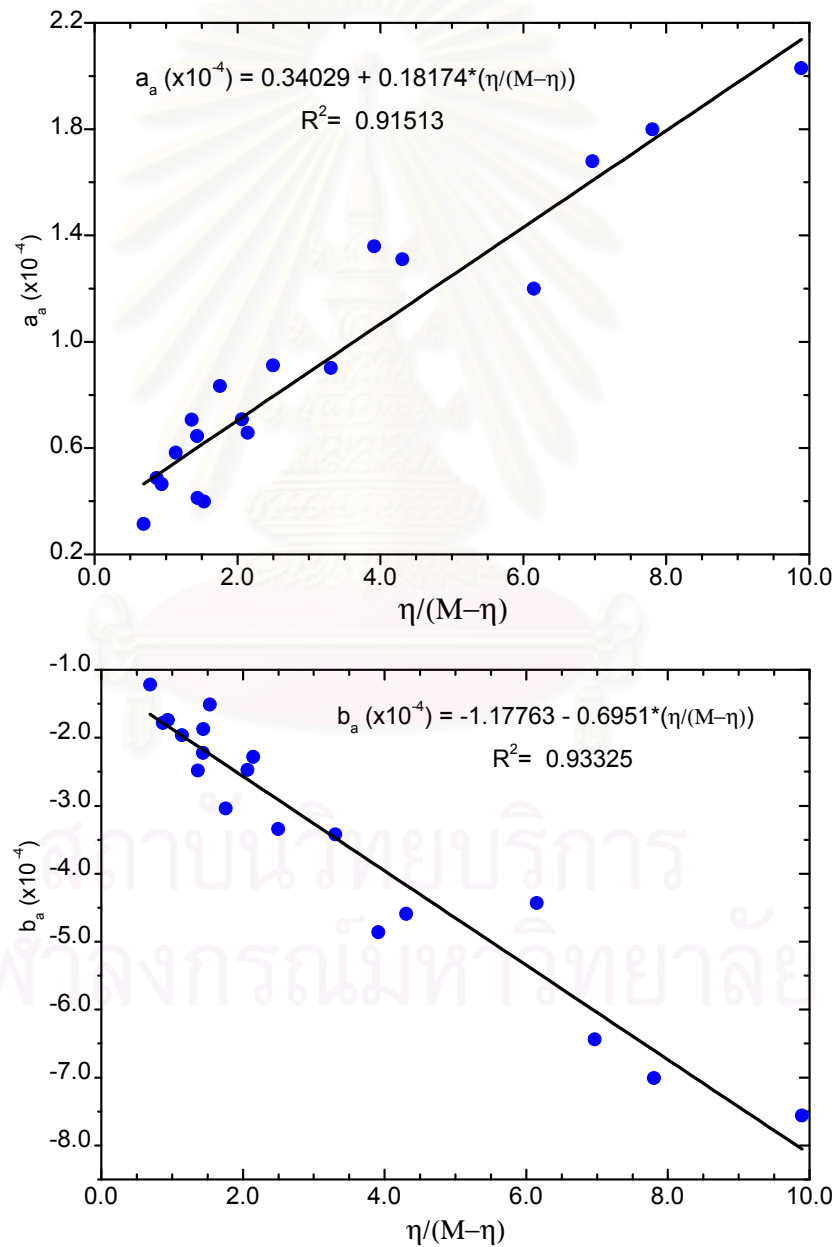


Figure 4.24. Coefficient a_a and b_a of axial strain rate $\dot{\epsilon}_a$

The strain rate of axial and radial direction was determined on CK₀DUC and CK₀UUC tests. When the stress state did not reach critical state ($\eta/M \leq 0.85$), both those strain rates decreased with time.

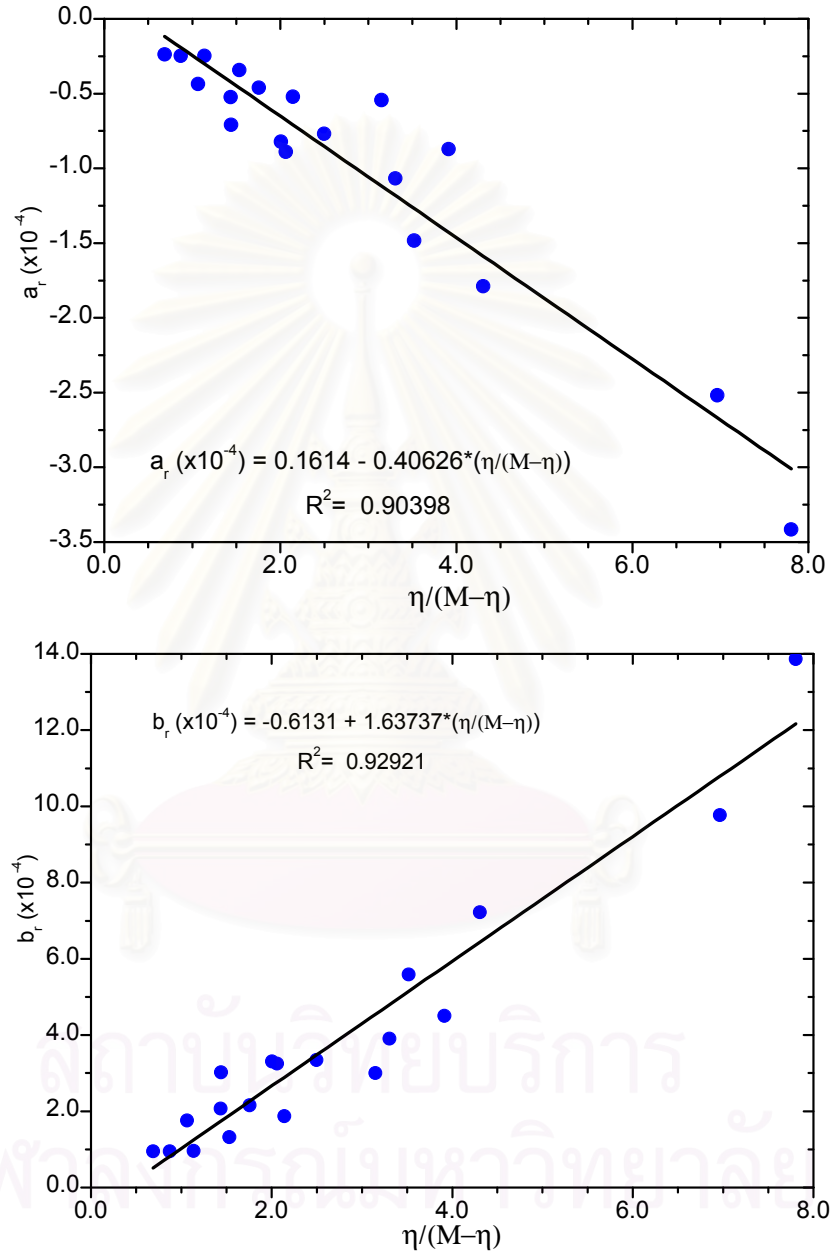


Figure 4.25. Coefficient a_r and b_r of radial strain rate $\dot{\epsilon}_r$

CHAPTER V

FINITE ELEMENT ANALYSIS

At present, many finite element (FE) codes can be used in analyzing the effects of deep excavation in soft ground. The commercial FE program PLAXIS (Vermeer & Brinkgreve, 1995) is proposed to be used in this research. Two soil models applied for FE back analysis the lateral displacement of DW are linear elastic-perfectly plastic (Mohr Coulomb model) and Soft Soil Creep models.

5.1 Background

The 2D-FE problem was used to study the response of ground and diaphragm wall around deep excavation area of BOT project. The section of DW at inclinometer B4 was selected for FE model to analyze the lateral displacement of DW during basement construction. At this section, the concrete F1 floor was replaced by steel strut because there was an existing function zone. The plane element of PLAXIS could not model the leg pile and the column system of the basement structure. Therefore, the model of problem was simplified as shown in Figure 5.1. The back and front zones of DW were more than 2.5 times the depth of excavation. The properties of DW, concrete basement floor and the strut were shown in Table 5.1.

Table 5.1. The properties of diaphragm wall and the basement floors

Structure	Thickness (m)	E (MPa)	Area (m ² /m)	I (m ⁴ /m)	ν	γ (kN/m ³)
Diaphragm wall	1.0	2.8×10^4	1	0.08333	0.2	25
F1 floor	0.4		0.4	0.00533		
P1 floor	0.3		0.3	0.00225		
P2 floor	0.3		0.3	0.00225		
P3 floor	0.3		0.3	0.00225		
P4 floor	1.3		1.3	0.18308		
Temporary strut	H350	$2.05 \times 10^{+5}$	$1.74 \times 10^{-6}(\text{m}^2)$	N.A.	0.2	N.A.

The soil model was selected so that the output data from FE back analysis could approach the field data. Two soil models were applied for FE back analysis without and with account of creep. The linear elastic-perfectly plastic model, which was based on the Mohr-Coulomb model of PLAXIS program, was selected for the soil model without account of creep. As some of previous researchers (P. Tanseng,

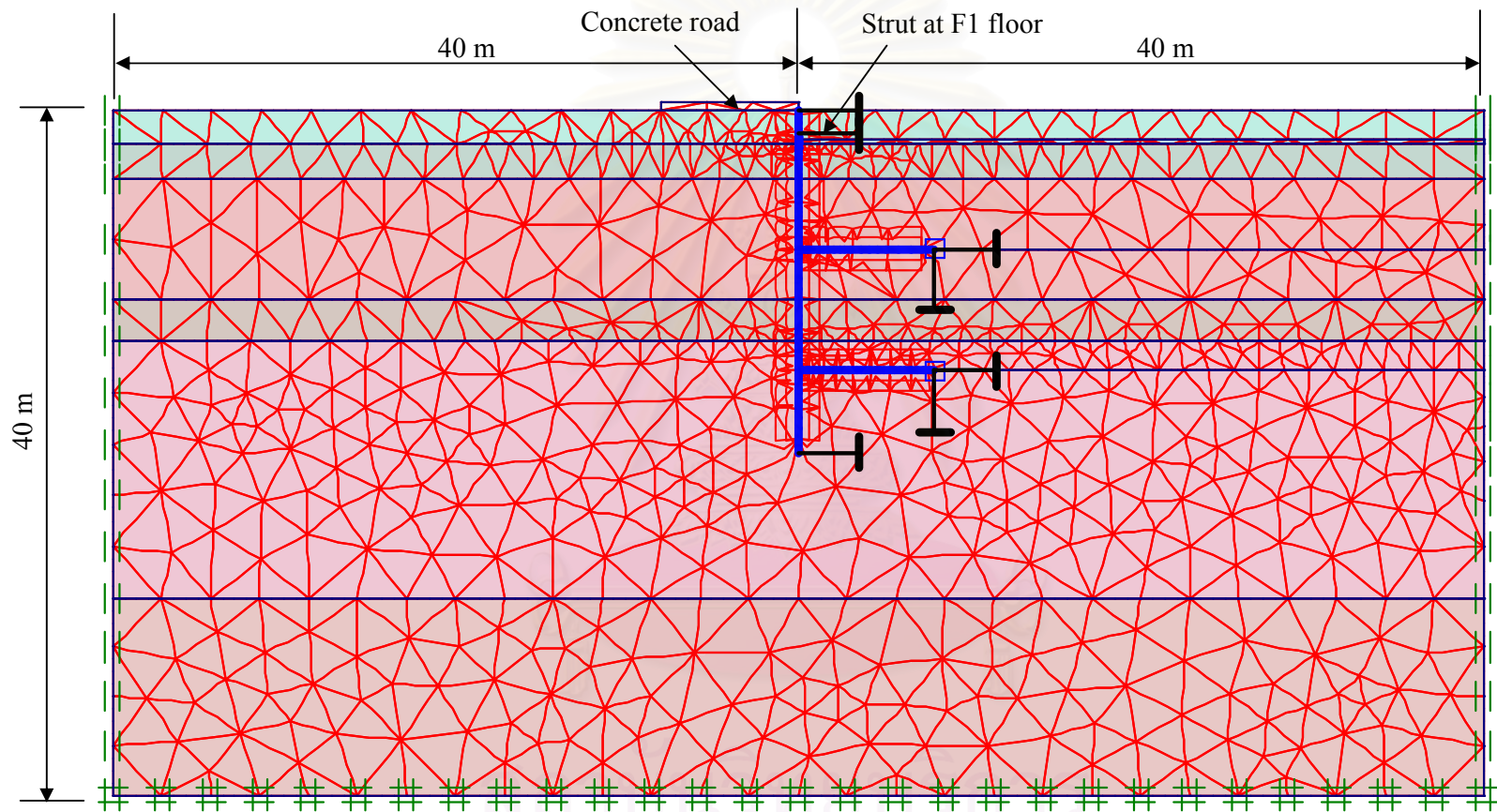


Figure 5.5. Modeling the basement floors of BOT project at section of inclinometer B4

จุฬาลงกรณ์มหาวิทยาลัย

1997 and S.B. Tamrakar, 2001) concluded that the linear elastic soil model was relatively good enough for predicting small ground deformation associated with excavation work with stiff retaining wall structure. Moreover, for this model, there were only three soil parameters considered: undrained Young's modulus, undrained shear strength and Poisson's ratio as shown in Table 5.2. The behavior of soil element on this model was affected by the undrained condition; therefore, this soil model might not describe the behavior of soil on elapsed time. However, the lateral displacement of DW on elapsed time could be estimated by reducing the undrained Young's modulus.

Table 5.2. Parameters for linear elastic-perfectly plastic model

<i>Parameter</i>	<i>Symbol</i>	<i>Formulation</i>	<i>Unit</i>
Undrained Young's modulus	E_u	$E_u = \alpha s_u$	kN/m ²
Poisson's ratio	ν	(correlation)	
Undrained shear strength	s_u		kN/m ²

The soil model with account of creep, which was selected for analyzing the lateral displacement of DW with the effects of creep, was Soft Soil Creep model on the PLAXIS program. This model required the parameters from the consolidation test and triaxial tests as shown in Table 5.4. For a rough estimate of the model parameters, P.A. Verneer and H.P. Neher (2000) suggested the correlation between λ^* , κ^* and μ^* as follows:

$$\lambda^* = I_p (\%) / 500; \quad \lambda^* / \mu^* = 15 \sim 25 \quad \text{and} \quad \lambda^* / \kappa^* = 5 \sim 10 \quad (5.1)$$

where $I_p (\%)$ – plasticity index.

The duration of each construction stage at the section of inclinometer B4 assigned for FE analysis was shown in Table 5.3. The stages in this table were the same as those stages in Figure 3.2. There were three durations of elapsed time at three excavations with the depth of 1.75m, 8.1m and 15.2m.

Table 5.3. Duration of each construction stage

Stage 2	Stage 3	Stage 4	Stage 5	Stage 6	Stage 7
Excavate to 1.75m	Elapsed time	Excavate to 8.1m	Elapsed time	Excavate to 15.2m	Elapsed time
7 days	30 days	19 days	82 days	20 days	78 days

According to the observation of ground water when excavation was carried out at the site of BOT project, the real ground water table existed only on the sand layer. Even though, when the ground was excavated to 15.2m deep to the stiff clay layer the water was unavailable on excavated zone. Hence, the phreatic line on the FE model was not assigned on the clay layers.

Table 5.4. Parameters for Soft Soil Creep model

<i>Parameter</i>	<i>Symbol</i>	<i>Formulation</i>	<i>Unit</i>
Failure parameter as in Mohr-Coulomb model			
- Cohesion	c		kN/m ²
- Friction angle	φ		0
- Dilatancy angles	ψ		0
Parameter of the Soft-Soil-Creep			
- Modified compression index	λ*	$\lambda^* = \frac{\lambda}{1+e} = \frac{C_c}{2.3(1+e)}$	
- Modified swelling index	κ*	$\kappa^* = \frac{\kappa}{1+e}$ $\approx \frac{3}{2.3} \frac{1-v_{ur}}{1+v_{ur}} \frac{C_r}{1+e}$	
- Modified creep index	μ*	$\mu^* = \frac{C_\alpha}{2.3(1+e)}$	
- Poisson's ratio for unloading-reloading	v _{ur}		
- Slope of the so-called "critical state line"	M		

5.1 Linear elastic-perfectly plastic model

The parameters of soil layer used for FE analysis with linear elastic-perfectly plastic soil model was shown in Table 5.5. The subsoil profile was divided into six layers: weathered crust (0.0 ~ 2.0 m), soft clay beneath the crust (2.0 ~ 4.0 m), soft clay (4.0 ~ 11.0 m), soft clay upper the stiff clay (11.0 ~ 13.5 m), stiff clay (13.5 ~ 28.5 m) and sand (28.5 ~ 40.0 m). For four soil layers from 0.0 to 13.5 m, the

undrained Young's modulus E_{u0} and undrained shear strength s_u were the average values selected from the CK_0UC tests of the samples. On the stiff clay layer (13.5 to 28.5m), the undrained shear strength was the value at 14m deep from field-vane-shear test (Figure 3.7). In addition, the E_{u0} of this soil layer was determined by the correlation $E_{u0} = \alpha s_u$ with $\alpha=2000$.

The coefficient of earth pressure at rest (K_0) was average values taken from the automatic K_0 procedure of CK_0UC , CK_0DUC , CK_0UUC tests.

Table 5.5. Properties of soil for Mohr-Coulomb model (linear elastic-perfectly plastic)

Layer (m~m) (1)	γ_t (kN/m ³) (2)	K_0 (3)	E_{u0} (kN/m ²) (4)	$E_u = 60\% \times E_{u0}$ (kN/m ²) (5)
0.0 ~ 2.0	17.1	0.60	$3.00 \times 10^{+4}$	$1.800 \times 10^{+4}$
2.0 ~ 4.0	17.4	0.53	$2.44 \times 10^{+4}$	$1.464 \times 10^{+4}$
4.0 ~ 11.0	16.1	0.45	$2.09 \times 10^{+4}$	$1.254 \times 10^{+4}$
11.0 ~ 13.5	16.5	0.44	$2.58 \times 10^{+4}$	$1.548 \times 10^{+4}$
13.5 ~ 28.5	17.5	0.45	$1.80 \times 10^{+5}$	$1.080 \times 10^{+5}$
28.5 ~ 40.0	19.0	0.50	$9.00 \times 10^{+4}$	(13.5~20.0m)

$E_{umin} = 46\% \times E_{u0}$ (kN/m ²) (6)	$S_{u(CK0UC)}$ (kN/m ²) (7)	$S_{u(FVS)}$ (kN/m ²) (8)	ϕ (°) (9)	ν (10)
$1.380 \times 10^{+4}$	22.9	34.7	0	0.3
$1.122 \times 10^{+4}$	17.8	41.7		0.49
$0.961 \times 10^{+4}$	32.0	33.9		0.49
$1.187 \times 10^{+4}$	43.3	46.0		0.49
$0.828 \times 10^{+5}$	90.0			0.35
(13.5~20.0m)	N.A.		30	0.30

Table 5.6. The ratio of undrained Young's modulus and undrained shear strength of soft clay layer

Layer (m~m)	$E_{u0}/S_{u(CK0UC)}$	$E_{u0}/S_{u(FVS)}$	$60\% \times E_{u0}/S_{u(CK0UC)}$	$60\% \times E_{u0}/S_{u(FVS)}$	$E_{umin}/S_{u(CK0UC)}$	$E_{umin}/S_{u(FVS)}$
0.0 ~ 2.0	1310.0	864.6	786.0	518.7	602.6	397.7
2.0 ~ 4.0	1370.8	585.1	822.5	351.1	630.3	269.1
4.0 ~ 11.0	653.1	616.3	391.9	369.8	300.3	283.4
11.0 ~ 13.5	595.8	560.5	357.5	336.3	274.1	257.9

As mentioned in the summary of chapter IV, the Young's modulus depended not only on the strain level but also on the stress state on all three kinds of tests.

Besides, the excavation of BOT project was paused at three main stages 2, 4 and 6. At those stages, the stress state and strain levels of soil behind the diaphragm wall were not at the same values. During the elapsed time, the lateral displacement of DW was increasing or the strain level of soil element behind the DW changed. Therefore, on the linear elastic-perfectly plastic soil model, the Young's modulus was changed to have the corresponding Young's modulus with strain level. There were three values of Young's moduli E_{u0} , $E_{u60\%}=60\%E_{u0}$ and $E_{umin}=46\%E_{u0}$ (shown in Figure 4.7) to be considered for FE back analysis.

Figures 5.2 and 5.3 showed the observation data and FE results of lateral displacement of DW at inclinometer B4. The smooth dark blue, pink and red lines were the results of FE analysis when the undrained Young's moduli were E_{u0} , $E_{u60\%}$ and E_{umin} respectively. At stage 4, when the Young's modulus was assigned with the E_{u0} value, the FE result of lateral displacement of DW was approximately equal to last lateral displacement line of elapsed time (Figure 5.2). However, when the Young's modulus was decreased to $E_{u60\%}$ and E_{umin} values the lateral displacement line of FE results were deviated the observation lines of lateral displacement. As a result, when the ground was excavated to 8.1m deep (stage 4), the lateral displacement of DW as well as the strain of soil element behind the DW was still a small value. Therefore, in this case, the linear elastic-perfectly plastic soil model with initial Young's modulus of CK_0UC test could not predict the lateral displacement of DW immediately after excavation time. The Young's modulus with a smaller strain level was needed in this case.

At stage 6, when the initial Young's modulus E_{u0} was applied to soil model for FE analysis, the lateral displacement of DW of FE result was approximated to the observation data of lateral displacement of DW immediately after finishing the excavation to 15.2m deep (Figure 5.3). In addition, when the E_{u0} value was replaced by $E_{u60\%}$ the lateral displacement of DW of FE result was almost the same as the last observation line of elapsed time. In this case, the initial Young's modulus was suitable to apply for FE analysis to analyze the lateral displacement of DW after excavation time.

Conclusively, when the FE analysis is carried out for the deep excavation with elapsed time existing at some depths, the Young's modulus should be adjusted to be larger when the excavation goes deeper.

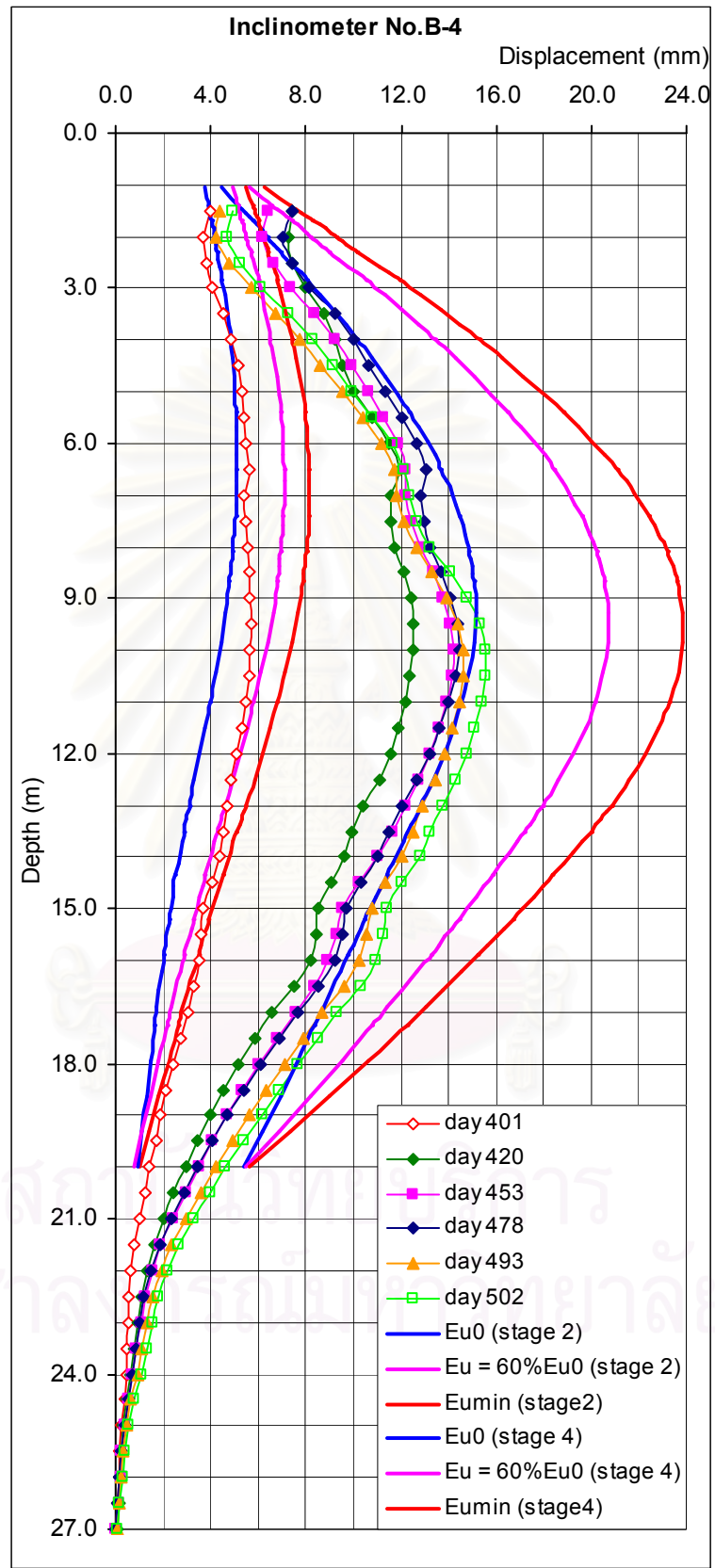


Figure 5.2. Lateral displacement of DW on stage 2 and stage 4

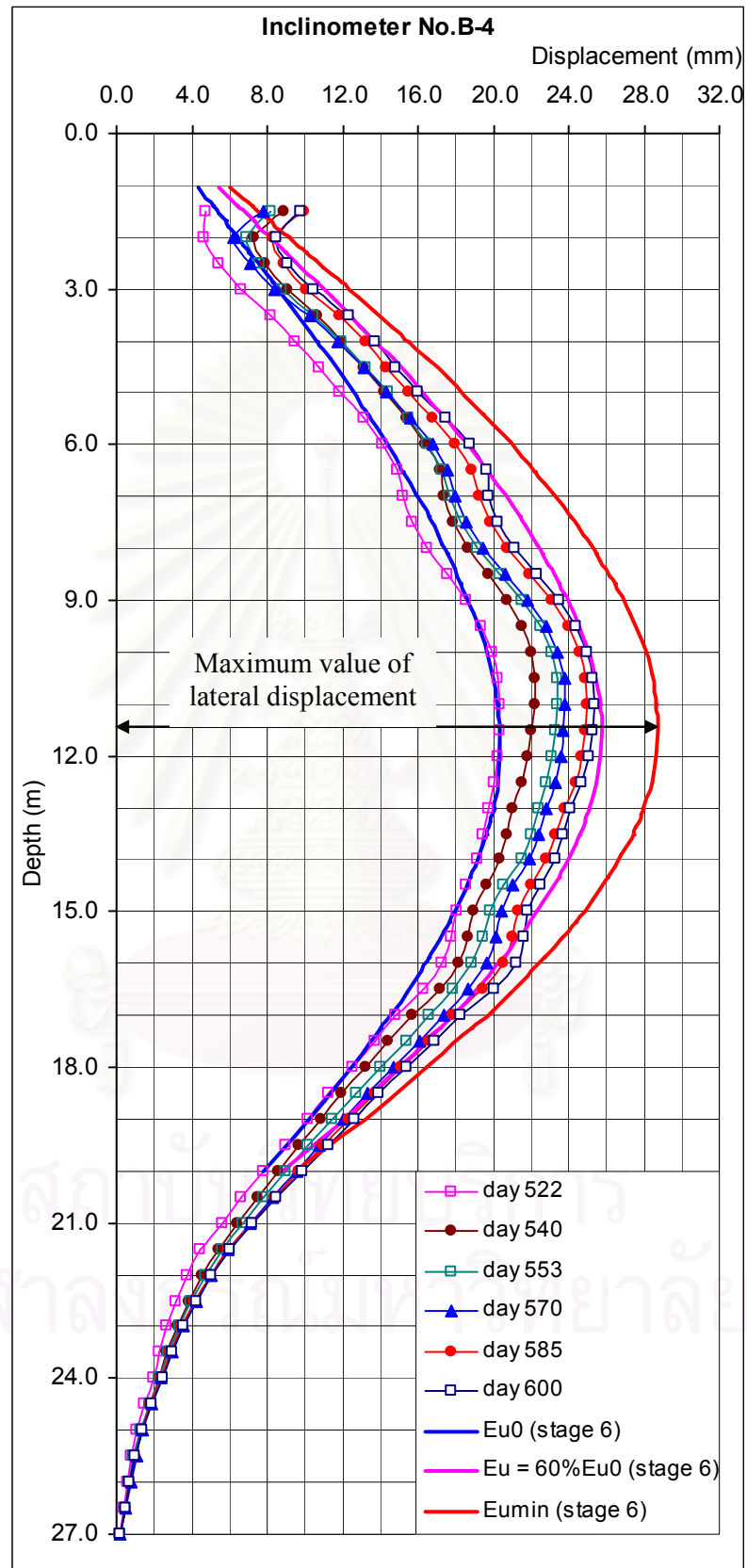


Figure 5.3. Lateral displacement of DW on stage 6

5.2 Soft Soil Creep model

The parameters for Soft Soil Creep (SSC) model were shown in Table 5.6. The slope of critical state line (M) and internal friction angle (ϕ) were selected from the results of CK₀UC tests. The parameter λ^* , κ^* and μ^* were calculated by the correlation of equations (5.1).

Table 5.7. Parameters of soil for Soft Soil Creep model for BOT project

Layer (m~m)	γ_t (kN/m ³)	K_0	λ^*	κ^*	μ^*	M	ϕ ($^\circ$)	ψ ($^\circ$)
0.0 ~ 2.0	17.1	0.60	0.108	0.022	0.005	2.17	50	0
2.0 ~ 4.0	17.4	0.53	0.103	0.021	0.005	1.74	42	
4.0 ~ 11.0	16.1	0.45	0.145	0.029	0.007	1.50	37	
11.0 ~ 13.5	16.5	0.44	0.137	0.027	0.007	1.53	38	

The results of lateral displacement of DW, which was analyzed with the undrained SSC model, were shown in Figures 5.4 and 5.5. The FE results showed that the lateral displacement of DW did not increase during elapsed time.

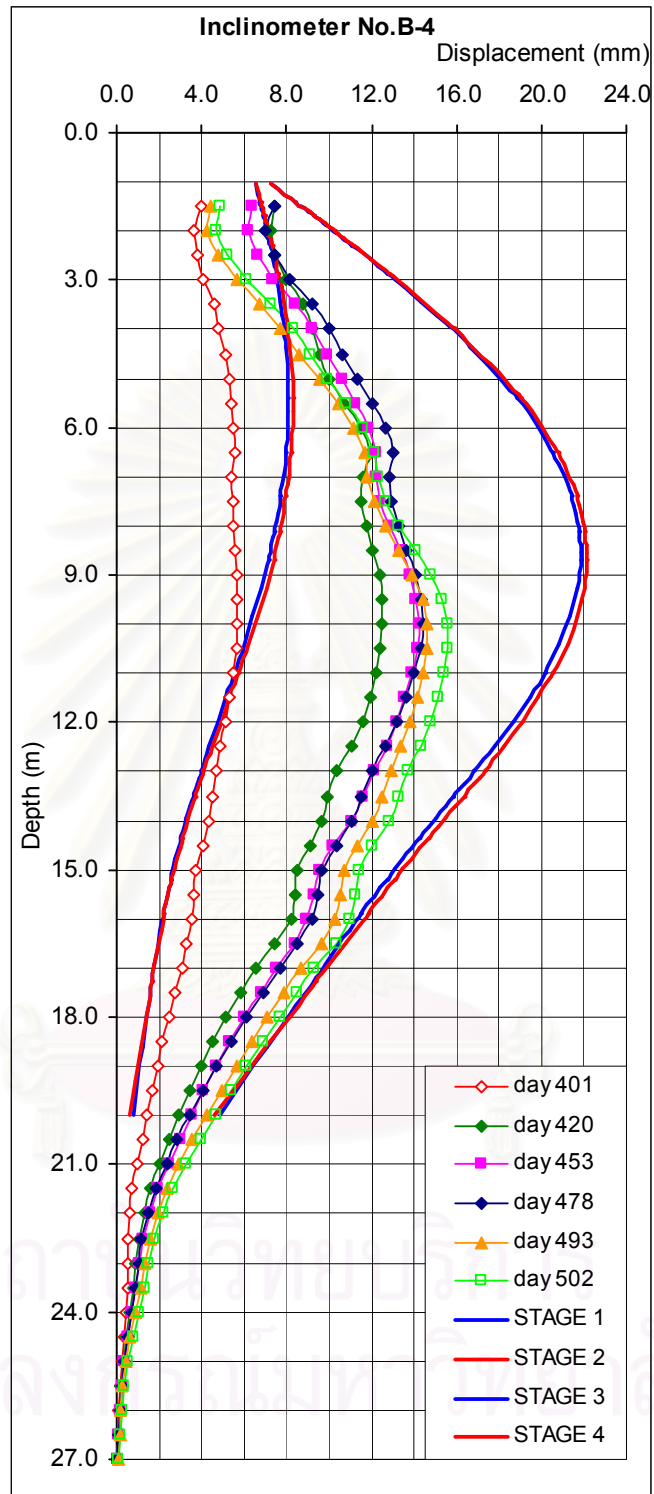


Figure 5.4. Lateral displacement of DW on stage 2,3,4 and 5.

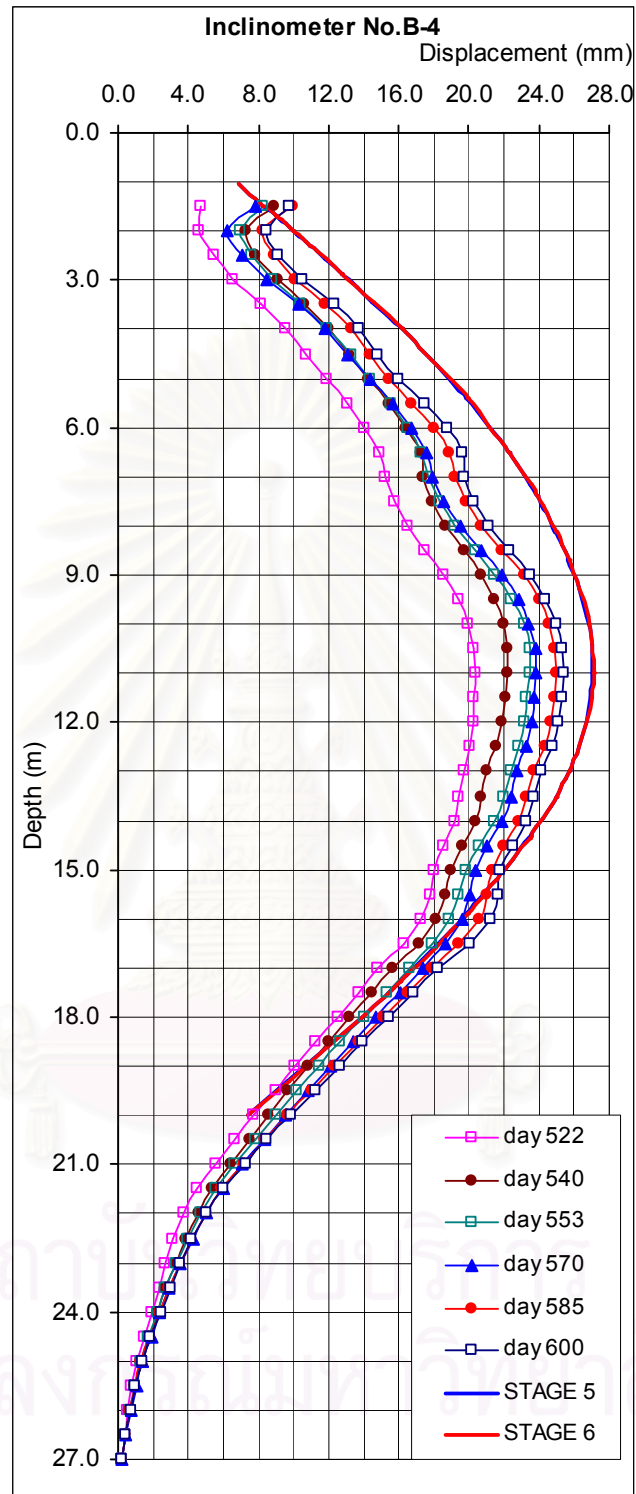


Figure 5.5. Lateral displacement of DW on stage 6 and 7

CHAPTER VI

RESULTS AND DISCUSSION

In this chapter, the results of experimental work, laboratory tests and finite element analysis will be discussed.

6.1 Parameters of soil models

The undrained shear strength s_u determined from three different tests was plotted and shown in Figure 6.1. The simple unconfined compression test experimented upon the samples from three boreholes at different positions had the smallest value. The s_u value from FVS test plotted in that figure was without Bjerrum's correction and almost approximately the same as the results obtained from CK_0UC test. The FVS test was carried out at two positions with and without effects of excavation. The FVS-11 and FVS-12 were tested at the same position without the effects of excavation. Otherwise, the FVS-21 was test at a position near the excavation zone. Comparing three s_u data of those FVS tests, the s_u value of FVS-11 and FVS-12 were a bit larger than the s_u value of FVS-21. This was a preliminary result because the shear strength of soil behind the DW might be changed by the alteration of stress state behind the wall. In fact, the sensitivity of FVS was probably not high; therefore, more tests needed to be conducted to achieve a valid result.

The relationship between volume strain and logarithm of mean effective stress of three CK_0DUC tests was shown in Figure 5.3. In those tests, the horizontal stress as well as the mean effective stress was decreased; therefore, the lines in Figure 5.3 described the unloading process. The swelling index (C_r) could be determined from the slope of the lines.

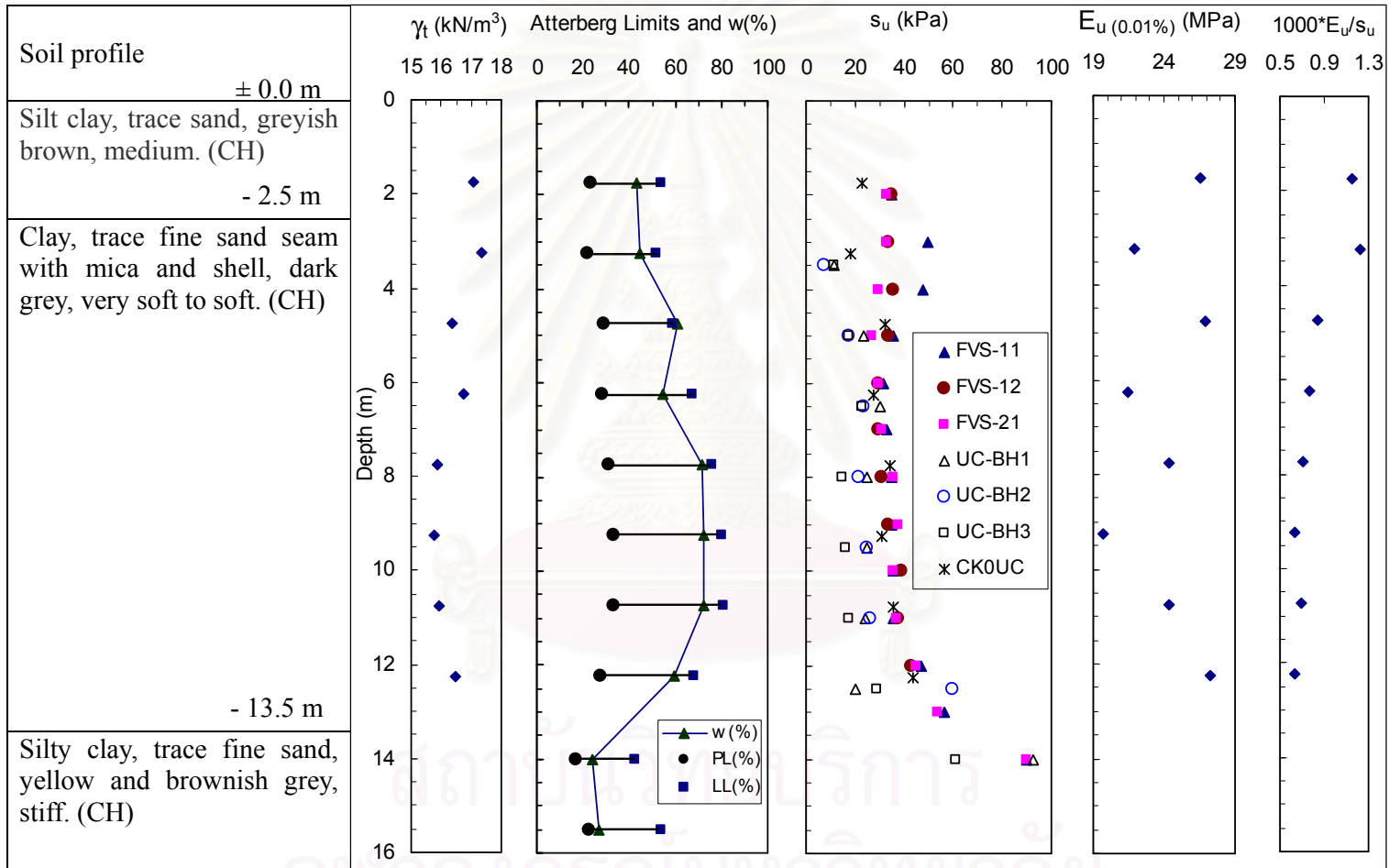


Figure 6.1. Geotechnical properties at BOT site project

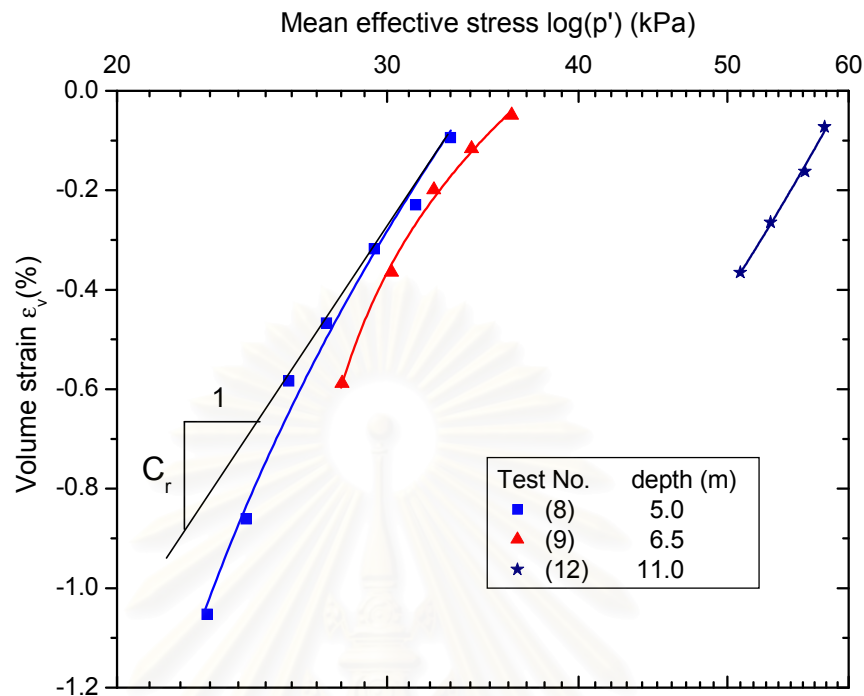


Figure 6.2. Relationship between mean effective stress p' and volume strain ϵ_a of CK_0 DUC test

6.1 Finite Element Analysis

The linear elastic-perfectly plastic model with undrained condition of soil behavior could not be used to predict the lateral displacement of DW during the elapsed time if the set of parameters (E_u , s_u and ν) was unchanged. Based on the collected inclinometer data during the elapsed time, the lateral displacement of DW was non-stop increasing. In other words, the strain of soil behind DW was also increasing. By the simple way, elastic-perfectly plastic model could be used to predict the lateral displacement of DW on the elapsed time by reducing the Young's modulus. However, in three kinds of tests, no matter whether the sample was drained or undrained, the minimum Young's modulus was limited by the lower bound value as shown in Figures 4.7, 4.11 and 4.14. Consequently, the lateral displacement of DW would be a maximum value when undrained Young's modulus reduced to lower bound value.

When the ground was excavated to 15.2 m deep (stage 6), the maximum lateral displacement of DW of inclinometer B4 during excavation and elapsed time was plotted in Figure 6.2. The non-stop increment of lateral displacement of DW

during elapsed time was approximated by the exponent equation. From this equation, the lateral displacement of DW reached an upper bound value ($\Delta h = 26.90$) when the variable of time moved towards unlimited ($t \rightarrow \infty$). Meanwhile, the maximum lateral displacement of DW (Δh) from back FE analysis with E_{umin} ($E_{\text{umin}} = 46\%E_{\text{u0}}$) at stage six was equal to 28.8 (Figure 5.3). Hence, at stage 6, the linear elastic-perfectly plastic soil model could to be used to predict the bound of lateral displacement of DW by using the undrained Young's modulus E_{umin} .

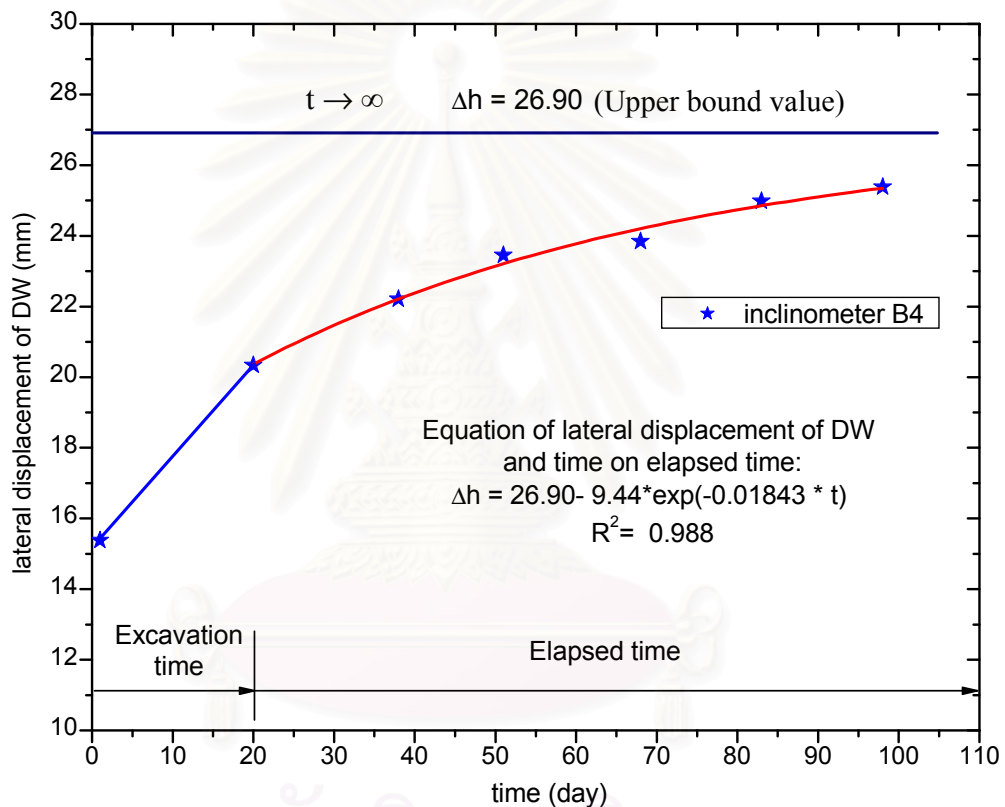


Figure 6.3. The approximate equation of lateral displacement of DW and time during elapsed time of inclinometer B4 at stage 6

CHAPTER VII

CONCLUSION AND RECOMMENDATION

7.1 Summary and Conclusion

To determine the soil behaviors at the elapsed time of excavation behind the diaphragm wall of the Bank of Thailand project in Bangkok by means of top down construction, the series of triaxial testes (CK₀UC, CK₀DUC, and CK₀UUC) and FE back analysis were performed. Based on the field experiment, the series of triaxial tests and the results of FE analysis, the following conclusions can be drawn.

1. To predict the initial lateral displacement of DW by using elasto-perfectly plastic model, the undrained Young's modulus of soil could be determined based on the ratio $s_u/E_{u(0.01\%)}$ and undrained shear strength at peak of CK₀UC test or field vane-shear test. For the Bangkok clay at BOT project, the ratio $s_u/E_{u(0.01\%)}$ is from 1100 to 1300 for weathered clay layer upper 4 m deep and 600 to 800 for soft soil layer deeper than 4 m. It should be taken the residual shear strength of clay from the CK₀UC test to secure the stability of DW in the case that the excavation takes a long time to complete. The ratio (s_u/σ'_{v0}) of undrained shear strength of FVS test as well as CK₀UC tests and overburden effective stress is around 0.45 at the depth from 6m to 12m.

2. Unloading Young's modulus (E_{un}) reduces as the ratio η/M increases and this depends on the amplitude of the decrement step of horizontal pressure.

3. For the soil samples below 6.0m deep, the Slope of Critical State Line (CSL) is equal to 1.5 for two kinds of CK₀UC tests and CK₀DUC tests.

4. Volume strain depends not only on the drainage condition but also on the amplitude of applied unloading lateral stress.

5. According to the results obtained from CK₀DUC and CK₀UUC tests, the coefficient of deformation with time (C_α) as well as strain rate depends not only on the deviator stress level, elapsed time and drainage condition but also on the direction of deformation. The horizontal coefficient of deformation ($C_{\alpha r}$) which could be applied for FEM analysis to predict the lateral displacement of DW versus time should be studied further.

6. The parameter Young's modulus of linear elastic-perfectly plastic model must be suitable to the strain level of the soil behind the wall.

7.2 Recommendations for Further Research

The linear elastic-perfectly plastic soil model can be applied to predict the lateral displacement of DW during excavation time and elapsed time. The final displacement of DW can be estimated by using the lower bound of un-reloading modulus E_u . However, the lateral displacement of DW is predicted discontinuously with time by using EPP soil model. The displacement of DW is only obtained at the point of time when the un-reloading Young's modulus is known. To know the reduction of E_u with time is difficult problem even if the E_u can determined from CK_0DUC and CK_0UUC tests. Meanwhile, the SSC model can be used for FE analysis to predict the ground movement. On SSC model, the ground settlement can be estimated by using the vertical coefficient of deformation $C_{\alpha a}$. Conclusively, the horizontal coefficient of deformation ($C_{\alpha r}$) which could be applied for FEM analysis to predict the lateral displacement of DW versus time should be studied further.

REFERENCES

- Augustesen, A., Liingaard, M., and Lade, P. V. (2004). "Evaluation of time-dependent behavior of soils." *International Journal of Geomechanics* 4, 3: 137–156.
- Barden, L. "Time dependent deformation of normally consolidated clays and peats". *Journal of The Soil Mechanics and Foundations Division, ASCE* 95 (1969): 1-31.
- Borja, R.I., and Kavazanjian, E. 1985. A constitutive model for the stress–strain–time behaviour of 'wet' clays. *Géotechnique* 35, 3: 283–298.
- Duncan, J.M., and Chang, C.Y. 1970. Non-linear analysis of stress and strain in soils. *Journal of the Soil Mechanics and Foundations Division, ASCE* 96(SM5): 1629–1654.
- Graham, J., Crooks, J.H.A., and Bell, A.L. 1983. Time effects on stress–strain behaviour of natural soft clays. *Géotechnique* 33, 3: 327–340.
- Head, K. H. *Manual of Soil laboratory testing 1,2,3*. Robert Hartnoll Ltd., Cornwall, Great Britain. 1982.
- Jardine R. J., Symes M. J., Burland J. B. 1984. The measurement of soil stiffness in the triaxial apparatus. *Geotechnique* 34, 3: 323-340.
- Kutter, B.L., and Sathialingam, N. 1992. "Elastic–viscoplastic modelling of the rate-dependent behaviour of clays". *Géotechnique* 42, 3: 427–441.
- Leroueil, S., Kabbaj, M., Tavenas, F., and Bouchard, R. 1985. Stress – strain – strain rate relation for the compressibility of sensitive natural clays. *Géotechnique* 35, 2: 159–180.
- Lingnau, B.E., Graham, J., Yarechewski, D., Tanaka, N., and Gray, M.N. 1996. "Effects of temperature on strength and compressibility of sand–bentonite buffer". *Engineering Geology* 41: 103–115.
- Lo Presti, D. C. F., Pallara, O., Cavallaro, A., and Jamiolkowski, M., "Influence of Reconsolidation Techniques and Strain Rate on the Stiffness of Undisturbed Clays from Triaxial Tests," *Geotechnical Testing Journal, GTJODJ* 22, 3 (September 1999): 211–225.
- Malcolm Puller, CEng, DIC, FICE, FIStructE (1996). "Deep Excavation a practical manual" Thomas Telford Publishing, Thomas Telford Services Ltd., 1 Heron Quay, London E14 4JD.

- Mimura M. and Jang W. "Evaluation of Time-dependent Behavior of Osaka Pleistocene Clay by Elasto-viscoplastic Finite Element Analysis". *Annals of Disas. Prev. Res. Inst., Kyoto Univ.*, No. 46 B, 2003.
- Mitchell, J. K. 1993. *Fundamentals of Soil behavior*, 2nd ed., John Wiley & Sons, Inc., New York.
- O. Kusakabe, K. Fujita, Y. Miyazaki (1999). "Geotechnical Aspects of Underground Construction in Soft Ground" *Proceedings of the International symposium on geotechnical aspects of underground construction in soft ground-IS-Tokyo '99 Tokyo/Japan/19-21 July 1999*.
- Ou, C. Y. and Lai, C. H. (1994). "Finite element analysis of deep excavation in layered sandy and clayey soil deposits", *Canadian Geotechnical Journal* 31, 4: 204–214
- Ou, C. Y., Liao J. T., and Lin, H. D. (1998). "Performance of Diaphragm wall constructed using Top-down method", *Journal of Geotechnical and Geoenvironmental Engineering* 124, 9.
- Pornpot Tanseng (1997). "Instrumented deep excavations Bangkok subsoils" M.Eng. Thesis, AIT, Bangkok, Thailand, April 1997.
- P. Thirapong (1999). "Application of F.E.M. to Excavation of Soft Clay" M.Eng. Thesis, Tokyo Institute of Technology, Japan.
- Sheahan, T. C., Ladd, C. C., and Germaine, J. T., "Rate-Dependent Undrained Shear Behavior of Saturated Clay". *Journal of Geotechnical Engineering* 122, 2 (February 1996): 99-108.
- Sheahan, T. C., Ladd, C. C., and Germaine, J. T., "Time-Dependent Triaxial Relaxation Behavior of a Resedimented Clay", *Geotechnical Testing Journal*, GTJODJ 17, 4 (December 1994): 444-452.
- Stolle, D.F.E., Vermeer, P.A. and P.G. Bonnier. (1999). A consolidation model for a creeping clay. *Canadian Geotechnical Journal* 36, 4: 754–759.
- Tamrakar, S. B. (2001). "Design parameters for elasto-plastic FE analysis of soft clay ground", Dr. Engineering Dissertation, Hokkaido University, Japan.
- Tanaka, N., Graham, J., and Crilly, T. 1997. "Stress–strain behaviour of reconstituted illitic clay at different temperatures". *Engineering Geology* 47: 339–350.
- Tavenas, F., Leroueil, S., LaRochelle, P., and Roy, M. 1978. "Creep behaviour of an undisturbed lightly overconsolidated clay". *Canadian Geotechnical Journal* 15: 402–423.

- Teparaksa, W. (1994). "Movement and Its Influence Zone of Flexible Sheet Pile Wall for Deep Basement Excavation in Soft Bangkok Clay." Proceedings of Conference on Deep Foundation and Ground Improvement Schemes, 21-24 November 1994, Bangkok, Thailand 1, 233-242.
- Teparaksa, W. (1999). "Analysis of lateral wall movement for deep braced excavation of Bangkok subsoils" Proceedings of Civil and Environmental Engineering Conference New Frontiers & Challenges 8-12 November 1999, Bangkok, Thailand 2, Part I, 67-76.
- Vermeer, P. A. and Neher H. P. "A soft soil model that accounts for creep". Beyond 2000 in Computational Geotechnics – 10 Years of PLAXIS International © 1999 Balkema, Rotterdam.
- Wedage A. M. P., Morgenstern N. R. and Chan D. H. 1997. "A strain rate dependent constitutive model for clays at residual strength". Canadian Geotechnical Journal 35: 364-373.
- Wood, D.M. 1990. Soil behaviour and critical state soil mechanics. Cambridge University Press, Cambridge, England.
- Yin, J.-H., and Graham, J. 1989. Viscous-elastic-plastic modelling of one-dimensional time-dependent behaviour of clays. Canadian Geotechnical Journal 26: 199-209.
- Yin, J.-H., and Graham, J. 1999. Elastic viscoplastic modelling of the time-dependent stress-strain behaviour of soils. Canadian Geotechnical Journal 36: 736-745.
- Yin, J.-H. and Zhu, J.-G. 1999. Elastic viscoplastic consolidation modelling and interpretation of pore-water pressure responses in clay underneath Tarsiut Island. Canadian Geotechnical Journal 36, 4: 708-717.
- Yin, J.-H. and Zhu, J.-G. 1999. Measured and predicted time-dependent stress-strain behaviour of Hong Kong marine deposits. Canadian Geotechnical Journal 36, 4: 760-766.
- Zhu, J.-G., Yin, J.-H., and Luk, S.-T., June 1999. "Time-Dependent Stress-Strain Behavior of Soft Hong Kong Marine Deposits," Geotechnical Testing Journal, GTJODJ 22, 2: 112-120.
- Zhu, J.-G., Yin, J.-H. 2000. Strain-Rate-dependent stress-strain behavior of overconsolidated Hong Kong marine clay. Canadian Geotechnical Journal 37: 1272-1282.



APPENDICES

สถาบันวิทยบริการ
จุฬาลงกรณ์มหาวิทยาลัย

APPENDIX A

DATA OF INCLINOMETERS

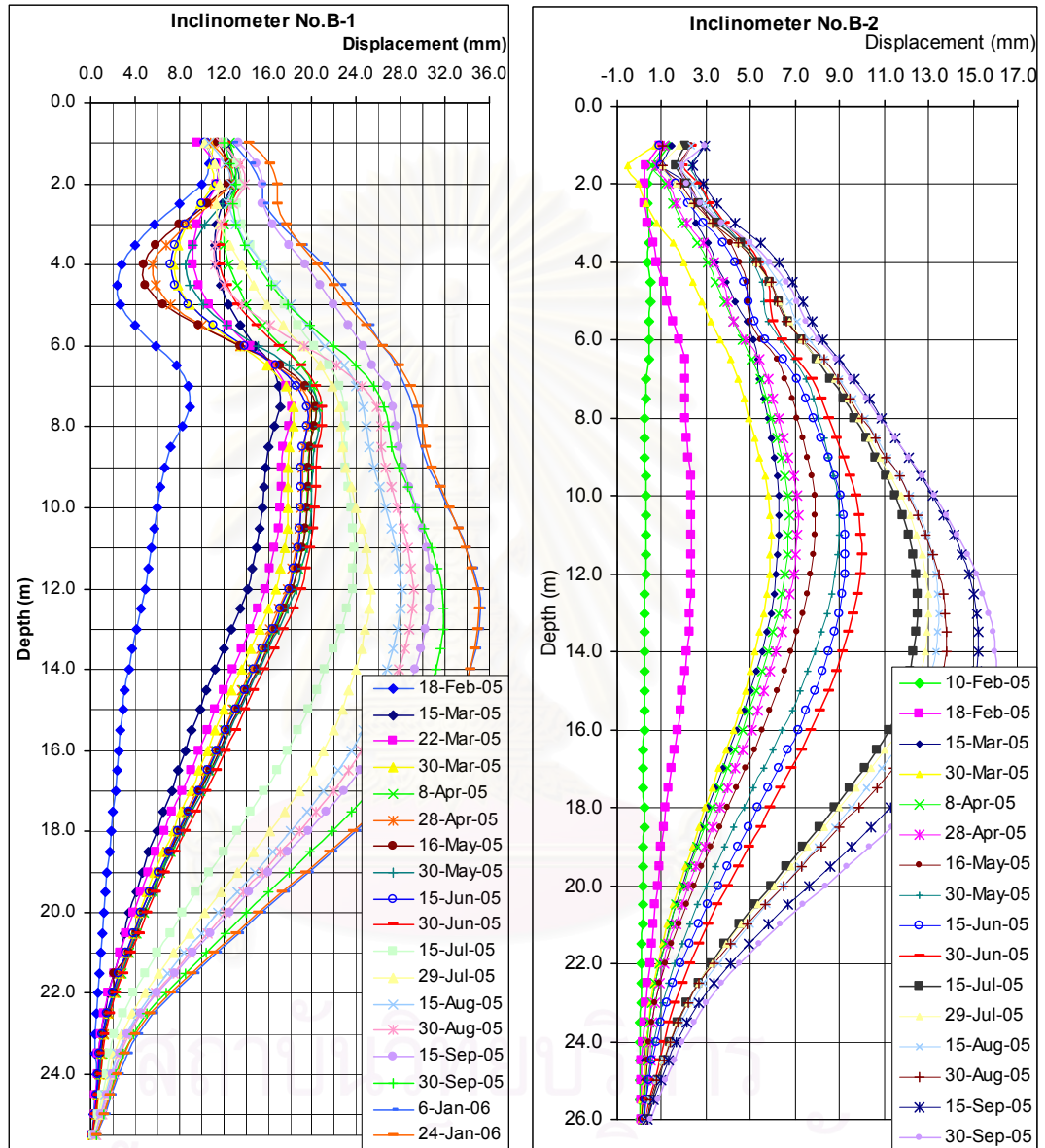


Figure A.1. Horizontal displacement of diaphragm wall at inclinometers B1 and B2 during basement construction

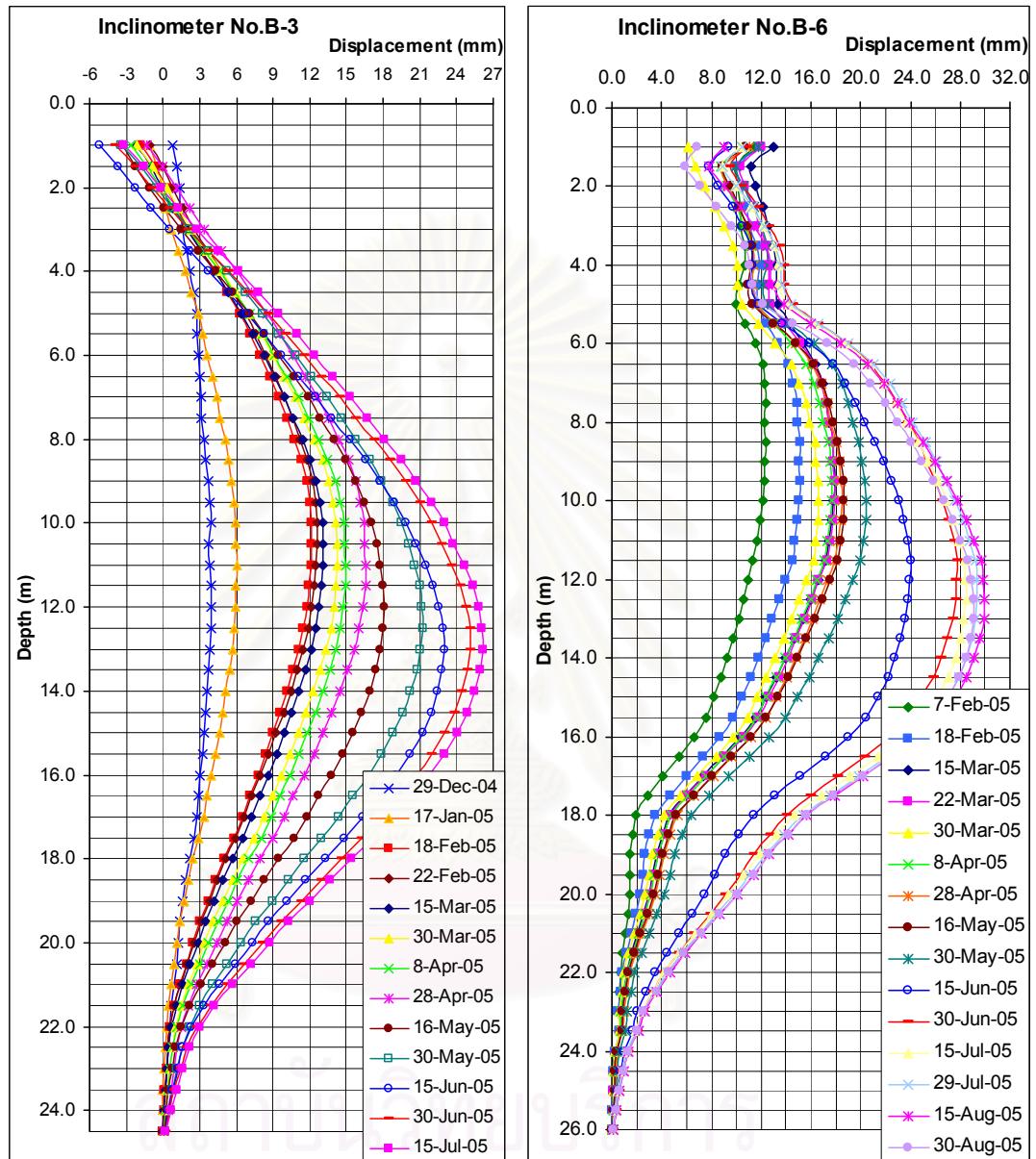


Figure A.2. Horizontal displacement of diaphragm wall at inclinometers B3 and B6 during basement construction

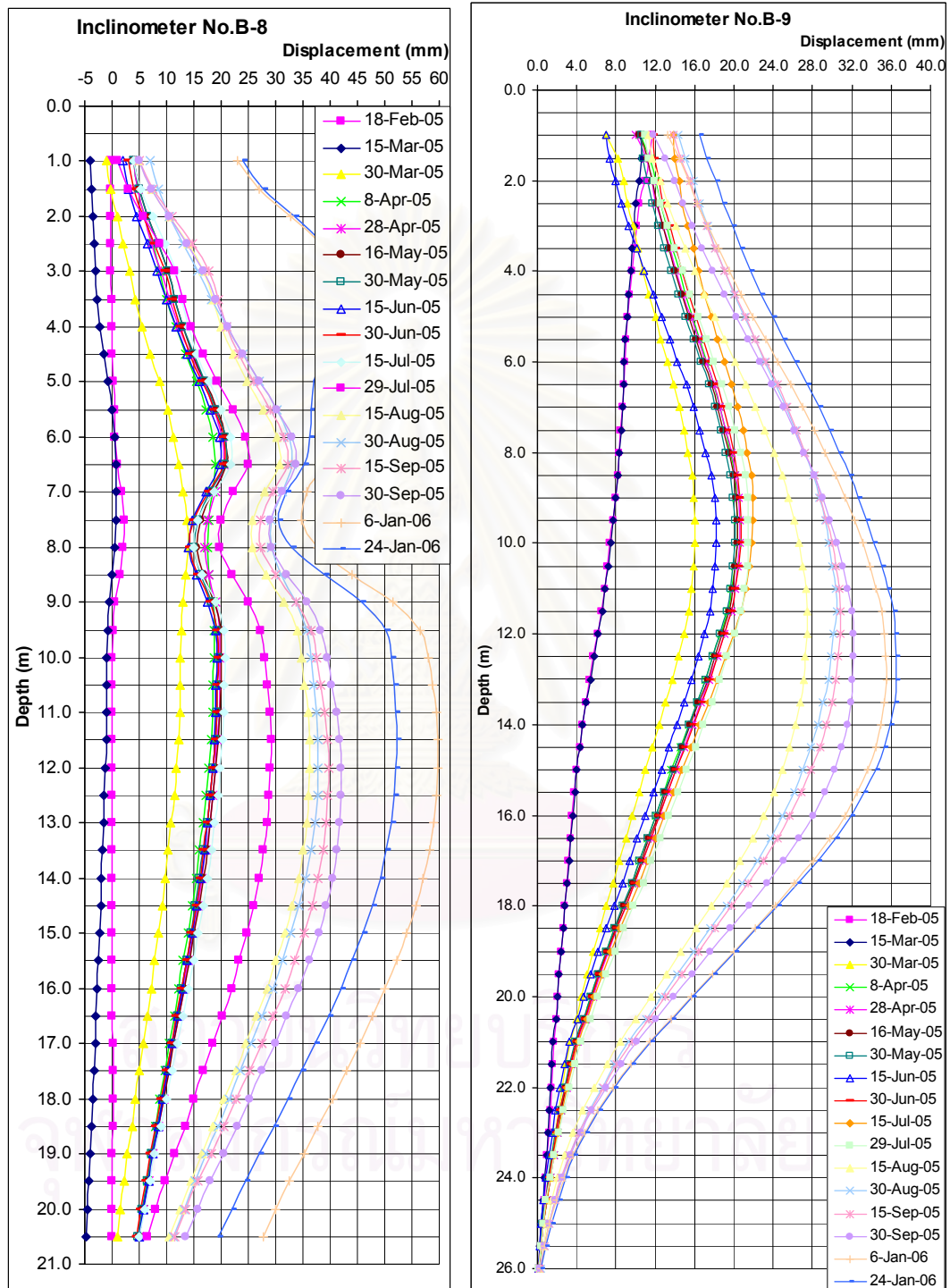


Figure A.3. Horizontal displacement of diaphragm wall at inclinometers B8 and B9 during basement construction

APPENDIX B
TRIAXIAL TEST APPARATUS



Figure B.1. Picture of Triaxial test system for carrying out the CK_0UC , CK_0DUC and CK_0UUC tests

สถาบันวิทยบริการ
จุฬาลงกรณ์มหาวิทยาลัย

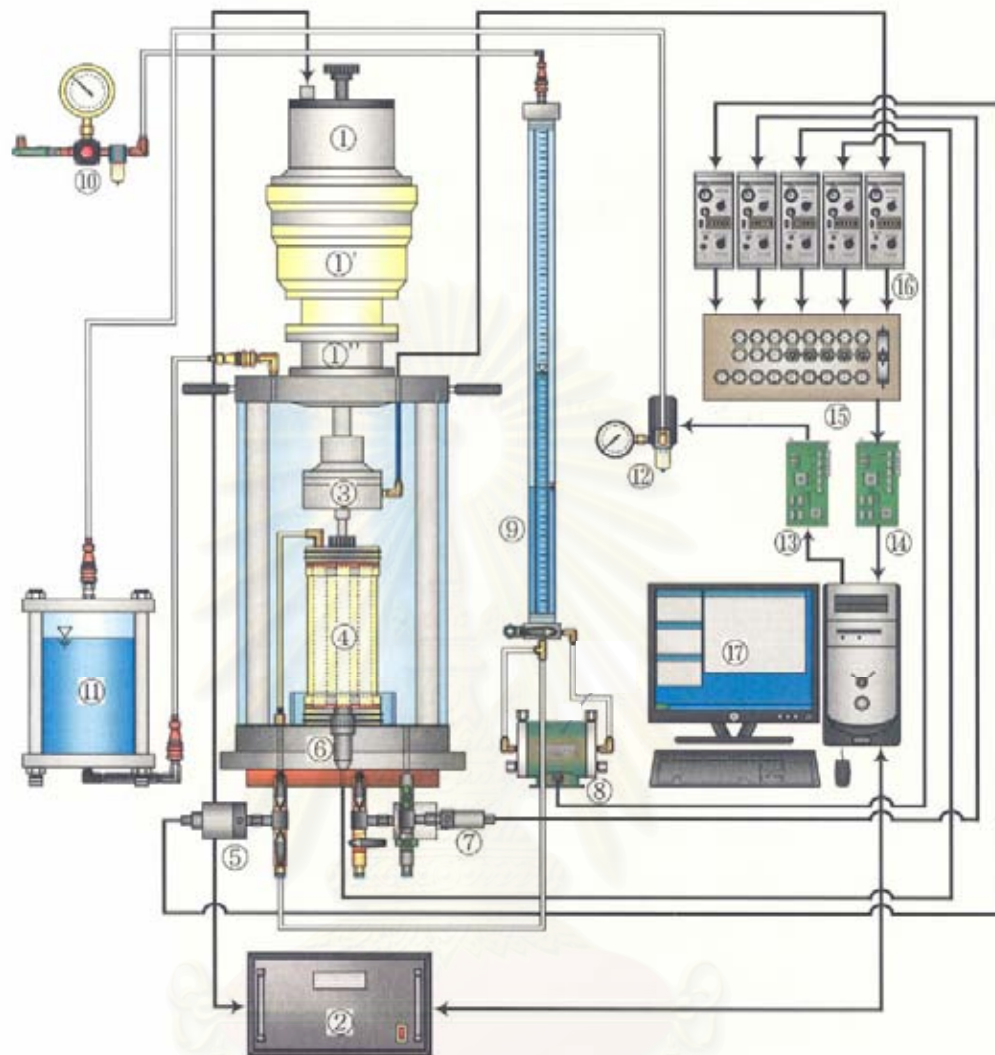


図 3.2.1 Mark I 概要図

- | | | |
|---------------|----------------|---------------|
| ① デジタルサーボモーター | ⑥ 間隙水圧計 (直下) | ⑬ DA変換ボード |
| ①' 減速機 | ⑦ セル圧計 | ⑭ AD変換ボード |
| ①'' フランジ | ⑧ 差圧計 | ⑮ ターミナル |
| ② ドライバーボックス | ⑨ 二重管式ビュレット | ⑯ ストレインアンプ |
| ③ ロードセル | ⑩ レギュレータ | ⑰ パーソナルコンピュータ |
| ④ 供試体 | ⑪ 側圧載荷用小型セル | |
| ⑤ 背圧計 | ⑫ 電空変換器 (E.P.) | |

Figure B.2. Triaxial test system for carrying out the CK₀UC, CK₀DUC and CK₀UUC tests

a. 注水タンク
 a-1. 注水タンクバルブ-1
 試験前日準備段階において、真空ポンプへ接続し脱気を行う。

a-2. 注水タンクバルブ-2
 二重負圧の初期段階では閉じておき、通水段階において開放する。

b. 集水タンク
 通水段階において、a・bの水頭差を用いて供試体内部・周辺に蒸留脱気水を循環させる。

b-1. 集水タンクバルブ-1

b-2. 集水タンクバルブ-2

b-3. 集水タンクバルブ-3

集水タンクを大気開放し、セル圧・背圧を大気圧にするときに使用する。

c. 注水タンクルート

間隙水圧測定ルートへ接続する。

e-1. 注水タンクルートの切り替えバルブ
 二重負圧の初期段階ではb側、通水段階ではa側へと切り替える。

d. 集水タンクルート

背圧測定ルートへ接続する。

d-1. 集水タンクルートのバルブ

e. 三軸セル用真空レギュレータ

セル圧を制御する。

f. 供試体内部用真空レギュレータ

間隙水圧・背圧を制御する。

g. セル圧用負圧ルート

側圧载荷用小型セルへ接続する。

h. 負圧供給用元圧

真空ポンプへ接続され、 -98kPa 程度の負圧が安定供給されている。

i. エアフィルター

真空レギュレータへの水蒸気の混入を防ぐことを目的としている。

j. 集水タンク（混入防止用）

供試体周辺などから吸引された水がe・fに混入しないよう、ここで集水する。

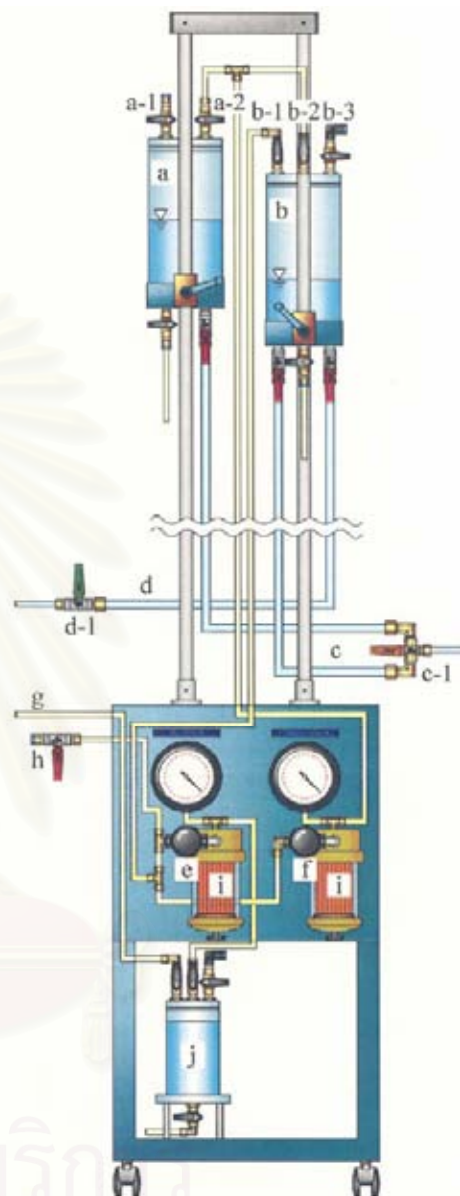


図 3.2.5 二重負圧装置の概要図

Figure B.3. Double Negative Pressure (DNP) system for saturation the soil sample

VITEA

Family name: LE

Last name: TRONG NGHIA

Gender: Male

Nationality: VIETNAMESE

Home address:

No. 164 Block 1, Area 2, Cho Gao town, Tien Giang province, Vietnam

Tel. (+84) 73 651 006

Office address:

Division of Geotechnical Engineering

Faculty of Civil Engineering

HoChiMinh City University of Technology

No. 268 Ly Thuong Kiet Street, District 10, HoChiMinh City, Vietnam

Tel. (+84) 8 863 68 22

Email address:

nghiacehut@yahoo.com or ltnghia@hcmut.edu.vn

Background

2006: obtained an award of excellent presentation at KKCNN symposium in Kyoto University, Japan.

2003: graduated Master degree of Engineering in Geotechnical Engineering (Construction on Soft Soil) at HoChiMinh City University of Technology.

2001: graduated Bachelor degree of Engineering in Civil Engineering at HoChiMinh City University of Technology with 1st honor class.